uOttawa

L'Université canadienne
Canada's university

**FACULTÉ DES ÉTUDES SUPÉRIEURES ET POSTOCTORALES**

uOttawa

L'Université canadienne
Canada's university

**FACULTY OF GRADUATE AND POSDOCTORAL STUDIES**

Samantha Murphy
AUTEUR DE LA THÈSE / AUTHOR OF THESIS

M.Sc.
GRADE / DEGREE

Department of Earth Science
FACULTÉ, ÉCOLE, DÉPARTEMENT / FACULTY, SCHOOL, DEPARTMENT

Characterization of a TCE-Contaminated Aquifer Using Tritium-Helium Dating and Geochemical Tracers, Valcartier, Quebec, Canada

TITRE DE LA THÈSE / TITLE OF THESIS

Ian Clark
DIRECTEUR (DIRECTRICE) DE LA THÈSE / THESIS SUPERVISOR

CO-DIRECTEUR (CO-DIRECTRICE) DE LA THÈSE / THESIS CO-SUPERVISOR

EXAMINATEURS (EXAMINATRICES) DE LA THÈSE / THESIS EXAMINERS

Michel Robin

Fred Michel

Gary W. Slater
Le Doyen de la Faculté des études supérieures et postdoctorales / Dean of the Faculty of Graduate and Postdoctoral Studies

**Characterization of a TCE-contaminated aquifer using tritium-helium dating and geochemical tracers, Valcartier, Quebec, Canada**

by

Samantha E. M. Murphy

A thesis submitted to the Faculty of Graduate and Postdoctoral Studies

in partial fulfillment of the requirements

for the degree of M.Sc. in Earth Sciences

OTTAWA CARLETON GEOSCIENCE CENTRE

AND

UNIVERSITY OF OTTAWA

OTTAWA, CANADA

*Your file Votre référence*
*ISBN:* 978-0-494-61293-4
*Our file Notre référence*
*ISBN:* 978-0-494-61293-4

## Abstract

The groundwater supply in the Valcartier area of Quebec is contaminated with trichloroethylene (TCE) from multiple sources, and hydrogeologic characterization is being carried out to understand its origin and migration patterns. A geochemical investigation was undertaken to independently verify groundwater flow and TCE transport in Valcartier groundwater to improve a numerical model that is currently being developed.

$^{3}H$-$^{3}He$ ages were obtained along flow paths stemming from two main source zones and compared with advective model ages produced at corresponding locations. Ages obtained above and below a prodeltaic silty aquitard in the eastern part of the study area were used to calculate an average vertical hydraulic conductivity ($K_v$) of 1.3-3.1x$10^{-8}$ m/s. $^{3}H$-$^{3}He$ ages were compared with modelled agesat different values of porosity ($n$) and recharge; the bestcorrespondence was found to be at 0.35 and 300 mm/yr, respectively. Anomalously high concentrations of terrigenic He and unexpectedly old $^{3}H$-$^{3}He$ ages in some areas indicate areas where groundwater in the underlying proglacial aquifer may flow upward into the deltaic sand aquifer.

Geochemical parameters measured in groundwater along the flow paths as well as in Shannon and in the proglacial aquifer were examined for patterns. Multivariate statistics (Principal components analysis and cluster analyses) were applied to the data to distinguish different types of groundwater; the geochemistry of each group reflects recharge origin and lithology encountered. The groups verify flow paths delineated by the groundwater model, and help distinguish groundwater of different origins downgradient of source zones. One facies in particular is associated with high TCE concentrations and occurs where groundwater upflow from the proglacial aquifer in Shannon inferred from the $^{3}H$-$^{3}He$ data. This appears to be TCE coming from a previously unrecognized source in the south part of the study area, possibly an old bedrock dump.

This study demonstrates the value of integrating geochemical information in groundwater characterization programs with existing information to refine the understanding of groundwater flow, especially in the development of numerical models.

# Contents

## List of Tables

## List of Figures

## Acknowledgements

There are many people who have helped with my thesis work over the past two years, and I would like to thank all of them for their efforts, their patience, and their insight. This work would not have been possible were it not for their continued support and encouragement.

An enormous thanks to my supervisors, Dr. Ian Clark and Dr. Rene Lefebvre, for their guidance and support for the project and for helping me make some important decisions both academically and professionally over the past two years.

Thank you to Jean-Marc Ballard and Thomas Ouellon, for their help with field work and with modelling. Thanks to Ratan Mohapatra for his help in the Noble Gas Lab; his dedication to running a mass spectrometer that sometimes seemed to have a mind of its own were crucial to the completion of my samples analysis.

To Nicholas Utting, for help with data processing and lab work, advice on projects and reports, and and empathetic ear that have helped me deal with the ups and downs of graduate work. Thanks to Simone Dumas and Lillian Navaro for being fantastic to work with during my Teaching Assistantships, Erwan Gloaguen for criticism and advice on statistical applications, Jamil Sader for helping me out in a tight spot, and Paul Middlestead and Wendy Abdi for their top notch work in the G.G. Hatch lab. Special thanks to fellow graduate students have offered their wisdom and friendship over coffee breaks and after-school beer sessions.

I am very grateful to the Natural Sciences and Engineering Research Council of Canada for financial support during the course of my Masters degree. Thanks also to Institut national de la recherché scientifique and the Department of National Defence for funding my work in Valcartier.

Finally, I'd like to thank my family (Tommy, Marm and Fifi) and my partner (Sandy) for always making life interesting and challenging and wonderful. You have all been so important in helping me grow emotionally and intellectually over the past years, and your love and support have carried me through above all else.

# 1.0 Introduction

## 1.1 Geochemical Tracers as Constraints on Groundwater Flow

In areas with contaminated groundwater it is essential to understand the groundwater system to establish contaminant history and mitigate further contamination. Traditionally, a characterization program is undertaken where wells are drilled into the aquifer of interest to obtain measurements of hydraulic head and perform pumping tests (Lefebvre *et al.*, 2003). This is done to estimate the physical properties of the contaminated aquifer and to determine groundwater flow direction, which may be used in a numerical model. Such models should represent groundwater flow and contaminant migration as realistically as possible, and require some measurable parameter of the aquifer that the model strives to replicate in order to calibrate the model (Konikow & Bredehoeft, 1992; Sheets *et al.*, 1998). Hydraulic head measurements are a readily available parameter that are commonly used to validate numerical models (Szabo *et al.*, 1996; Sheets *et al.*, 1998; Tompson *et al.*, 1999; Weissman *et al.*, 2002). The problem with having only one calibration target for a numerical model is that a unique set of parameters and boundary conditions does not exist for a given match to hydraulic head measurements, as other combinations may also lead to an adequate match (Konikow & Bredehoeft, 1992; Oreskes *et al.*, 1994). The selection of parameters and boundary conditions used in the model remain uncertain, as are the predictions made by such models, and a wide range of possible velocities and flow paths exists other than those predicted by the model.

Groundwater models offer a way to better understand the behaviour of a contaminant in groundwater, and decisions pertaining to mitigation and remediation measures are often made based on model predictions. A high degree of confidence is required in a numerical model used

for such purposes, so it is critical to constrain the model with data that is unrelated to the original calibration target. Groundwater geochemistry can provide information about groundwater flow independently of measured physical parameters, and may be used to reduce uncertainty in numerical models. In this study, two geochemical investigations are undertaken to accomplish this.

The first technique is tritium-helium dating, which can be used in young (<50 years), shallow groundwater systems to produce unambiguous residence times of groundwater at any point in the flow system that can be sampled (Schlosser *et al.*, 1988; Solomon *et al.*, 1992). Groundwater age increases along a flow path, so tritium-helium ($^3$H-$^3$He) dating establishes an age gradient which can be directly compared to simulated travel times from numerical models. The ages can then be used to re-evaluate parameters and boundary conditions used in numerical models to improve their predictive capabilities (Ekwurzel *et al.*, 1994; Szabo *et al.*, 1996; Sheets *et al.*, 1998).

The characterization of relevant geochemical parameters can also provide indications of flow conditions in systems fed by groundwater of different origins. The stable isotope composition of groundwater reflects the origin and degree of evaporation that meteoric waters have undergone, and can provide an indication of recharge conditions (Clark & Fritz, 1997). Groundwater chemistry provides valuable information about origin and flow paths, especially in areas where anthropogenic activities have led to inputs to the subsurface. Characteristics of the recharge location and of the aquifer may impart a distinct geochemical character to groundwater. Water chemistry can change as it flows through the system by interacting with other components of the groundwater system, allowing the classification of groundwater at different points in the system based on flow origin and history (Freeze & Cherry, 1979; Stuyfzand, 1999). Methods of geochemical classification may employ multivariate statistical techniques to help identify groups

of groundwater samples with similar characteristics, which have been successfully applied in other studies to understand recharge origins and flow paths in groundwater systems (Melloul & Collin, 1992; Farnham *et al.*, 2000; Cloutier *et al.*, 2008). This study will examine the geochemical patterns in groundwater, with the aid of multivariate statistics, to distinguish groundwater of different origins and relate it sources of contamination in groundwater.

## 1.2 Potential application of geochemical tracers in the Valcartier sector

The groundwater supply at the Canadian Forces Base Valcartier, northwest of Quebec City (Figure 1.1), is contaminated with chlorinated organic solvents, particularly trichloroethylene (TCE). Prior to the 1970's, TCE was commonly used in industrial operations as a metal degreaser, but its use has largely declined in Canada as health studies have revealed TCE to be toxic and potentially carcinogenic to humans. However, improper disposal by dumping or storage in large ponds has led to large-scale releases of TCE to groundwater systems at many sites in industrialized countries, and the quality of groundwater for drinking supply has been degraded (Pankow & Cherry, 1996). The maximum allowable concentration (MAC) of TCE in drinking water in Canada is 5 µg/L (Health Canada, 2008); concentrations of TCE in the Valcartier aquifer, and the neighboring town of Shannon, are up to 4500 µg/L, rendering groundwater supplies unfit for consumption (Lefebvre *et al.*, 2003).

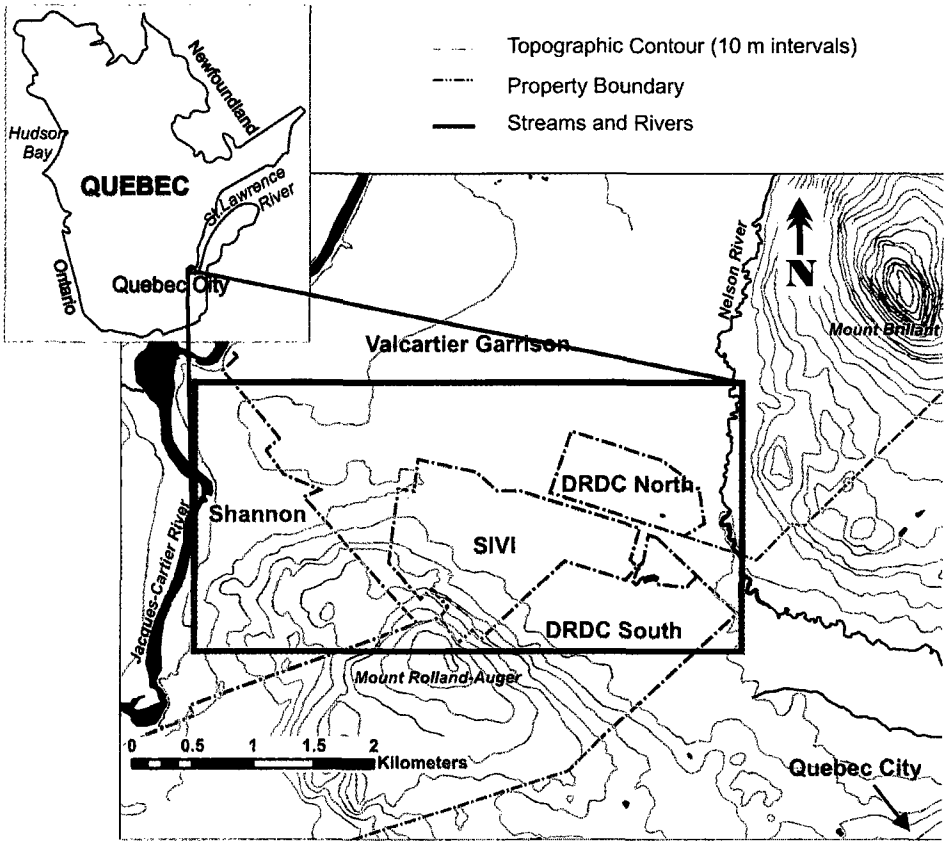


**Figure 1.1.** Map of the study area showing topography, rivers and property limits. Canadian Forces Base Valcartier includes the Valcartier Garrison in the north as well as properties owned by Defense R&D Canada and Société Immobiliére Valcartier Inc.; the town of Shannon lies to the west.

Extensive characterization of the hydrogeology at Valcartier has been ongoing since TCE was discovered in 1997, with efforts focussing on delineating the dissolved TCE plume and describing properties of the principal aquifer where most of the TCE resides (Lefebvre *et al.*, 2003). However, studies have revealed several potential source zones (Figure 1.2) that operated as waste disposal sites on property owned by DND and Société Immobilière Valcartier Inc. (SIVI, formerly owned and operated by SNC-TEC) over the last 60 years or so, although records of disposal activity and the types of substances in the waste are sparse or nonexistent. Despite

this difficulty, a firm understanding of the history of TCE release in Valcartier is crucial to developing a realistic model to predict future behaviour of the contaminant.

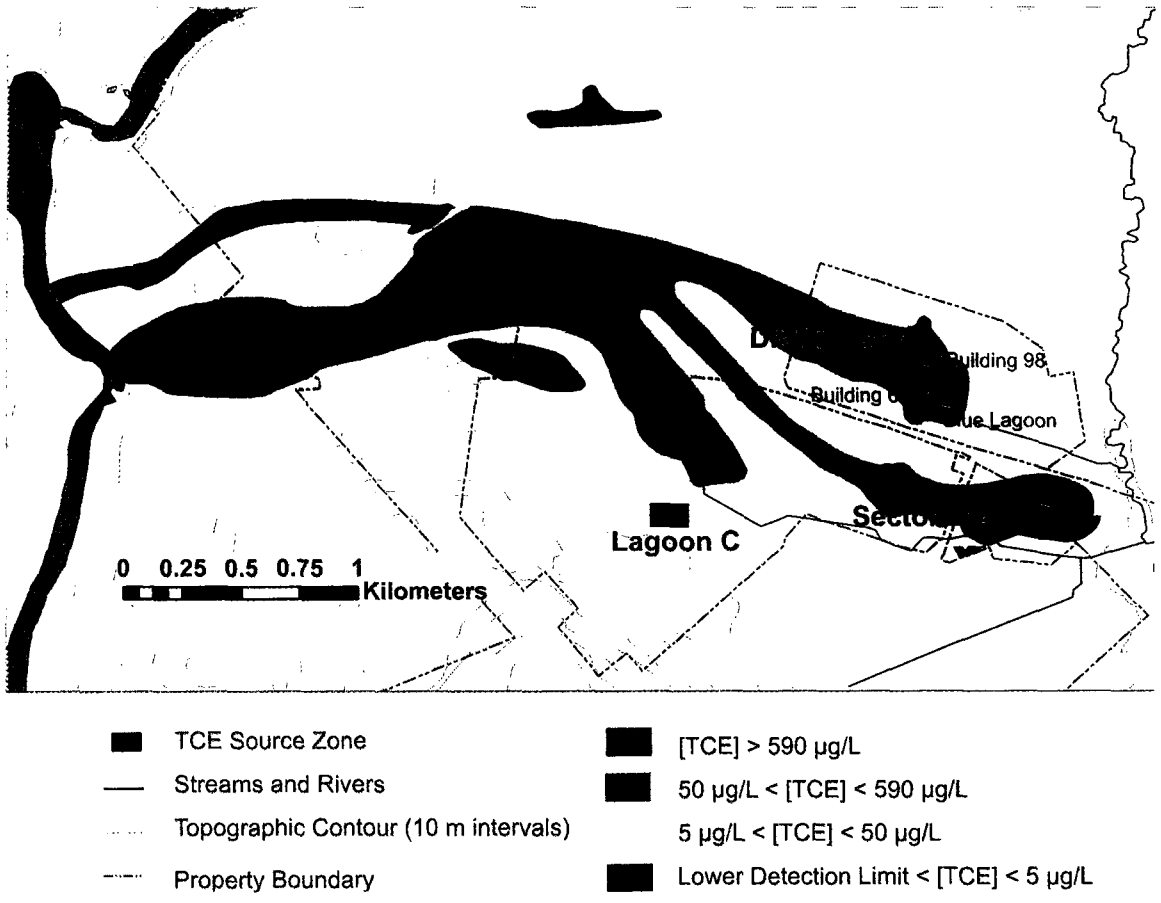


**Figure 1.2**. Map of the Valcartier area showing the maximum historical concentrations of TCE in the deltaic aquifer from 2000-2008 (adapted Ouellon *et al.*, 2008b). Three main TCE source zones at Valcartier include DRDC North, which includes 3 potential waste sites, and Sector 214 and Lagoon C on SIVI property.

The numerical groundwater model currently being developed strives to replicate hydrogeological conditions at Valcartier in order to understand the origin and migration of TCE through the

groundwater system. The model will be used to help make decisions to remediate the groundwater, so it is important for the model to be as close to reality as possible. A detailed study by Ouellon *et al.* (2008a) characterized heterogeneities in the aquifer in an effort to define the hydraulic conductivity field of the model. Several other techniques have been used to estimate other properties of the aquifer and to choose appropriate values for parameters used in the model as outlined in Section 2.5 (Lefebvre *et al.*, 2003; Murphy *et al.*, 2009). Like many numerical models, the Valcartier model used hydraulic heads as a calibration target, but the model needs to be further constrained to minimize uncertainty. Accurate results from the model such as TCE velocity and travel time depend on appropriate choice of parameters (recharge, porosity, hydraulic conductivity), so it is important to validate these values that have been estimated using other techniques (Lefebvre *et al.*, 2003).

The nature of TCE contamination at Valcartier, with its complex disposal history and the heterogeneous hydrostratigraphy, makes it an ideal site for a geochemical investigation. As mentioned previously, $^{3}H$-$^{3}He$ dating can provide unambiguous groundwater ages at any point in the system, which allows estimates of groundwater transit times to be made that can be compared with model results. It is also important to relate TCE distribution in the plume to the multiple source zones, which is difficult to do using the numerical model. If waste that entered the water table at the various source zones has different chemical compositions, or flow paths travelled by the TCE impart a particular geochemistry on the groundwater, there is potential to trace TCE in the plume to its various origins. The suitability of Valcartier for using geochemical tracing techniques allows a conceptual model of groundwater flow and TCE migration to be constructed that is independent of the numerical model.

## 1.3 Purpose of the Study

The purpose of this project is to strengthen the understanding of groundwater flow and TCE origin and migration at Valcartier by employing the techniques of $^{3}H$-$^{3}He$ dating and isotopic and geochemical tracing. This is being done as part of an integrated study of the Valcartier groundwater system that aims to characterize hydrogeological conditions and understand TCE behaviour, so results of this investigation will be closely compared with the numerical model. The goals of the investigation to be addressed in this report are:

- To obtain estimates of groundwater and TCE transit times
- To assess the appropriateness of physical parameters used in the numerical groundwater model of the Valcartier aquifer
- To trace TCE migration in the subsurface in order to
    - verify groundwater flow patterns;
    - understand TCE origin; and
    - relate TCE in the plume in Shannon to its source zones

The results of this study will be used to strengthen the conceptual model of TCE movement in Valcartier groundwater, as well as to re-evaluate the parameters used in the current numerical model so that improvements can be made to reduce uncertainty.

## 1.4 General Methodology

This study will be pursued using two techniques, $^{3}H$-$^{3}He$ dating and geochemical tracing, which are suitable to address the specific objectives of the Valcartier study. The general goal is to use these geochemical methods to examine properties of the groundwater system and how they affect TCE distribution in groundwater at Valcartier.

Many hydrogeological studies have used $^{3}H$-$^{3}He$ dating to address a wide range of groundwater issues (Solomon *et al.*, 1992; Ekwurzel *et al.*, 1994; Reilly *et al.*, 1994; Solomon *et al.*, 1995; Szabo *et al.*, 1996; Aeschbach-Hertig *et al.*, 1998; Dunkle-Shapiro *et al.*, 1998; Portniaguine & Solomon, 1998; Price *et al.*, 2003). The $^{3}H$-$^{3}He$ age represents the mean residence time of water since it entered the saturated zone at discrete points. At Valcartier, ages can be obtained along flow paths identified, using the numerical model, a originating from TCE source zones. The ages along a particular flow path can be compared with ages derived from model simulations to evaluate the parameters being used in the model. $^{3}H$-$^{3}He$ groundwater ages within the TCE plume also provide insight on the history of TCE in the aquifer, which can be related to the timing of its release from source zones.

Groundwater chemistry can be a significant indicator of groundwater flow once spatial patterns are identified (Stuyfzand, 1999; Glynn & Plummer, 2005). Although geochemical data are commonly collected in groundwater studies, they are seldom examined closely enough to make interpretations on groundwater origin. Hierarchical cluster analysis and principal components analysis are statistical techniques that are used to help establish groups of related groundwater samples from Valcartier that can be traced to a common source (Davis, 2002; Güler *et al.*, 2002).

Geochemical "fingerprinting" may be especially useful at Valcartier, as the groundwater being traced originates from sites where TCE was likely disposed of with other geochemical constituents. Effluent from the different sites may have had different chemical compositions that would mix with groundwater once it reached the water table, imparting distinct chemical characteristics to groundwater. Groundwater geochemistry can be examined to identify the influence of lithology, microbial activity, and anthropogenic inputs (Appelo & Postma, 2005). The Valcartier groundwater system consists of several geological units, and land use includes military and industrial activities, so there is potential to trace groundwater flow using geochemistry.

The information obtained from the geochemical investigations will advance the understanding of groundwater flow and TCE migration in the Valcartier groundwater system. Estimates of groundwater travel time in different parts of the deltaic aquifer can be used to assess the extent of the TCE contributions from each source zone to the overall TCE plume, and give some indication of the timing of TCE release. Geochemical patterns will be used to identify the contribution of each source zone to the overall TCE plume, as well as further delineate flow patterns. Finally, this information will be used to evaluate the reliability of the numerical model, and aid in the selection of parameters that will minimize the uncertainty of model predictions.

## 1.5 Organization of the thesis

This Master's thesis is structured to present results of the study in the style of peer-reviewed journal articles, while the initial chapters and the concluding section are written and organized as a traditional thesis report. In addition to the Introduction as the first chapter, the second chapter

(Study Area) outlines the physical details such as geology and hydrogeology, as well as a history of the site's land use and efforts to establish the TCE contamination of groundwater. The third chapter (Characterization Program) explains how the sampling program was specifically designed to address the objectives of the study. Background information on $^{3}H$-$^{3}He$ dating and geochemical tracing and their applicability to the Valcartier groundwater study are also presented in this chapter.

The fourth chapter is written as a journal article, and presents the results of the integrated study of groundwater age distribution in Valcartier groundwater by comparing $^{3}H$-$^{3}He$ ages with ages produced by the numerical model. Transit times derived from $^{3}H$-$^{3}He$ ages are used to assess the use of different model parameters such as recharge, hydraulic conductivity, and different values of effective porosity to aid in the optimization of the numerical model. The fifth chapter is the journal article that describes the geochemical tracing of Valcartier groundwater. Spatial patterns are identified initially to establish groundwater flow patterns, and multivariate statistical techniques are applied to the data to help identify distinct groundwater groups, or facies. Geochemical signatures are established for groundwater recharging near the suspected TCE source zones, which helps to determine the relative contributions from each source to the overall dissolved TCE plume.

The concluding chapter summarizes the interpretations on groundwater flow and TCE migration in Valcartier drawn from the $^{3}H$-$^{3}He$ ages and geochemical characterization, and it is written in the style of a traditional Masters-level thesis. In this chapter, interpretations made in both papers are incorporated to draw conclusions about the origin of TCE in Valcartier.

## 1.6 Contribution of the Author

The work presented in this thesis is one part of a large scale study of the Valcartier groundwater system that began in 2001, shortly after TCE was discovered in private wells in Shannon. This is largely being undertaken by R. Lefebvre and his research group at the Institut national de la recherché scientifique – Eau Terre Environnement (INRS-ETE). This group is characterizing the groundwater system and developing a numerical groundwater model to guide decisions made on the control and potential clean-up of TCE in the groundwater. The study is being funded by the Department of National Defence.

A great deal of work has been done on the Valcartier project since it began. Over 990 wells have been installed and 435 slug tests performed, and groundwater has been monitored multiple times in for TCE and other contaminants in many of these wells. The stratigraphy has been characterized using borehole logs, cone penetration testing (CPT), grain size analysis and column testing. On this basis, a 3-D geologic model has been developed that defines the hydrostratigraphy of Valcartier (Michaud *et al.*, 1999; Martel *et al.*, 2000; Lefebvre *et al.*, 2003). Extensive work has been done to obtain estimates of the physical properties of the system (hydraulic conductivity, porosity, recharge, retardation factor) and to establish groundwater flow patterns, so that a numerical model could be developed to help interpret TCE migration in Valcartier groundwater (Lefebvre *et al.*, 2003; Boutin *et al.*, 2004; Lefebvre *et al.*, 2004; Maltais, 2006; Ouellon *et al.*, 2008a,b,c).

The sampling program for this study was initially designed by R. Lefebvre with the aid of modelling done by T. Ouellon at INRS-ETE, for the purpose of targeting flow paths originating from TCE source zones in Valcartier. A preliminary study was carried out with I.D. Clark and R. Mohapatara at the University of Ottawa in the spring and summer of 2007 to determine the

feasibility of performing $^{3}H$-$^{3}He$ dating on Valcartier groundwater; this study laid the groundwork for planning and obtaining funding for a more extensive groundwater dating program.

The author collected water and gas samples and took field measurements in wells selected by R. Lefebvre and T. Ouellon in November 2007, which was done with the help of T. Ouellon. For complementary sampling done in the summer of 2008, the author selected several additional wells to be sampled in Valcartier and in Shannon, which was done with the help of J.-M. Ballard, who also conducted the particle tracking with the model to produce model ages to compare with the $^{3}H$-$^{3}He$ ages. The author conducted laboratory analyses of all gas samples required for $^{3}H$-$^{3}He$ dating. Chapter 4 is a paper addressing $^{3}H$-$^{3}He$ dating in the context of the overall characterization of the Valcartier aquifer system, and includes sections on the numerical model and other characterization efforts that were written by R. Lefebvre. Sections specifically pertaining to the $^{3}H$-$^{3}He$ dating, especially in the Methods, Results and Discussion sections, were written primarily by the author. Chapter 5 was written mostly by the author, with contributions from co-authors (particularly R. Lefebvre). Chapters 1, 2, 3 and 6 are entirely the work of the author.

Finally, the author contributed to a research report for the Department of National Defence from INRS-ETE on the Valcartier groundwater dating and geochemistry project (Murphy *et al.*, 2009).

# 2.0 Study Area

## 2.1 Location

The study site is located 25 km northwest of downtown Quebec City, Quebec, Canada and includes Canadian Forces Base Valcartier, the town of Shannon in the west and Val Belair (now Quebec City) to the east (Fig. 1.1). The study area is relatively flat and surrounded by large hills, the nearest being Mount Rolland-Auger in the south and Mount Brillant in the northeast. Two rivers running north-south bound the area, the Jacques-Cartier River west of Shannon and the Nelson River in the East.

Valcartier is in the humid continental climate zone, with hot, humid summers and cold winters, with high amounts of precipitation throughout the year. Temperatures vary annually from an average of -12.8°C in January to 19.2°C in July. The area receives 1230 mm of precipitation annually, with 316 mm falling as snow and 924 mm falling as rain (Environment Canada, 2008).

Land use on CFB Valcartier is primarily residential and military, and Shannon is almost entirely residential. Industrial activity is ongoing in the property owned by Defence R&D Canada (DRDC), and there have been industrial activities on the SIVI property, which was formerly owned by SNC-TEC. Mixed-coniferous forest occupies the hills and undeveloped parts of Valcartier and Shannon. The water is supplied entirely from groundwater, and mostly withdrawn from an unconfined deltaic sand aquifer that underlies the area (described in Sections 2.3 and 2.4).

## 2.2 History

In 1997, TCE was found in water from municipal and private wells of CFB Valcartier at concentrations exceeding the maximum allowable concentration (MAC) at the time of 50 μg/L, which was reduced to 5 μg/L in 2005 (Health Canada, 2008). Programs to study the groundwater system at Valcartier were initiated at this time to characterize the dissolved TCE plume, and the water supply was relocated to an area with uncontaminated groundwater. High levels of TCE were discovered in private wells in Shannon in December of 2000, to the west of Valcartier. Residents of Shannon with high TCE levels in their wells were provided with treatment systems to filter the TCE, but poor results led to the extension of the Valcartier water distribution system in 2003 to supply drinking water to Shannon via aqueduct.

A large-scale program was begun in 2001 by INRS to characterize the Valcartier groundwater system and to delineate the extent of TCE in the groundwater. The TCE plume,found mostly within the deltaic sand aquifer, and is about 4.5 km long from east to west, 650 m at its widest north-south, and has an average plume thickness of 20 m (Fig. 1.2). Modelling efforts of the groundwater system in Valcartier began in 2003, and have expanded to include Val-Belair (now part of Quebec City) and Shannon since characterization of the plume in those areas began in 2005.

There have been three pilot tests run on plume control technologies in Valcartier from 2006-2008. Implementation of such technologies to manage TCE in groundwater is tentatively planned for 2009, once characterization and modelling of the aquifer system is complete.

## 2.3 Geology

The site is located in the Grenville Province of the Canadian Shield. Bedrock of the area consists of granitic gneiss, the roots of the Laurentian Mountains formed by the Grenville Orogeny 1.1 Ga ago (Natural Resources Canada, 2008). Erosion of the bedrock formed a crescent-shaped valley that runs west-east in the study area, which has topography of up to 50 m. The valley splits in two directions in the west, with a less-defined valley continuing under the Jacques-Cartier River (Lefebvre *et al.*, 2003).

During the Quaternary, about 12 Ka ago, the isostatically depressed land allowed the invasion of the Atlantic Ocean into the region to form the Champlain Sea. As the glaciers retreated, sediment was deposited on the bedrock in a sequence of till, then proglacial sands and gravels, and then finally silts when the area was inundated by the sea. Through time, the crust rebounded isostatically and rivers carrying high-sediment load continued to drain into the sea, forming deltas and depositing sand and silt on top of the glacial sediments. Alluvial sediments constitute the most recently deposited overburden in the area (Fagnan *et al.*, 1999; Natural Resources Canada, 2008).

The stratigraphic units that make up the sediments at Valcartier include, from bottom to top: glacial till, proglacial sand and gravel , glacio-marine silt, deltaic sand, prodeltaic silt and alluvial sands (Lefebvre *et al.*, 2004). Figures 2.1 and 2.2 show the surficial geology of the area and a 3-D representation of the stratigraphy, respectively.

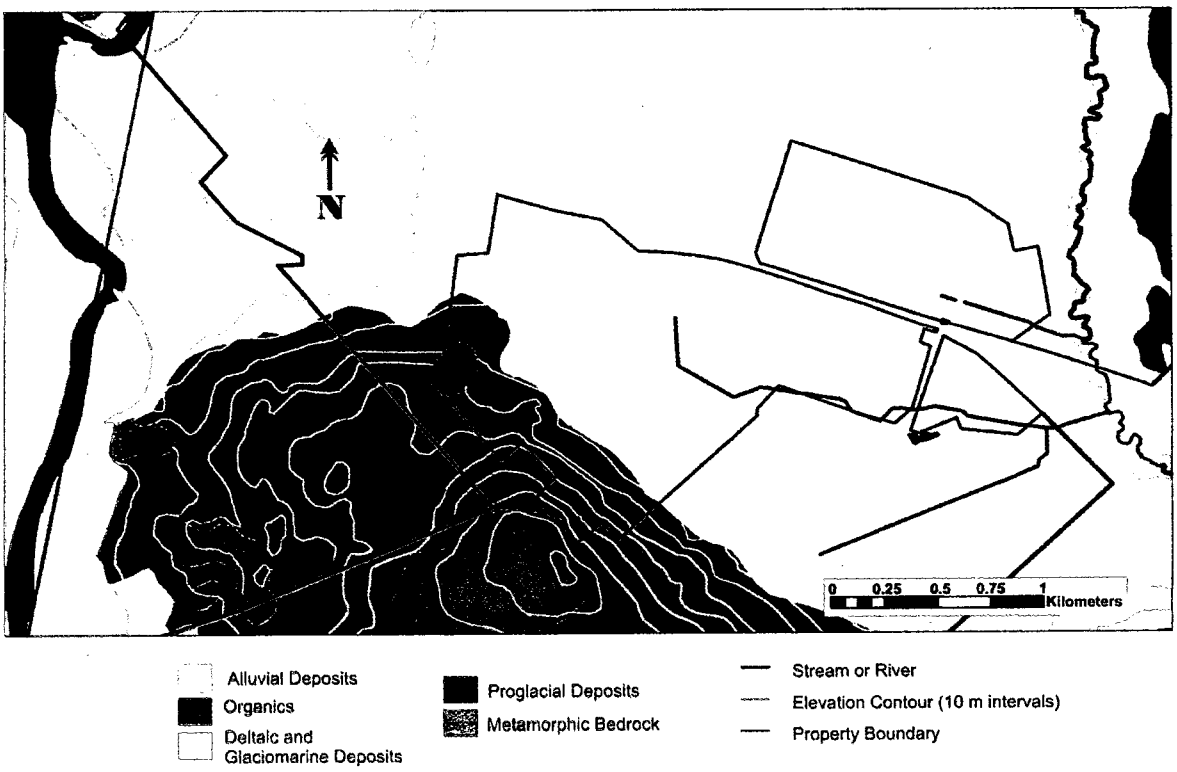


**Figure 2.1**. Map showing the surficial geology of the Valcartier area. Quaternary sediments fill the valley running west-east, and bedrock outcrops on the mounts.

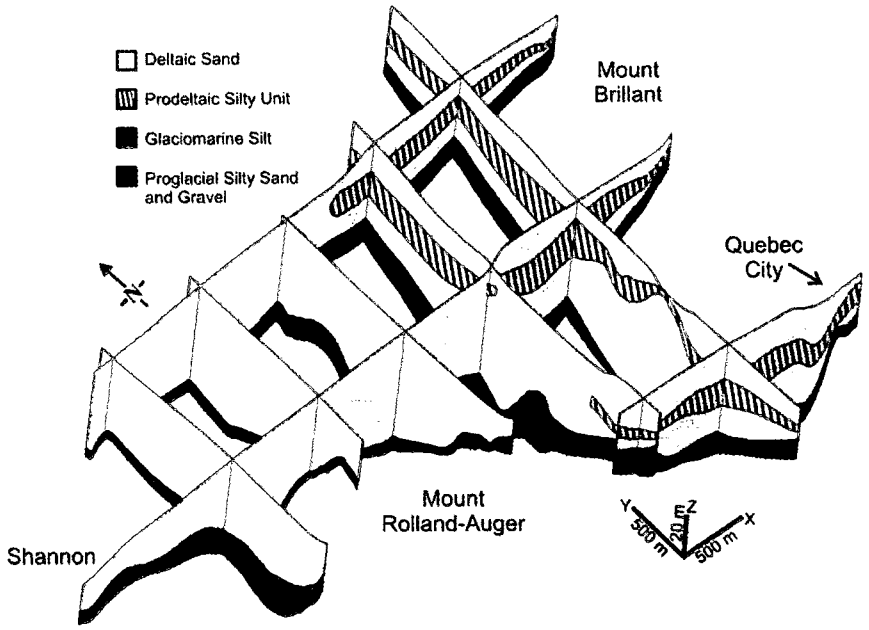


**Figure 2.2**. 3-D geological model of the study site showing the stratigraphy of Quaternary sediments above the bedrock (modified from Lefebvre *et al.*, 2004).

## 2.4 Hydrogeology

The main aquifer at Valcartier is the deltaic sand unit, which has medium- to coarse-grained sand and is hydraulically connected to the underlying proglacial sediments where the glacio-marine silt is discontinuous (Figure 2.3). The deltaic sand in the eastern part of the study area is split into upper and lower units by a wedge of prodeltaic silt. This unit consists of fine layers of silt, clayey silt and sandy silt that form an aquitard (Lefebvre *et al*, 2004). The deltaic aquifer is semi-confined where it is overlain by the prodeltaic silty aquitard, and unconfined where it is stratigraphically above the silt and where the silt unit is not present in the western part of the study area. Potentiometric maps indicating the direction of groundwater flow in the deltaic sand aquifer and in the proglacial aquifer are shown on Figure 2.4.

The thickness of the deltaic sand unit ranges from very thin up to 45 m due to the topography of the underlying bedrock. Mean hydraulic conductivity (K) for the stratigraphic units as estimated from slug tests is $3.2 \times 10^{-4}$ m/s for the deltaic sands and $1.6 \times 10^{-5}$ m/s for the prodeltaic silts; however, the sediments are quite heterogeneous, making it difficult to accurately calculate groundwater velocities. In general, groundwater moves on the scale of 100 m/a near the hills where the gradient is high, and slower within the valley (10 – 100 m/a). Groundwater also moves slower in the east where the finer-grained silt unit restricts flow velocity. A horizontal gradient dominates the study area where water generally flows westward toward the Jacques-Cartier River. Groundwater moves downward in the recharge area near the groundwater divide in the east, and across the silt unit where there is a downward gradient of 0.1-0.3 m/m (Lefebvre *et al.*, 2004).

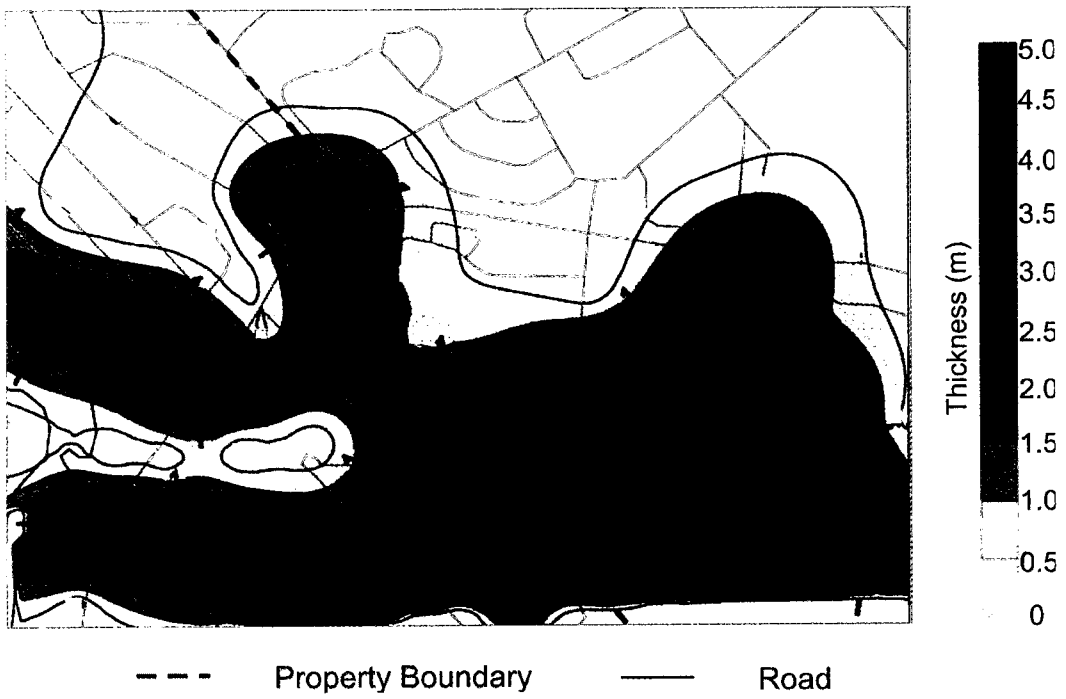


**Figure 2.3**. Map of the western part of the study area showing the thickness of the proglacial silt aquitard.

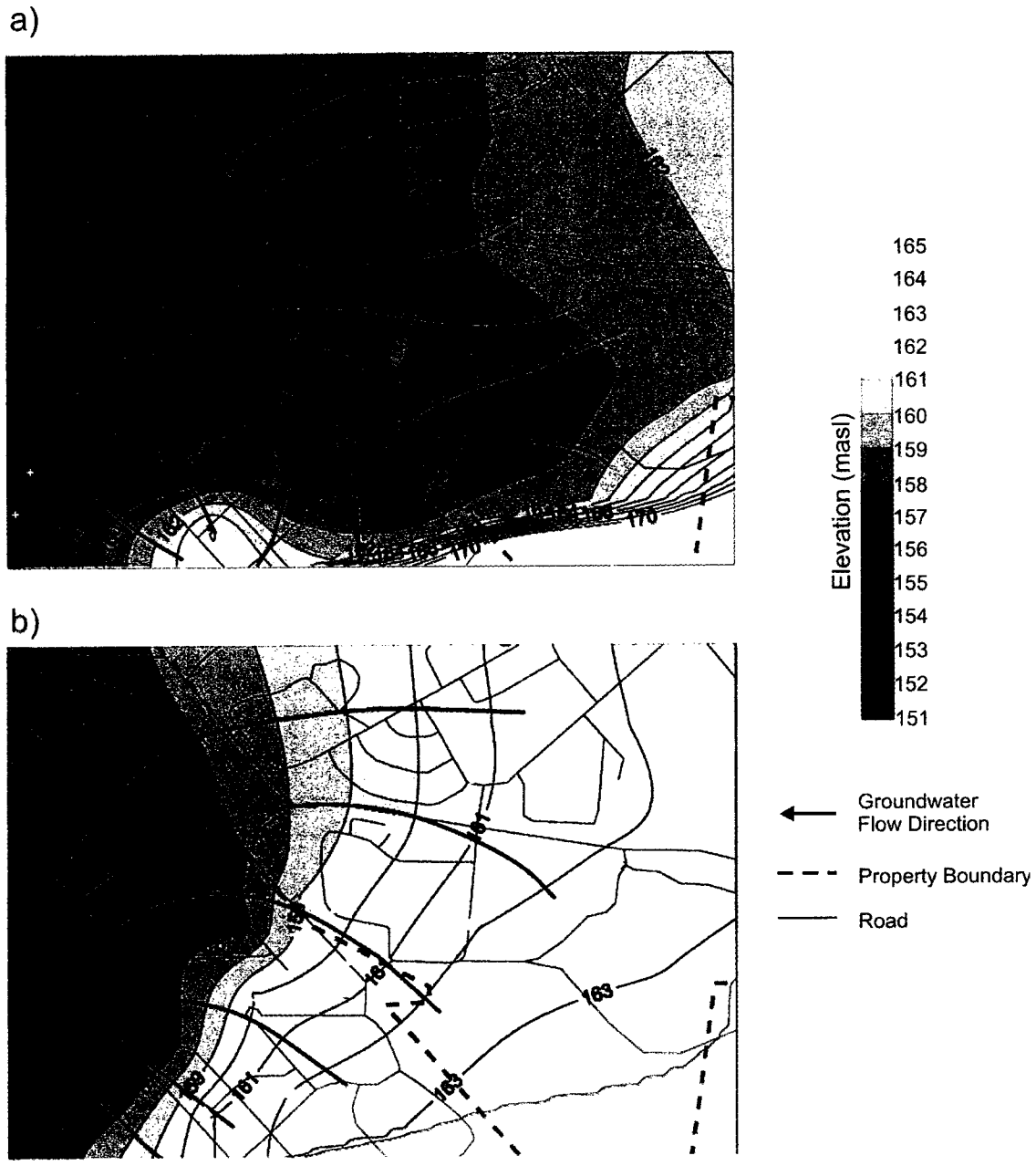


**Figure 2.4**. Maps showing potentiometric surfaces in the western part of the study area in a) the deltaic sand aquifer and b) the proglacial aquifer.

## 2.5 Available Data

The Valcartier groundwater system has been extensively characterized to understand TCE origin and migration patterns. Since characterization began, numerous wells have been installed to measure groundwater levels and contaminant concentrations, and to perform slug tests to estimate the hydraulic conductivity of the stratigraphic units. A summary of characterization measures undertaken from 1997 to present is listed in Table 2.1.

**Table 2.1**. Available data to support the Valcartier groundwater characterization program.

| **Stratigraphy** (locations / total length, m) | |
|---|---|
| Borehole logs | 394 / 9580 |
| CPT soundings | 28 / 365 |
| **Observation wells** (≈2 per borehole) | |
| Screened intervals | 991 |
| **Water samples** (including repeats) | |
| Well sampling | > 2350 |
| Direct push sampling | 1460 |
| **Hydraulic conductivity** | |
| Slug tests | 435 |

Estimates of physical parameters of the Valcartier groundwater system have been made through various techniques (Table 2.2), with a focus on the deltaic sand aquifer. Estimates of recharge and other hydrological parameters are derived from well hydrograph records and water balance calculations (Lefebvre *et al.*, 2009). Hydraulic conductivity estimates of the main hydrostratigraphic units were made from slug test results and by calibrating the numerical model to match groundwater heads. Other relevant parameters were quantified using CPT sounding (porosity) and column tests (porosity, retardation factor).

**Table 2.2**. Estimates of physical parameters of the Valcartier groundwater system.

| Parameter | Value | Units | Method |
|---|---|---|---|
| **Deltaic Sand** | | | |
| Total Porosity | 0.40 | - | Column Tests (Lefebvre *et al.*, 2003) |
| Total Porosity | 0.44 | - | CPT (Fauveau *et al.*, 2005) |
| Specific Yield | 0.22 | - | Column Tests (Lefebvre *et al.*, 2003) |
| Specific Yield | 0.25 | - | CPT (Fauveau *et al.*, 2005) |
| Hydraulic Conductivity | $3x10^{-5}$ to $1x10^{-3}$ | m/s | Slug tests and hydrofacies (Ouellon *et al.*, 2008a, b) |
| Retardation Factor | 1 | - | Column tests (Lefebvre *et al.*, 2003) |
| Groundwater Recharge | 308 to 500 | mm/a | Well Hydrographs (Lefebvre *et al.*, 2003) |
| Groundwater Recharge | 300 | mm/a | Numerical modelling calibration (Ouellon *et al.*, 2008a, b) |
| **Prodeltaic Silt** | | | |
| Total Porosity | 0.36 | - | Column tests (Lefebvre *et al.*, 2003) |
| Hydraulic Conductivity (vertical) | $3x10^{-9}$ to $3x10^{-8}$ | m/s | Numerical modelling calibration and hydrofacies (Ouellon *et al.*, 2008a, b) |
| Retardation Factor | 1.7 | - | Column tests (Lefebvre *et al.*, 2003) |
| **Glaciomarine Silt** | | | |
| Hydraulic Conductivity | $5x10^{-5}$ | m/s | Slug Tests (Lefebvre *et al.*, 2003) |
| **Proglacial Aquifer** | | | |
| Hydraulic Conductivity | $1.9x10^{-4}$ | m/s | Numerical modelling calibration (Boutin *et al.*, 2004) |
| **Bedrock** | | | |
| Hydraulic Conductivity | $5.6x10^{-6}$ | m/s | Slug Tests (Blais, 2006) |

The TCE plume in Valcartier groundwater is well-defined, and is shown in Fig. 1.2. From the patterns of TCE concentration and knowledge of groundwater flow direction, several potential source zones have been identified. In the DRDC property there are three closely-spaced locations from which TCE may have been emitted: Buildings 67 and 98, and the Blue Lagoon, which are grouped as one source zone. The second and third TCE source zones are on SIVI property, namely Sector 214 and Lagoon C; there are other suspected waste disposal sites in this area where no TCE has been detected thus far. Of the known source zones, Building 98 and Sector 214 are located above the prodeltaic silty aquitard, whereas Building 67, the Blue Lagoon, and Lagoon C overlie the deltaic sand aquifer where the aquitard is absent. Wells thatencounter the TCE plume are sampled at least annually, along with concentrations of other volatile organic compounds, perchlorate and several other contaminants, although few compounds other than TCE have been found at concentrations of concern. The most recently available report on contaminant levels in Valcartier groundwater was done by Dessau-Soprin in July 2008, based on measurements taken throughout 2007 (B. Michaud, pers. comm., 2008).

# 3.0 Characterization Program

## 3.1 Objectives

This program was undertaken to address specific questions pertaining to the Valcartier groundwater system, which are outlined in the following objectives:

1. ***Provide Evidence of Groundwater Flow Conditions***

    a. *Groundwater Recharge.* In unconfined aquifer systems such as the one at Valcartier, groundwater recharge controls circulation, and it is difficult to obtain accurate estimates of this parameter. Values for the recharge rate at Valcartier have been estimated using other techniques (daily water balance, water table fluctuation method; Maltais, 2006). A vertical profile of groundwater age provides a way to estimate the vertical flux of groundwater; if a sampling location can be selected that is close to a groundwater divide, where groundwater flow is predominantly vertical, such a profile could be compared with other recharge estimates.

    b. *Control of Prodeltaic Silty Unit.* Two TCE source zones in Valcartier are located above a prodeltaic silty unit within the deltaic sand aquifer (B98 and Sector 214), which the TCE must traverse prior to reaching the deltaic sand aquifer (Figures 1.2 and 2.2). This unit affects the initial vertical migration of TCE, and hence controls overall transit time of TCE from these source zones.It is therefore important to estimate accurately the properties of the unit to understand its influence on TCE migration. There are no direct measurements available with which to estimate the vertical hydraulic conductivity of this unit, but this can be

done if groundwater ages are obtained above and below the silty unit. These data could be used to determine groundwater transit time through the silt unit, which can then be applied to estimating TCE migration time and hydraulic properties of this unit.

2. ***Groundwater Transit times and Velocities***. Groundwater models that are calibrated using hydraulic heads may not realistically represent groundwater velocities and contaminant transit times. Sensitivity testing shows that this calibration target is highly sensitive to hydraulic conductivity, which is well constrained at Valcartier, but the model is less sensitive to recharge and independent of porosity under steady-state flow conditions (R. Lefebvre, pers. comm., 2008). Recharge and porosity exert strong control on groundwater velocity under unconfined conditions such as Valcartier, so it is important to assess these parameters to determine whether or not the velocities produced by the model are reliable. Ages obtained along a flow path can be compared with simulated ages from the model to assess the model's ability to replicate the $^{3}H$-$^{3}He$ age distribution, which serves as an alternate calibration target. Once the model has been optimized by selecting parameters that provide the closest match to $^{3}H$-$^{3}He$ ages, estimates of groundwater velocity and transit times from TCE source zones to receptor areas in Shannon can be obtained using the numerical groundwater model.

3. ***Distinguish TCE Plume Origins and Migration Paths***

    a. *Source zones at the Origin of the TCE Plume*. There are three main source zones in Valcartier contributing to the TCE plume in the deltaic aquifer (Fig. 1.2); the current understanding is that TCE emitted from DRDC North and Sector 214 has

a relatively longer transit time to the town of Shannon to the west of the source zones, which lies downgradient of the plume, than TCE from Lagoon C. Presently, the conceptual model of TCE migration in Valcartier implies that TCE from DRDC North and Sector 214 may have not yet passed the western limit of the Valcartier Garrison. This idea must be verified in order to implement future controls on the westward migration of the TCE plume, which can be done using groundwater ages. Particle tracking using the model shows that DRDC North and Sector 214 have parallel flow paths and similar transit times (Murphy *et al.*, 2009), so a general flow path can be found that represents TCE transit time from both of these source areas. Groundwater ages along the flow path can be compared with groundwater ages along the flow path stemming from Lagoon C to see if a difference exists in the migration time of groundwater (and thus TCE) from the source zones to receptors in Shannon. If groundwater originating from the two groups of source zones have different geochemical signatures, tracers may be used to independently verify flow paths and origins of different portions of the TCE plume.

b. *TCE plume transit time from source zones.* Assessment of the time it takes for TCE to migrate from source zones to receptors in Shannon can be done by identifying groundwater flow paths from TCE source zones (objective 2.a.) and estimating groundwater transit time and velocity (objective 1.c.). If groundwater velocities predicted by the model can be validated by groundwater age data, past and future evolution of TCE migration from source zones can be assessed.

*4. **Provide Evidence for Source Zones of the TCE found in Shannon.*** Shannon, where many private wells are contaminated with TCE, lies to the west of the TCE source zones in Valcartier. TCE emitted from all source zones that have had time to reach Shannon are integrated into the plume downgradient, and it is difficult to distinguish contributions from individual source zones. Geochemical characteristics and ages of groundwater in Shannon can be used to relate TCE found in Shannon to its origins at the TCE source zones found in Valcartier.

## 3.2 Design of Sampling

### 3.2.1 Delineating Flow Paths

The sampling program was designed to facilitate the use of tracers (age and geochemistry) as evidence of groundwater flow conditions and TCE origin and migration. The data collected will be used as independent evidence to constrain the groundwater model, and as such the selection of sample locations needed to be done in a manner that allowed direct comparison with numerical simulation results. For this reason, sampling focussed on TCE migration pathways from the two main source zones in Valcartier, which were identified using the numerical model. Wells in Valcartier and Shannon that lie close to these flow lines were selected to help answer the questions outlined in Section 3.1.

TCE derived from the two source zones being targeted, as mentioned previously, are thought to have different migration paths and travel times into Shannon. Particle tracking was used to identify a north flow path (NFP) originating to the west of the prodeltaic silty aquitard between the DRDC North and Sector 214 source zones, and a south flow path (SFP) that begins at

Lagoon C, as indicated on Figure 3.1. It is a technique where a "particle" in the numerical model is released at a point of interest in the aquifer system, and the "track" taken by the particle is recorded by a simulator. This was done at closely-spaced intervals along the water table starting at each of the source zones and progressing downgradient into Shannon, establishing a cross section of particle tracks for both the NFP and SFP in the deltaic sand aquifer (shown in Chapter 4, Figure 4.5).

Once flow paths were defined, observation wells that lie on or close to the paths were selected for sampling. The saturated thickness of the deltaic aquifer generally increases from south to north, so wells that were offset from the flow paths had to be projected onto the particle track cross sections. Projection was done using the same X-coordinate as the sample points, but by normalizing the elevation at the sample location to match the same relative position within the saturated thickness on the particle track section. This was necessary to be able to associate sampling points with particle tracks on each flow path to directly compare model ages to ages obtained through $^{3}H$-$^{3}He$ dating (details on sample locations and the projection of locations onto cross sections are provided in Appendix A).

### 3.2.2 Selection of Sampling Locations

The sample locations chosen to support the objectives to be met specifically using groundwater ages are screened in the deltaic sand aquifer, the unit in which most TCE resides. These sampling locations were selected because they provide access to groundwater at multiple depths in the aquifer as well as the following:

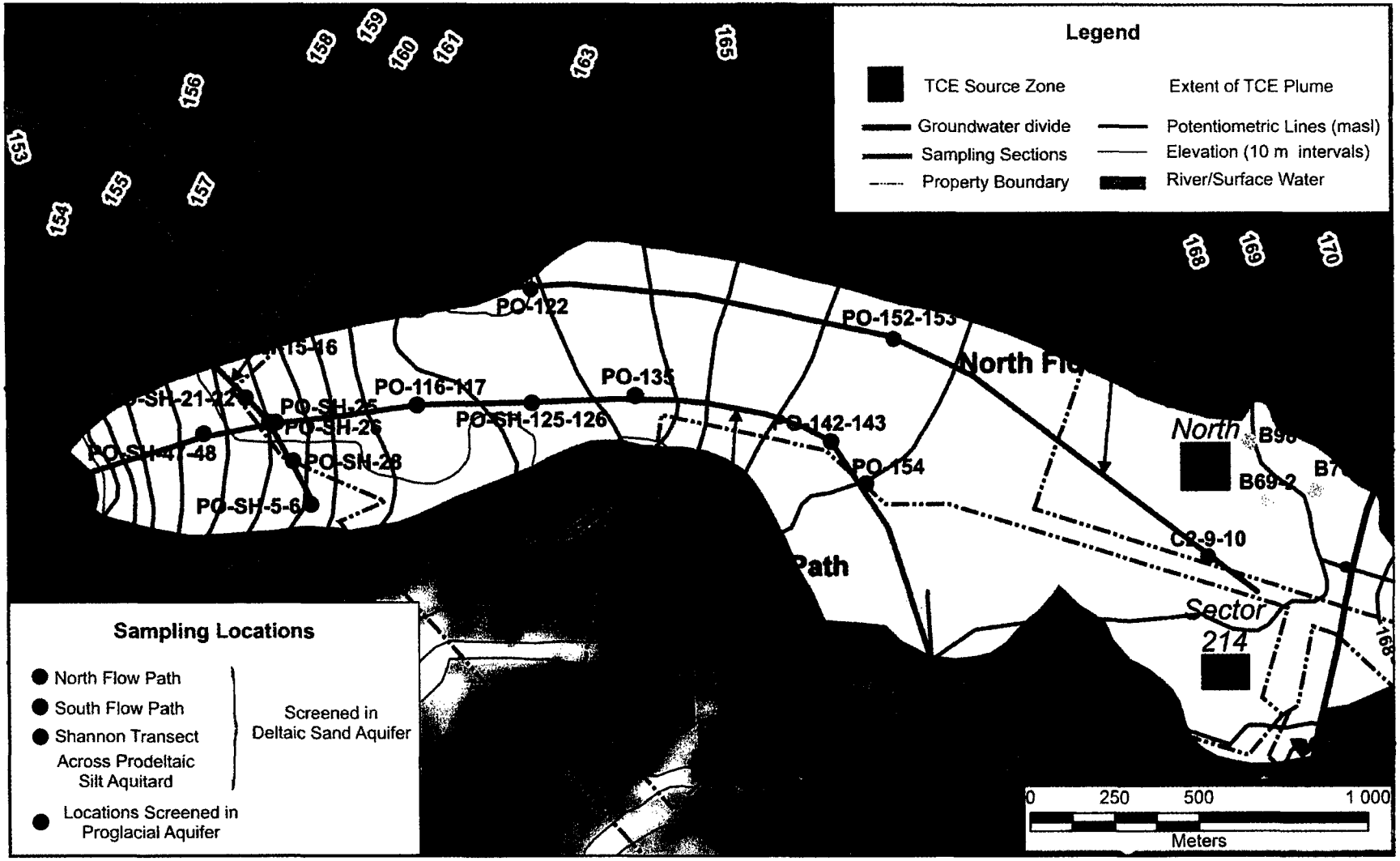


**Figure 3.1**. Map of the Valcartier area showing the North and South Flow Paths and the transect through Shannon, as well as locations selection for sampling groundwater in the deltaic sand aquifer and in the proglacial aquifer.

- Objective 1 - Provide evidence of groundwater flow conditions
    - C2-9-10: This location is close to the groundwater divide where flow is mostly vertical; its age profile can be used to estimate the rate of recharge.
    - B69, B70 and B98: These wells have screened intervals directly above and below the prodeltaic silty unit; ages from these wells can be used to calculate the transit time of groundwater and TCE across the silt.
- Objective 2 - Distinguish TCE origins and migration paths
    - C2-9-10, PO-152-153, PO-122, PO-SH-7-8 (North Flow Path) and PO-142-143, PO-125-126, PO-116-117, PO-SH-26, PO-SH-47-48 (South Flow Path): These locations fall on or near groundwater flow paths from the source zones, where changes in age between wells can be related to groundwater transit time and velocity. Comparison of transit times and velocities from the two main TCE source zones with results from the model will allow the selection of parameters that lead to the best match between simulated model ages and $^{3}H$-$^{3}He$ ages. The geochemical signature of each TCE source zone and the evolution of groundwater along flow paths can also be established by examining samples from these wells.
- Objective 3 - Evidence for Source Zones of the TCE found in Shannon
    - PO-SH-7-8, PO-SH-21-22, PO-25, PO-5-6: These sample locations form a transect running northwest to southeast across the downgradient end of the TCE plume in Shannon. Both groundwater ages and geochemical parameters can be used to distinguish contributions to the TCE plume from potential source zones.

The other important aspect of this study is the use of geochemical parameters to trace groundwater flow paths and TCE origins. Several sampling locations were chosen in addition to those listed above to provide a more complete data set to interpret spatial patterns for the following reasons:

- Obtain detailed cross sections of geochemical parameters in Shannon perpendicular to groundwater flow.
    - PO-SH-15-16 and PO-SH-28: More detail is required for distinguishing the distribution of geochemical parameters in Shannon groundwater. Gaps of information along the transect in Shannon can be filled in using samples collected from these wells, which are easily projected onto the Shannon cross section (Figure 3.2).
- Characterize groundwater flowing in proglacial aquifer
    - The source zone targeted on the south flow path, Lagoon C, consists of a pit that may be excavated to the proglacial aquifer, which is suggested by high concentrations of dissolved TCE in this unit. There are also some locations south of the SFP on the flanks of Mount Rolland-Auger where waste disposal is thought to have occurred in the past that may have included TCE. If waste from these southern potential source zones recharges the proglacial aquifer, it would flow northward towards the SFP, so it is important to understand the extent of hydrologic interaction between the proglacial aquifer and the deltaic sand aquifer. Groundwater geochemistry in the proglacial aquifer must be characterized, so it is

important to select samples screened in the proglacial aquifer, with a focus on locations near the SFP.

- PO-154 and PO-135: These wells are screened in the proglacial aquifer and intercept groundwater containing TCE that was likely released by Lagoon C. They may be used to establish a geochemical fingerprint of the Lagoon C source released to the proglacial aquifer that may be entering the deltaic sand aquifer downgradient.

- PO-128, PO-SH-25, PO-SH-45-46: These wells are screened in the proglacial aquifer outside of (or beneath, in the case of PO-SH-25) the TCE plume. The range of background geochemical conditions in the proglacial aquifer can be established by examining groundwater from these sample locations.

Information on the wells selected for this study is given in Appendix A, and Figure 3.1 shows their location on a map. Figure 3.2 shows the locations of samples taken along the North and South Flow Paths and the Shannon transect in cross section.

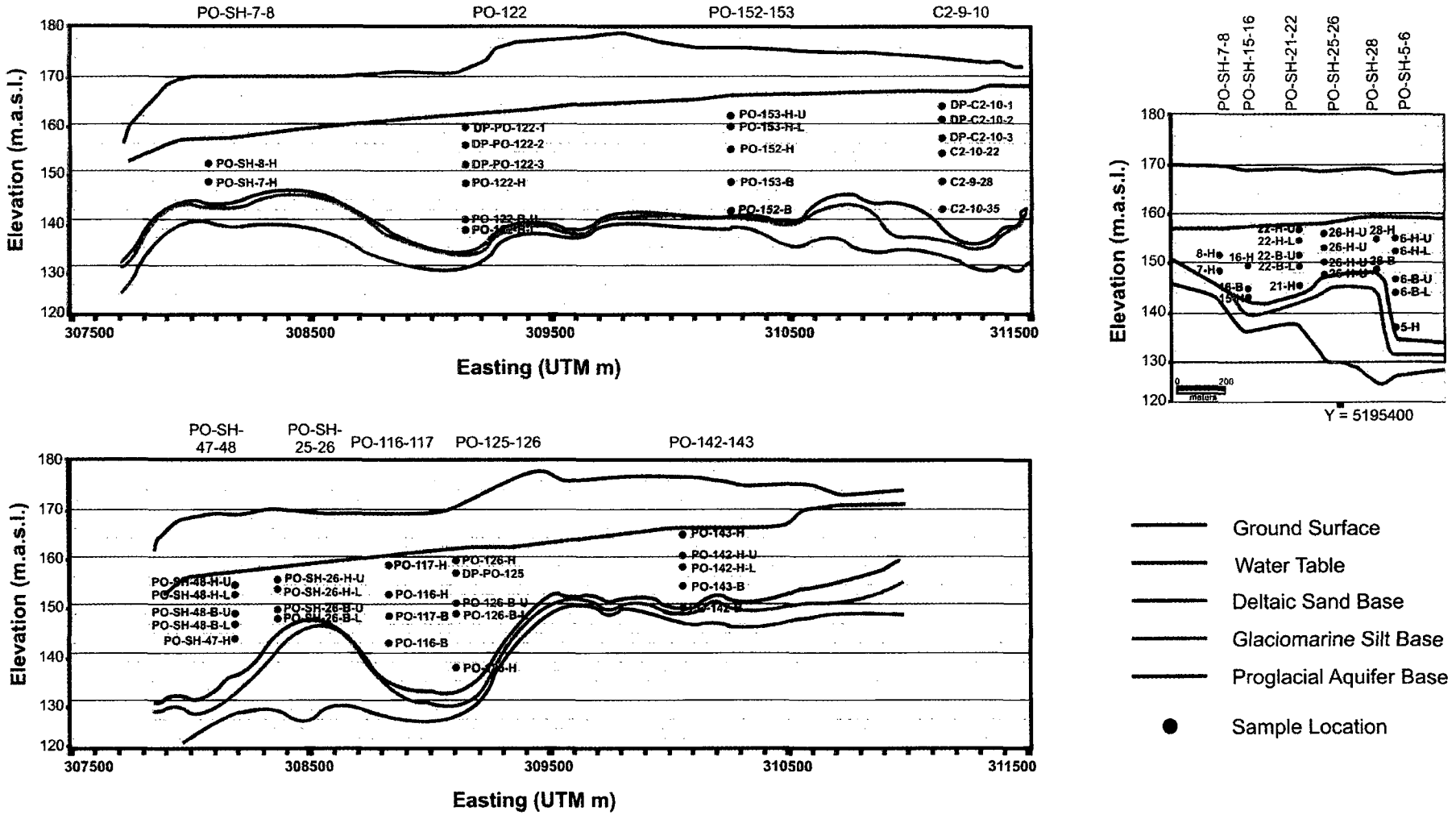


**Figure 3.2**. Cross sections of the North and South Flow Paths and the Shannon transect showing sampling locations in the deltaic sand aquifer.

## 3.3 $^{3}H$-$^{3}He$ Dating

### 3.3.1 Theory

Tritium ($^{3}H$) is a radioactive isotope of hydrogen that decays to $^{3}He$ via beta decay, with a half life of 12.32 years. It is created naturally in the atmosphere through spallation reactions from cosmic rays, and natural background levels range from 1-15 tritium units (TU, where 1 TU = 1 $^{3}H$ atom per $10^{18}$ H atoms), depending on global location. $^{3}H$ produced in the atmosphere is incorporated into the hydrological cycle when it is oxidized to water, and subsequently reaches Earth's surface as precipitation (Kipfer *et al.*, 2002).

Levels of atmospheric $^{3}H$ rose dramatically during thermo-nuclear weapons testing in the 1950's and 60's, with concentrations spiking two to three orders of magnitude above background levels. Changes in $^{3}H$ concentration in precipitation since the 1960's have been documented by the International Atomic Energy Agency and groundwaters around the globe show a pulse of very high $^{3}H$ levels corresponding to precipitation that recharged at that time (Figure 3.3). Early attempts to date groundwater sought to identify the peak $^{3}H$ concentration from 1963 to use as a reference point to estimate the time elapsed since recharge. However, this method is often complicated by dispersion of the high $^{3}H$ groundwater (Schlosser *et al.*, 1988; Solomon & Sudicky, 1991) and a dampened peak signal as $^{3}H$ decays to $^{3}He$. Local sources of $^{3}H$ production from either nuclear power generating stations or manufacturing facilities can overprint the bomb peak and make it difficult to identify (Solomon & Sudicky, 1991; Dunkle-Shapiro *et al.*, 1998). This method, therefore, provides only a qualitative estimation of groundwater age.

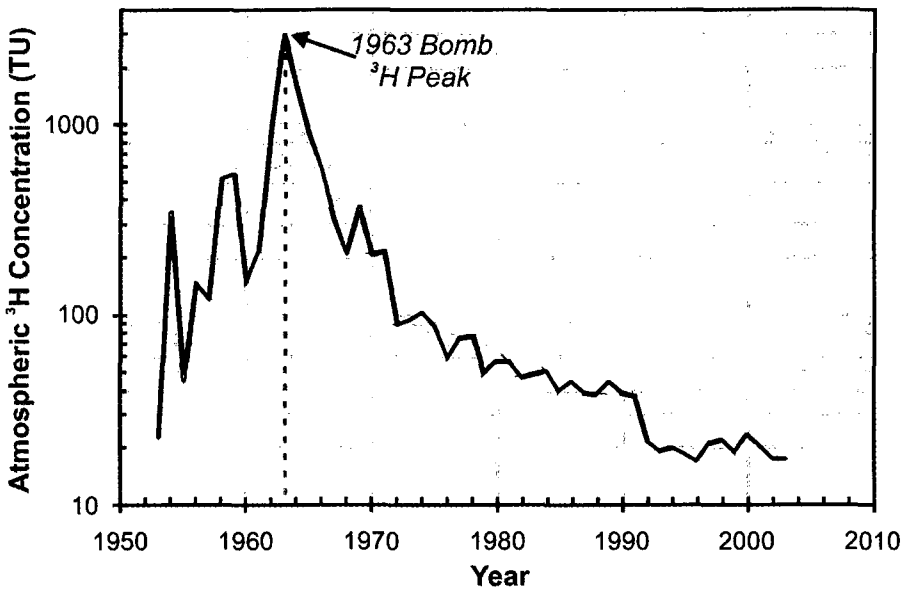


**Figure 3.3**. Graph showing tritium concentrations in precipitation in Ottawa from 1953-2004 (from IAEA/WMO, 2006). The maximum concentration of tritium occurred in 1963 is referred to as the Bomb Peak, and has been used in many in hydrogeological studies.

The $^3H/^3He$ dating method was first proposed by Tolsikhin and Kamenskiy (1969) but was not applied until the 1980's when advances in sampling and analytical techniques allowed the measurement of $^3H$ in lower concentrations as well as its decay product, $^3He$. If both parent and daughter concentrations are found, the age (in years) of the water can be calculated:

$$\mathbf{Age = t_{1/2}/ln2*(1 + {}^3He_{trit}/{}^3H)} \qquad 3.1$$

Where $t_{1/2}$ is the half life of $^3H$ (12.32 years) and $^3He_{trit}$ is the helium produced from the decay of $^3H$. This relation is based on the principle that as precipitation falls through the air and infiltrates the unsaturated zone, it equilibrates with the air so that $^3He$ generated from $^3H$ decay is able to escape to the atmosphere. Once the water reaches the saturated zone, it is effectively isolated from atmospheric gas exchange and acts as a closed system, so that $^3He$ builds up as $^3H$ decays and concentrations decline (Figure 3.4).

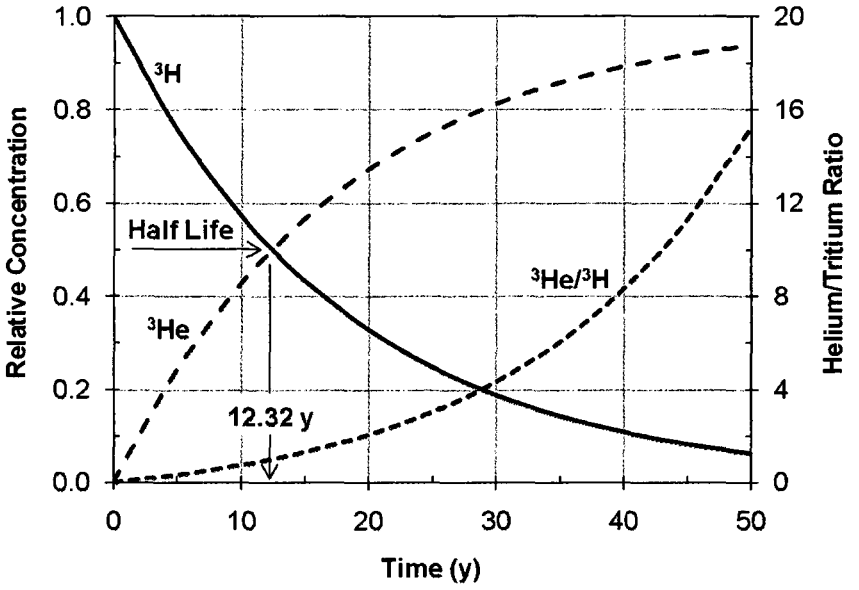


**Figure 3.4.** Graph showing changes in $^3$H and $^3$He concentration through time. Once $^3$H in precipitation reaches the water table, radioactive decay in groundwater leads to a $^3$He/$^3$H ratio that can be related to groundwater age (modified from Kipfer *et al.*, 2002).

Both $^3$H (incorporated into the water itself) and $^3$He (a noble gas) are geochemically non-reactive in the groundwater system; their conservative behavior prevents them from being affected by processes such as biodegradation or sorption, making them ideal tracer substances in groundwater studies. This method, unlike the $^3$H peak method, can be used independently of the knowledge of the $^3$H input function for a particular area, as the age is based on a ratio ($^3$He$_{tri}$/$^3$H) rather than absolute concentrations.

There are several assumptions made when dating groundwaters by the $^3$H/$^3$He method:

1) No mixing of groundwater from different recharge sources/times can occur. If two or more groundwaters have different $^3$He/$^3$H concentrations or ratios, then the resultant age of the mixed

waters will be biased towards the component of water with a higher initial concentration of $^3H$ (Kipfer *et al.*, 2002).

2) Dispersion is minimal. $^3H$ in the water molecules and dissolved $^3He$ are assumed to travel via advection only, at the same rate and direction of flow as the water parcel. If $^3H$ or $^3He$ diffuses into surrounding groundwater, the ages calculated for that point in the system may be incorrect.

3) Complete confinement of $^3He$ beneath the water table. Loss of $^3He$ across the water table into the atmosphere leads to younger computed ages for the groundwater that is dated. Although some $^3He_{trit}$ loss is inevitable very near to the water table, studies have shown that as long as vertical flow velocity in the recharge area is greater than 0.25 m/a, $^3He$ loss is negligible (Schlosser *et al.*, 1989; Solomon and Sudicky, 1991). However, $^3H/^3He$ ages are usually considered to be the minimum residence time.

### 3.3.2 Processing

Calculation of groundwater ages based on $^3H/^3He$ dating is complicated by the fact that groundwater contains dissolved $^3He$ from sources other than the decay of tritium in the water. The atmosphere is a natural reservoir for $^3He$, and some of this $^3He$ will dissolve into water (as precipitation and as infiltrating water in the unsaturated zone) as it equilibrates with the atmosphere. The amount of gas that dissolves into a liquid is proportional to their partial pressures in the gaseous phase (and is temperature dependent), according to Henry's Law:

$$\mathbf{K = C/P} \qquad 3.2$$

Where K (mol/(L*atm)) is Henry's constant whose value depends on temperature , P (atm) is the partial pressure of a gas in the atmosphere, and C (mol/L) is the concentration of dissolved gas in

aqueous form. If the recharge temperature is known, the amount of $^3He$ that has dissolved into the groundwater can be determined. Fortunately, the atmospherie maintains constant concentrations of $^3He$ and $^4He$; once the equilibrium concentrations of dissolved $^3He$ and $^4He$ are determined from Henry's Law, a characteristic equilibrium $^3He/^4He$ ratio in the groundwater can be used to separate the equilibrium component ($^3He_{eq}$) from the tritiogenic ($^3He_{tri}$).

Another source of $^3He$ in groundwater is excess air, which is the result of small air bubbles near the water table becoming entrained during recharge and dissolving as a result of increasing pressure. Although there have been several models proposed to explain this process (Heaton and Vogel, 1981; Stute *et al.*, 1995; Aeschback-Hertig *et al.*, 1998), the extent of $^3He/^4He$ fractionation between air bubbles and the groundwater is poorly understood. In any case, the $^3He/^4He$ ratio from excess air would be very close to that of the atmosphere, so it is assumed that the $^3He/^4He$ of excess air is the same as the $^3He/^4He$ of the atmosphere.

The amount of excess air can be determined by comparing it with the amount of another noble gas dissolved in the groundwater, neon (Ne). Ne is not generated in the subsurface, its only source being the atmosphere; thus Ne has only two components in groundwater, equilibrium ($Ne_{eq}$) and excess air ($Ne_{ex}$). This makes it possible to determine the solubility equilibrium concentrations (at a particular recharge temperature, according to Henry's Law) and compare those with the measured concentrations of Ne and He in groundwater (Appendix B). The amount of He and Ne in excess of air saturated water allows for the quantification of $^3He$ derived from excess air ($^3He_{ex}$).

Finally, $^3$He in groundwater may also have a terrigenic source. Primordial $^3$He diffuses to the surface slowly from the mantle, but this is usually negligible in shallow groundwater systems. Helium can also be generated from minerals in the aquifer or in underlying crustal rocks that contain radioactive isotopes, and diffuse into the groundwater. U and Th undergo alpha decay to produce $^4$He as well as a neutron flux that can produce $^3$He when Li is present according to the following reaction (Mamyrin and Tolstikhin, 1984):

$$^6\mathbf{Li} + \mathbf{n} \rightarrow \alpha + {}^3\mathbf{H};\ {}^3\mathbf{H} \rightarrow (\beta\text{-})\ {}^3\mathbf{He} \qquad 3.3$$

If the U, Th and Li content of surrounding rocks is well characterized then the $^3$He contribution from this source may be estimated from a characteristic $^3$He/$^4$He signature. The amount of terrigenic $^3$He ($^3$He$_{ter}$) depends on the geologic history of the study area; in some areas it may be unimportant, but in others it can constitute a proportion of the total $^3$He measured in the groundwaters large enough that it must be accounted for. The $^3$He$_{ter}$ concentration can be determined by using the characteristic $^3$He/$^4$He of the terrigenic source; estimates for different geologic settings can be found in the literature (Kipfer *et al.*, 2002).

The measured $^3$He in groundwater is therefore a combination of $^3$He from solubility equilibrium, excess air, radiogenic decay and decay of tritium in water molecules. Tritiogenic $^3$He in groundwater can be isolated from other $^3$He components by subtracting the concentrations of these components from the measured $^3$He :

$$\mathbf{^3He_{tri} = {}^3He_{meas} - {}^3He_{sol} - {}^3He_{ex} - {}^3He_{ter}} \qquad 3.4$$

Once the concentration of $^3$He$_{tri}$ in a groundwater sample is established, it can be used in Equation 3.1 with the corresponding $^3$H concentration to obtain a groundwater age. For a

description of how each component of $^3He$ in groundwater is determined, refer to Appendix B. A description of the quality check on $^3H$-$^3He$ data is outlined in Appendix C.

### 3.3.3 Consistency with Tritium Record

To evaluate the validity of $^3H$-$^3He$ data, the consistency of the results with tritium delivery to the groundwater system should be checked. The $^3H$ and $^3He_{tritiogenic}$ concentrations and groundwater ages can be used to reconstruct the concentration of $^3H$ in precipitation at the time of groundwater recharge. This method assumes that the sum of $^3H$ and $^3He_{tritiogenic}$ concentrations will equal the initial concentration of $^3H$ of the groundwater at the time of recharge:

$$^3H_{initial} = {}^3H_{present} + {}^3He_{tritiogenic} \quad 3.5$$

The recharge year is computed as:

$$\textbf{Year of Recharge} = \textbf{Year of Sampling} - {}^3\textbf{H}\text{-}{}^3\textbf{He Age (years)} \quad 3.6$$

Reconstructed $^3H$ estimates can be compared with historical concentrations of $^3H$ in precipitation, if such records are available. The nearest International Atomic Energy Agency station to Valcartier is Ottawa, Ontario, where $^3H$ levels have been measured since 1953 (Fig. 3.3). Valcartier is not close to nuclear power generating facilities or any known industry that emits $^3H$ to the atmosphere, so the Ottawa record can be considered a reliable basis for comparison with Valcartier $^3H$-$^3He$ age results.

### 3.3.4 Applicability

The $^{3}H$-$^{3}He$ dating technique was chosen for the Valcartier study because groundwater ages can serve as a calibration target for the numerical model, as well as provide estimates of hydrogeological properties of the system. It was initially chosen for its suitability in dating young groundwater in shallow aquifers, as circulation in the Valcartier deltaic aquifer is generally less than 50 years to depths of less than 50 m (Schlosser *et al.*, 1988; Schlosser *et al.*, 1989). The conservative behaviour of both $^{3}H$ and $^{3}He$ eliminates the need to account for retardation of the tracers; this would have been problematic in the prodeltaic silty aquitard in the eastern part of the study area which has TOC of 0.16% (Lefebvre *et al.*, 2003), which is known to retard TCE and could affect other environmental tracers such as chlorofluorocarbons (Reilly *et al.*, 1994; Cook & Solomon, 1997; Bauer *et al.*, 2001). The Valcartier deltaic aquifer is relatively homogeneous compared with other study areas where diffusive fractionation of $^{3}H$ and $^{3}He$ has been a problem, such as fractured rock aquifers or areas with large contrasts in hydraulic conductivity, so $^{3}H$-$^{3}He$ ages can be considered equivalent to advective ages (Aeschback-Hertig *et al.*, 1998; Dunkle-Shapiro *et al.*, 1998; Labolle *et al.*, 2006; Neumann *et al.*, 2008).

Another factor to be considered for $^{3}H$-$^{3}He$ dating is the ability to obtain spatially discrete groundwater samples. Ages obtained from wells with long screens or in areas near active (or recently active) production wells can contain a mix of groundwater spanning the vertical column. In this case a sample may contain groundwater with a range of ages and produce a $^{3}H$-$^{3}He$ age that will not necessarily reflect the true groundwater age, or even the mean groundwater age (Tompson *et al.*, 1999; Weissmann *et al.*, 2002; Zinn & Konikow, 2007). These problems are avoided during sampling of Valcartier groundwater due to strong horizontal gradients (which

maintain the age-stratification within the well), relatively short screened intervals, and the use of sampling equipment that minimizes disturbance to the water column.

The groundwater system being studied at Valcartier has both hydrogeological and logistical conditions that are conductive to obtaining reliable results from $^{3}H$-$^{3}He$ dating. A sampling program was designed to be able to use the $^{3}H$-$^{3}He$ ages to address the objectives of this project, as listed in Section 3.2.2.

## 3.4 Geochemical Characterization

### 3.4.1 Theory

Groundwater sampled at any point in the system contains information in its hydrogeochemical signature that, combined with other geologic and hydrologic data, may be used to interpret its origin and flow history. The spatial analysis and classification of groundwater based on its geochemical composition enables the interpretation of groundwater flow patterns (Freeze & Cherry, 1979; Stuyfzand, 1999). Conservative tracers do not significantly react with aquifer materials, and can be easily measured and examined to identify patterns as their concentrations align with the direction of groundwater flow (Glynn & Plummer, 2005). Constituents in groundwater that are subject to chemical reactions to varying degrees within the aquifer can also be used to characterize flow by the pattern of changes they undergo. The evolution of reactive solutes from recharge areas to downgradient locations can provide information on different types of lithology encountered, microbiological activity and hydrologic properties of the groundwater system (Tóth, 1999). The availability of geochemical tracers permits one to examine physical and chemical properties of a groundwater system and interpret its flow dynamics. Studies by

Fisher & Mullican (1997), Sracek & Hirata (2002) and Brenot *et al.* (2008) have all used geochemical tracing to characterize the hydrogeology of sites for a variety of purposes.

Stable isotopes of oxygen and hydrogen are another type of conservative tracer in groundwater. These isotopes constitute the water molecules themselves, and their relative abundance, measured in ratios ($^{18}O/^{16}O$ and $^{2}H/^{1}H$), provides important clues about groundwater recharge location. Fractionation between water molecules with heavy and light isotopes occurs during kinetic processes in the hydrologic cycle, leading to different isotopic compositions of vapour and water masses. Changes in the isotopic character of precipitation that recharges groundwater are due to temperature changes (season, altitude and latitude) and Rayleigh Distillation of the condensing air mass. The isotopic composition of groundwater can also be a product of secondary evaporation that can occur prior to entering the saturated zone. Such shifts in isotopic ratios are well understood, so even slight differences in the spatial and temporal origin and evolution of recharging groundwater will be reflected in its isotopic composition (Clark & Fritz, 1997). Information on recharge processes is inherent in the stable isotope composition of groundwater, so it can be used to estimate recharge location if conditions of the area are known. Many studies have used stable isotopes of water in combination with other geochemical parameters in many groundwater studies to examine recharge (Lee *et al.*, 1999), the impact of land use (Landon *et al.*, 2000), and distinguishing local and regional groundwater systems (Stimson *et al.*, 2001; Salem *et al.*, 2004; Cloutier *et al.*, 2006).

Multivariate statistical techniques can be done on groundwater samples using their geochemical composition to help classify groundwater into distinct groups, and can strengthen the interpretation of groundwater origin and migration. Principal components analysis is used to reduce the number of variables (geochemical parameters) to a lower dimension to make the data

easier to discriminate between groundwater groups. Hierarchical cluster analysis is another statistical method that compares samples based on their variables then groups them according to their similarity, producing a dendrogram that displays the relationship between samples (Davis, 2002). These techniques have been applied to geochemical data sets from a variety of groundwater studies (Steinhorst & William, 1985; Adar *et al.*, 1992; Melloul & Collin, 1992; Farnham *et al.*, 2000; Güler *et al.*, 2002; Cloutier *et al.*, 2008), and have generally led to an improved understanding of how hydrogeological processes influence groundwater geochemistry.

### 3.4.2 Applicability

The Valcartier groundwater system integrates recharge from the areas of suspected TCE release in downgradient areas, making it difficult to distinguish contributions from each source. Geochemical tracing can be used to distinguish inputs to the groundwater system to help refine the current understanding of TCE origin and migration in Valcartier, which is crucial to the development of mitigation and remediation strategies. The initial design of this study was to sample along groundwater flow paths stemming from source zones to facilitate the comparison of $^{3}H$-$^{3}He$ ages with ages derived from the numerical model. This approach is also amenable to examining groundwater chemistry and changes it undergoes as it moves through the saturated zone. It is particularly useful because of the nature of TCE release: each suspected source zone was a disposal site where many chemicals may have entered the water table at the same time and location as the TCE. Dissolved TCE at any point in the system is associated with a particular suite of other substances that share a history, so if the composition of groundwater at each suspected source zone can be established, there is a way to differentiate contributions from the source zones even when mixing has occurred.

An important aspect of this project is distinguishing theorigins of TCE found in Shannon at upgradient locations, and identifying migration pathways. Groundwater in the proglacial aquifer underlying the deltaic sand aquifer will also be examined in several areas (Fig. 2.2 and 3.1) to see if this unit plays a role in the transport of TCE into Shannon. Wells in Shannon that access groundwater in the deltaic unit in addition to those already chosen for $^{3}H$-$^{3}He$ dating were selected to generate a more detailed cross section of geochemical conditions in the aquifer perpendicular to groundwater flow. This will allow geochemical differences in Shannon to be examined in three dimensions, along with the NFP and SFP cross sections showing conditions parallel to flow.

# 4.0 Tritium-helium groundwater age used to constrain a groundwater flow model in a TCE-contaminated valley fill aquifer

## 4.1 Abstract

A numerical groundwater flow model was developed to better define dissolved TCE transport and guide the implementation of plume control systems in a deltaic sand aquifer. A geochemical characterization was carried out to further constrain the model with independent data, including tritium-helium ($^3H$-$^3He$) dating of groundwater, which is applicable for residence times under about 50 years. 58 discrete groundwater and dissolved gas samples were obtained along two parallel flow paths, respectively for $^3H$ and He/Ne analyses. Particle tracking with the numerical model was used to define these paths originating from two known TCE source zones whose related plumes converge to form a single plume with an overall length and width of about 4 500 m by 500 m. Sampling points in monitoring wells were projected on densely defined particle tracking vertical sections along the two flow paths. At these points, simulated advective ages obtained from particle tracking were matched to $^3H$-$^3He$ ages using porosity values between 0.30 and 0.45. A porosity of 0.35 corresponds best with the $^3H$-$^3He$ ages and agrees with soil moisture profiles obtained from a CPT/SMR cone penetrometer. $^3H$-$^3He$ ages were also obtained above and below a prodeltaic silty aquitard in the upgradient portion of the aquifer where some source zones are located. These ages provide groundwater and TCE transit times through the aquitard and a mean vertical hydraulic conductivity of the aquitard in agreement with previous estimates used in the numerical model. In certain locations, anomalously old $^3H$-$^3He$ ages with high terrigenic helium and a distinct geochemical signature indicate areas where groundwater from the underlying proglacial unit flows upward into the deltaic sand aquifer through aquitard windows. Upflow locations correspond with increased TCE concentrations, suggesting

significant TCE provenance through the proglacial unit originating from a previously unrecognized TCE source zone. The independent constraints offered by $^{3}H$-$^{3}He$ ages thus contributed to the development of a fully constrained numerical model providing representative predictions of groundwater velocities and transit times and using parameters supported by a variety of independent estimation methods.

## 4.2 Introduction

Contamination of aquifers is a common problem in the industrialized world, and often leads to the large-scale degradation of groundwater supplies. The effective mitigation and remediation of contamination at such sites relies on a firm understanding of hydrogeological conditions of the aquifer system, as well as knowledge of the contaminant origin and migration paths. Aquifer heterogeneity must also be assessed, as it controls flow and contaminant transport, and failure to consider heterogeneity may lead to inefficient contamination control and remediation (Marsily *et al.*, 2005). Although present-day numerical simulators have the capability to represent aquifer heterogeneity, conventional hydrogeological characterization techniques (hydraulic tests such as pumping tests or slug tests) are generally insufficient to define the spatial distribution of hydraulic conductivity, which must instead be inferred from indirect geological or geophysical information (Rubin and Hubbard, 2005).

A common limitation of numerical modeling also lies in conventional model calibration methods. Numerical models are often solely calibrated to observed hydraulic heads. However, even an adequate match does not provide a unique set of model parameters and boundary conditions, as other combinations could also have led to an adequate match, thus leaving much

uncertainty in parameters such as recharge and porosity (Konikow and Bredehoeft, 1992; Sheets *et al.*, 1998). Model predictions are thus uncertain as well, especially groundwater velocities and transit times, since steady state groundwater flow models are independent of porosity that exerts a strong influence on velocity. When model predictions are to be used to design contamination control or remediation methods, it becomes critical to constrain models with more independent data, other than hydraulic heads.

In order to develop a representative numerical model, it is thus crucial to have first a realistic conceptual model of contaminant migration in the aquifer system, then define a representative distribution of heterogeneous hydraulic conductivity, and finally to constrain the numerical model to a variety of independent data that can lead to a more unique and validated set of model parameters. Such independent data can be provided by the groundwater geochemistry, including geochemical tracers allowing the estimation of groundwater age (Clark and Fritz, 1997; Abbott *et al.*, 2000; Bassett *et al.*, 2008; Clark *et al.*, 1998; Koh *et al.*, 2006; Moore *et al.*, 2006).

The age of groundwater at any point in the saturated zone is a function of its velocity through the aquifer, which depends on the characteristics of the aquifer and on its recharge. Multiple groundwater age measurements made throughout an aquifer can provide a means of validating aquifer properties used in numerical models. Tritium-helium ($^3$H-$^3$He) dating is a method of estimating the time elapsed since groundwater recharge, and is referred to as groundwater "age". Among geochemical tracers, $^3$H-$^3$He dating is particularly well suited to young (less than 50 years), shallow groundwater systems, and can produce unambiguous residence times of groundwater (Solomon *et al.*, 1993). Both $^3$H (incorporated into the water itself) and $^3$He (a noble gas) are geochemically non-reactive in the groundwater system; their conservative behaviour prevents them from being affected by processes such as biodegradation or sorption, making them

ideal tracer substances in groundwater studies. The $^3H$-$^3He$ dating method was proposed by Tolsikhin and Kamenskiy (1969). This method, unlike the $^3H$ peak method, can be used independently of the knowledge of the $^3H$ input function for a particular area, as the age is based on a ratio ($^3He_{tri}/^3H$) rather than absolute concentration. However, this method was not applied to groundwater studies until sometime after it was proposed, awaiting advances in the past couple of decades in sampling and analytical techniques facilitating the application of $^3H$-$^3He$ dating.

The $^3H$-$^3He$ dating technique has been applied to establish age gradients in groundwater that are used to calculate recharge rates and groundwater velocities (Solomon and Sudicky, 1991; Solomon *et al.*, 1992; Ekwurzel *et al.*, 1994; Reilly *et al.*, 1994; Cook *et al.*, 1996; Dunkle-Shapiro *et al.*, 1998; Beyerle *et al.*, 1999). Many studies have used $^3H$-$^3He$ dating to validate numerical groundwater models by using the ages as a calibration target, adjusting model parameters and boundary conditions to match the ages and improve model validity (Solomon *et al.*, 1992; Ekwurzel *et al.*, 1994; Szabo *et al.*, 1996; Sheets *et al.*, 1998; Portniaguine and Solomon, 1998; Tompson *et al.*, 1999). At sites with contaminated groundwater, investigators have determined $^3H$-$^3He$ ages at points along a contaminant plume to understand the timing of contaminant release to the subsurface and its migration rates (Solomon *et al.*, 1995; Bohlke and Denver, 1995; Dunkle-Shapiro *et al.*, 1999; Moore *et al.*, 2006). $^3H$-$^3He$ groundwater ages are thus a valuable measurement that can be used to infer the properties of an aquifer system independently of physical measurements such as hydraulic head.

This paper reports on the uses of $^3H$-$^3He$ ages as part of an integrated study aiming to better represent groundwater flow and contaminant transport in a complex aquifer system where multiple TCE source zones are present. Since the numerical model of groundwater flow in this system must support environmental management decisions, its predictions must be reliable. For

that purpose, a practical approach was developed to 1) define the aquifer heterogeneity, 2) integrate this information on heterogeneity in a groundwater flow numerical model and 3) calibrate and validate the numerical model with various independent data in order to fully constrain the model, including with geochemical tracers and $^{3}H$-$^{3}He$ ages. Figure 4.1 illustrates the overall approach used to develop and validate the numerical model of groundwater flow. Ouellon *et al.* (2008a) used the data provided by the physical characterization of the aquifer both to develop a numerical model representative of geological conditions and to define aquifer heterogeneity. The numerical model development thus explicitly integrates the constraints of the geological context, including aquifer heterogeneity. In order to fully constrain the numerical model as part of the calibration and validation process, independent hydraulic and geochemical data were used. Hydraulic constraints are briefly described in Section 3. The use of geochemical tracers to better define groundwater origins and flow paths is presented by Murphy *et al.* (2009). This paper emphasizes the application of $^{3}H$-$^{3}He$ groundwater ages as part of the geochemical constraints used in the model calibration and validation process.

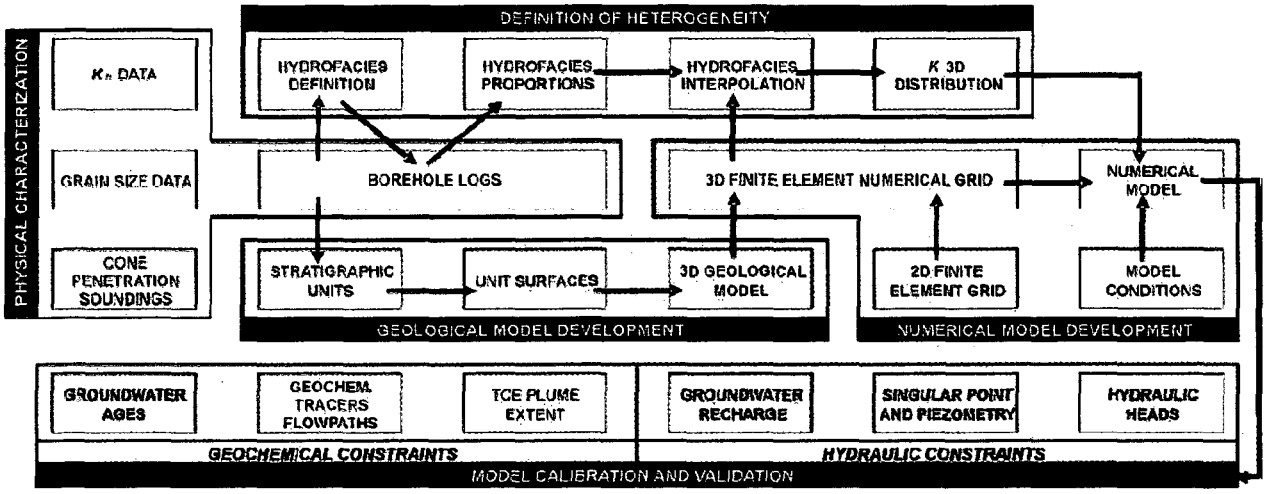


**Figure 4.1**. Approach used to develop and validate the numerical model of groundwater flow (modified from Ouellon *et al.*, 2008a). The present paper emphasizes the application of groundwater ages as part of geochemical constraints used in the model calibration and validation process. Hydraulic constraints are also briefly described.

## 4.3 Hydrogeological Context

Figure 4.2 shows the Valcartier sector, which is located 25 km from central Quebec City. The land surface is relatively flat in the central area and it is bordered by two mounts, to the south and to the east. The Jacques-Cartier and Nelson Rivers are found, respectively, to the west and east of the sector. This land is used mainly by the Ministry of National Defence (Valcartier Garrison and research facilities of DRDC-Valcartier) and a former industrial site (SIVI). In the underlying deltaic aquifer, a trichloroethylene (TCE) plume extends over a length of 4.5 km by a width of about 500 m, with concentrations mostly between 5 and a few hundred μg/L with local highs above 590 μg/L, mostly near source zones. Known source zones include locations on property belonging to DRDC North and SIVI's Sector 214 and Lagoon C (Lefebvre *et al.*, 2003). Groundwater flow conditions are such that TCE contributions from each source zone eventually combine to form a single large plume within which the origin of TCE is difficult to discriminate.

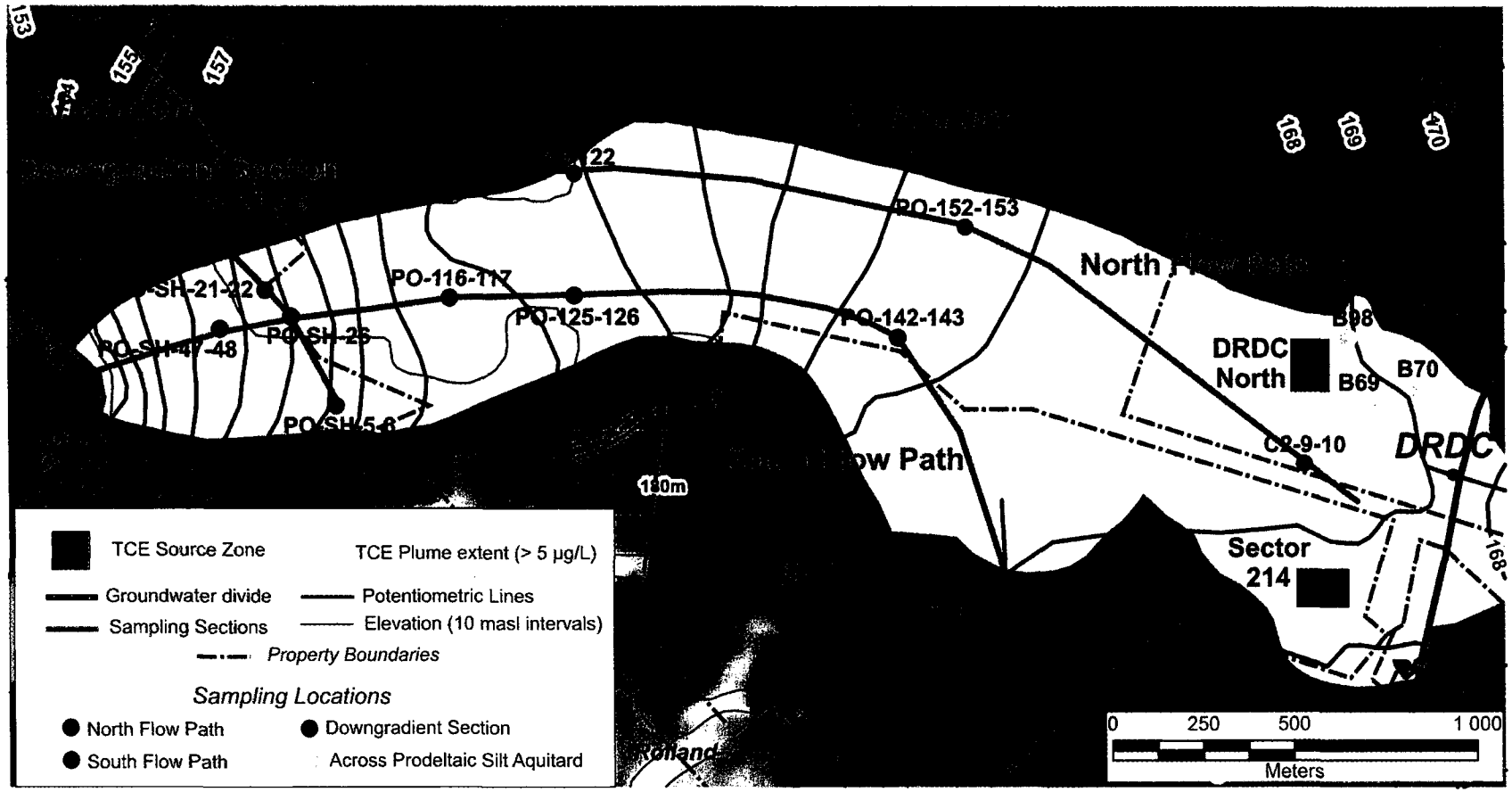


**Figure 4.2**. Location and physiography of study area. The overall extent of the TCE plume with concentrations above 5 µg/L in the deltaic aquifer is shown, as well as sampling locations along simulated flow paths originating from known source zones. The extent of the numerical model is also shown.

Figure 4.3 shows that although the land surface is relatively flat in the study area, it is overlying a buried valley filled by up to 50 m of sediments present in the central part of the Valcartier sector, extending from east to west. Figure 4.3 shows a perspective view of hydrostratigraphic units found above bedrock. Deltaic sediments are mainly formed of sand and gravel but an interlayered prodeltaic silty aquitard forms a wedge in the eastern part of the sector. A semi-confined aquifer made up of proglacial sediment (poorly sorted sand and gravel) is separated from deltaic sediments by a locally discontinuous glaciomarine silt aquitard. Although aquifer units are laterally continuous, the two silty aquitards are discontinuous, thus changing hydrogeological conditions found from west to east in the aquifer units. In the western and central parts of the sector, the prodeltaic silt aquitard is absent, so that the entire thickness of deltaic sediments constitutes what is referred to as the "regional deltaic unconfined aquifer". In the eastern part of the Valcartier sector, the pro-deltaic silt aquitard splits the deltaic sands in two, which results in two deltaic aquifers, the "upper deltaic unconfined aquifer" and the "semi-confined deltaic aquifer".

Figure 4.2 shows the potentiometric surface of the regional deltaic sand aquifer, which is semi-confined under the prodeltaic silty aquitard in the eastern part of the study area. Groundwater generally flows westward in the study area, except in the south where recharge from Mount Rolland-Auger causes groundwater to flow northward. In general, groundwater moves slower in the east (on the order of 10 m/y) and more rapidly downgradient in the west and on the flanks of the mountains where the hydraulic gradient is high (10-100 m/y). Vertical hydraulic gradients are very low in most of the study area so flow is predominantly horizontal, except near the groundwater divide where recharging groundwater has a greater vertical component. Vertical

groundwater flow also occurs across the prodeltaic silty aquitard from the upper to the lower deltaic sand, where there is a gradient of 0.1-0.3 (Lefebvre *et al.*, 2003).

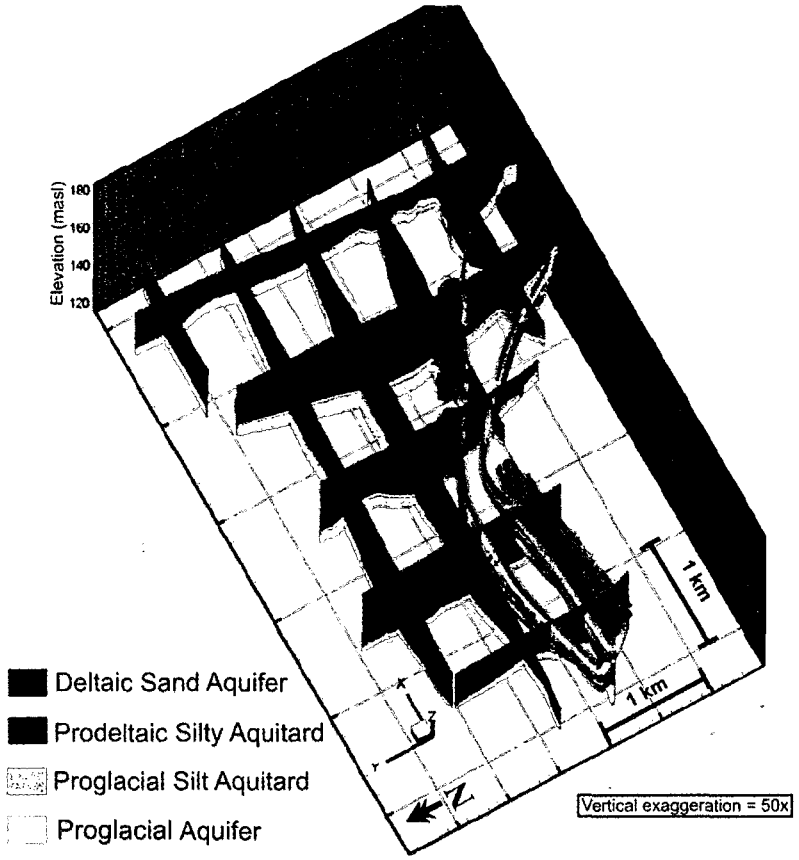


**Figure 4.3.** Hydrostratigraphy and locations of particle tracking flow paths. The view is from the northwest towards the southeast.

Most of the dissolved TCE is found within the deltaic aquifer, which was the focus of the $^{3}H$-$^{3}He$ groundwater dating program. At the eastern source zones, most TCE emissions occurred above the prodeltaic silt aquitard and TCE migrated downward through the aquitard, due to a strong vertical hydraulic gradient, prior to emerging under the aquitard. TCE then migrated mostly westward along the flow paths prevailing in the regional deltaic aquifer. Some of the TCE was emitted beyond the edge of the silt aquitard and therefore migrated directly into the regional

deltaic aquifer. The two simulated particle tracks originating from the main TCE source zones are shown on Figures 4.2 and 4.3. These traces are referred to as the North Flow Path (NFP) and South Flow Path (SFP), originating respectively from source zones DRDC North and Sector 214 (NFP) and Lagoon C (SFP) (see also Figure 4.5).

Following numerous hydrogeological characterization programs carried out across the Valcartier sector, an important data set has been accumulated (Table 4.1). All available borehole logs have used a standardized and coded geological facies (Parent *et al.,* 2008), which facilitate comparison and processing of geological information. In the past few years, cone penetration tests (CPT) combined with soil moisture resistivity (SMR) have been used to recognize hydrofacies and complement stratigraphic information where borehole logs are sparse (Fauveau, 2006; Fauveau *et al.*, 2005; Ouellon *et al.*, 2008a, b). CPT soundings with SMR also allow the measurement of volumetric water content, which is equivalent to porosity in the saturated zone (Shinn *et al.,* 1998). In the Valcartier sector, most boreholes are used to install two observation wells and many locations have two boreholes drilled side by side (total of 4 observation wells). This approach, combined with relatively long screens (about 4 m), was used to cover the entire saturated thickness and maximize the possibility to detect TCE. Nearly 1000 screened intervals thus allow measurement of water levels and groundwater sampling.

Since 2001, direct push groundwater sampling has been used in the Valcartier sector to delineate the TCE plume prior to drilling and installation of observation wells (Lefebvre *et al.*, 2003, 2004). Numerous TCE concentrations were obtained from such samplings. Most observation wells have also been repeatedly sampled, either to verify initial results or as part of a continuous TCE monitoring program. Slug tests have been carried out in almost all wells installed since

2001, thus providing 435 measurements of hydraulic conductivity (Ouellon *et al.*, 2008a). Besides the data listed in Table 4.1, other information is also available in the Valcartier sector.

**Table 4.1**. Available data in the Valcartier sector.

| **Stratigraphy** (locations / total length, m) | |
|---|---|
| Borehole logs | 394 / 9580 |
| CPT soundings | 28 / 365 |
| **Observation wells** (≈2 per borehole) | |
| Screened intervals | 991 |
| **Water samples** (including repeats) | |
| Well sampling | > 2350 |
| Direct push sampling | 1460 |
| **Hydraulic conductivity** | |
| Slug tests | 435 |

More than 260 grain size analyses are available on all sediments present in the sector (Ouellon *et al.*, 2008a, b). Two well hydrographs were recorded for a period of two years and correlated to a hydrograph that is being recorded for more than 10 years in the adjacent Pont-Rouge area in a similar deltaic aquifer also deposited by the Jacques-Cartier River. These records were used to estimate groundwater recharge (Maltais, 2006; Lefebvre *et al.*, 2009).

Physical parameters relevant for the interpretation of the groundwater dating program are compiled in Table 4.2. These parameters were obtained from previous work on the Valcartier aquifer system (Ouellon *et al.*, 2008a, b, c; Lefebvre *et al.*, 2003, 2004; Boutin *et al.*, 2004). Well hydrographs are suitable for the estimation of recharge in the context of the Valcartier and Portneuf aquifers (Scanlon *et al.*, 2002; Healy and Cook, 2002). A promising approach

combining daily soil water balance based on weather data and well hydrographs (Baalousha, 2005) was applied in Portneuf (Maltais, 2006; Lefebvre *et al.*, 2009). The Pont-Rouge location in Portneuf is a very good analog to Valcartier as it is located a few kilometres down the Jacques-Cartier River within a similar deltaic aquifer and has similar weather conditions (Fagnan *et al.*, 1999; Paradis *et al.*, 2007).

**Table 4.2**. Estimated physical parameters of the Valcartier deltaic aquifer.

| Parameter | Symbol | Value | Unit | Method (reference) |
|---|---|---|---|---|
| ***Deltaic Sand - Valcartier Sector*** | | | | |
| Total porosity | $n_t$ | 0.40 | - | Column tests (Lefebvre *et al.*, 2003) |
| Total porosity | $n_t$ | 0.38 | - | CPT/SMR (Fauveau, 2006; Fauveau *et al.* 2005; this study) |
| Drainage porosity (*Specific yield*) | $n_d$ | 0.22 | - | Column tests (Lefebvre *et al.*, 2003) |
| Drainage porosity (*Specific yield*) | $n_d$ | 0.23 | - | CPT/SMR (Fauveau, 2006; Fauveau *et al.* 2005; this study) |
| Horizontal hydraulic conductivity | $K_h$ | $3x10^{-5}$ to $1x10^{-3}$ | m/s | Slug tests and hydrofacies (Ouellon *et al.*, 2008a) |
| Retardation factor | $R_f$ | 1.0 | - | Column tests (Lefebvre *et al.*, 2003) |
| Groundwater recharge | $R$ | 376 and 491 | mm/y | Well hydrographs (Lefebvre et al., 2003) |
| Groundwater recharge | $R$ | 300 | mm/y | Numerical modeling (Ouellon *et al.*, 2008 a,b,c) |
| ***Prodeltaic Silt - Valcartier Sector*** | | | | |
| Total porosity | $n_t$ | 0.36 | - | Column tests (Lefebvre *et al.*, 2003) |
| Vertical hydraulic conductivity | $K_v$ | $3x10^{-8}$ to $3x10^{-9}$ | m/s | Hydrofacies and modeling (Ouellon *et al.*, 2008a, b, c) |
| Retardation factor | $R_f$ | 1.7 | - | Column tests (Lefebvre *et al.*, 2003) |

## 4.4 Numerical Model

As mentioned in the introduction, Figure 4.1 outlines the process followed to develop the numerical model by Ouellon *et al.* (2008a, b). Deltaic sediments form the major aquifers in the

Valcartier sector and they contain most of the TCE contamination. An effort was thus made to define the heterogeneity of deltaic sediments and the spatial distribution of hydraulic conductivity in this unit, as it controls groundwater flow and TCE transport (Ouellon *et al.*, 2008a). Heterogeneity is defined by the distribution of both hydrofacies and hydraulic conductivity ($K$). Hydrofacies are defined as lithologic facies with distinctive hydraulic conductivity ranges. Four site-specific deltaic hydrofacies were defined on the basis of lithologic descriptions used in borehole logs, supported by grain size analyses, slug tests and CPT mechanical response (Figure 4.1). Each hydrofacies includes a group of geologic facies found in borehole log descriptors. The spatial distribution of hydrofacies was first interpolated directly on the 3D grid of the numerical model. Finally, the proportions of hydrofacies were used to estimate horizontal $K_h$ and vertical $K_v$ components of $K$ using generalized means for layered media.

Figure 4.4 shows the 2D triangular finite element grid developed in Feflow (WASY, 2005) for the numerical model. The grid was refined both where high hydraulic gradients were expected, such as around production wells, and within the known TCE plume. Grid elements vary in side length between 15 and 50 m. To the south and east, the model extends to the base of mounts where imposed heads are applied on proglacial aquifer nodes to represent groundwater inflow in this unit from the adjacent highlands (red lines). The Jacques-Cartier River borders the model to the west and is represented by imposed heads on the upper three model layers (blue line). Heads were imposed only on the top layer for the smaller Nelson River present within the eastern limit of the model (blue line). The northern limit was set as a zero flux boundary as it is a streamline whose location was based on the potentiometric map (white line – Figure 4.2). A recharge of 300 mm/y was imposed evenly on the top nodes of the model. This is similar to the recharge obtained from the interpretation of a 10-year well hydrograph in Pont-Rouge, which is located to the west

of Valcartier in a deltaic aquifer also related to the Jacques-Cartier River and where weather conditions are analogous (Maltais, 2006; Lefebvre *et al.*, 2009). Short 2-year hydrographs available for two wells in the Valcartier sector match the hydrograph of Pont-Rouge. The two garrison wells P4 and P7 had their respective flow rates, 360 and 2020 $m^3/d$, imposed over nodes corresponding to their screened interval (Figure 4.2).

Figure 4.4 (lower left) also shows a west to east vertical section through the 3D numerical grid and the distribution of layers. Six guiding layers were first defined on the basis of the 3D geological model (numbers shown on Figure 4.4): 1) bedrock surface, 2) proglacial aquifer surface, 3) glaciomarine silt surface, 4) the base and 5) top surfaces of the prodeltaic silty aquitard, and 6) the water table surface. Since the silty prodeltaic aquitard is discontinuous, where this unit is absent its base and top were positioned respectively in the upper and lower third of deltaic sediments. Then, 23 layers of nodes were added, for a total of 29 layers of nodes: 21 in deltaic sediments, 3 in the glaciomarine silt, and 5 in proglacial aquifer. The grid has 1 249 640 elements and 655 893 nodes. In the eastern part of the model, the top 5 layers represent the upper deltaic unconfined aquifer. These layers use the adaptative grid option of Feflow, which allows these layers to remain fully saturated as they expand or contract, according to changes in the simulated water table surface elevation compared to its initial elevation.

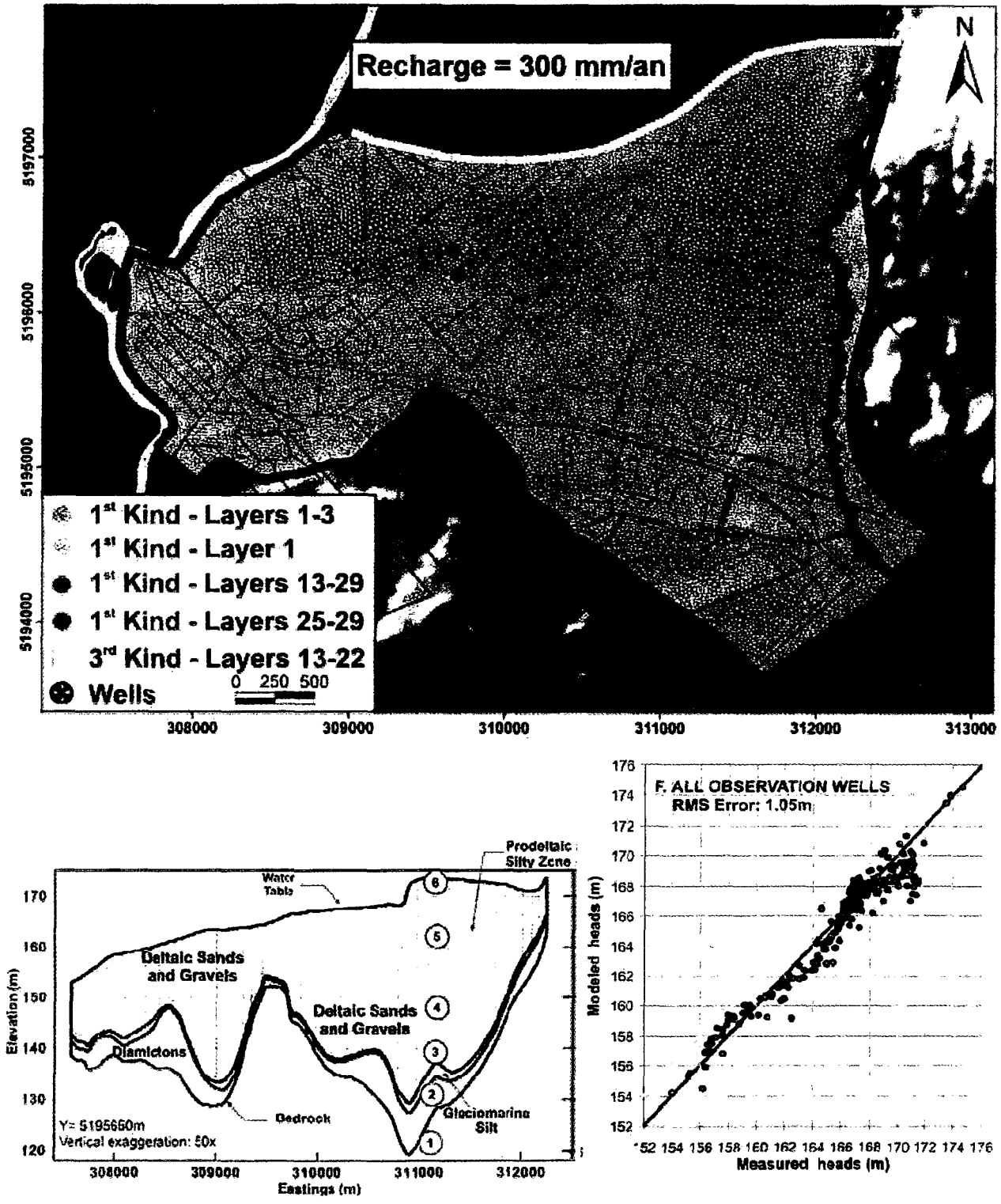


**Figure 4.4**. Numerical model: grid and boundary conditions (top), layers following the hydrostratigraphy (lower left), and comparison of measured and simulated hydraulic heads (lower right – unconfined heads are shown in blue and semi-confined heads in green).

Figure 4.4 (lower right) shows simulated and measured hydraulic heads, which were matched for each hydrogeological context and unit of the Valcartier sector. Given that the overall variation in heads is about 25 m in the system, a calibration target of 2.5 m (10%) was set. Most heads match within 2 m of observations, without any systematic bias, the overall median and RMS errors are respectively -0.005 and 1.05 m. These matches were obtained simply by small changes in boundary conditions. The initially imposed recharge and the 3D heterogeneous $K$ field derived by Ouellon *et al.* (2008a, b) did not require any change to obtain a satisfying match. An earlier model with a zoned distribution of $K$ could not reach such a satisfying match (Boutin *et al.*, 2004). The match obtained, without requiring changes in the estimated $K$ field or recharge, provides an indirect validation of these estimates. As indicated on Figure 4.1, besides aiming to match heads, model validation also aimed to reproduce the overall directions of groundwater flow, as indicated by potentiometric maps in unconfined and confined aquifers. The model especially had to match locations of groundwater divides and "singular points" (Figure 4.2). These points correspond to locations in the eastern part of the sector where groundwater converges from north and south and then diverges to the east and west. Locations of these points influence flow directions, especially TCE migration paths from source zones.

Groundwater flow paths are also indicated by the morphology of the TCE plume itself, whose extent was reproduced both by particle tracking and mass transport originating from known source zones (Ouellon *et al.,* 2008b). A detailed geochemical tracer study also distinguished water types from the multivariate interpretation of concentrations in major ions and stable isotopes (Chapter 5). The study showed that the spatial distribution of distinguished water types is coherent with the general flow directions obtained from the numerical model.

The constraints provided by hydraulic and geochemical data used in the model calibration and validation process provide confidence that the model represents groundwater flow conditions with a valid set of parameters. However, these steps are not sufficient to validate the prediction made by the model about groundwater velocities and transit time, which should depend in large part on porosity and recharge (Chesnaux *et al.*, 2005). Recharge could be further validated, and a mean value of porosity that would provide representative velocity estimates also needs to be determined. The $^{3}H$-$^{3}He$ groundwater age characterization program described in the next section was designed to provide an independent parameter that could be used to validate model predictions about transit time and velocity, as described later in Section 5.

For the geochemical study, the sampling program design and interpretation of results were integrated with numerical modeling, following two flow paths obtained from particle tracking (Figures 4.2 and 4.3). Such an approach assures that geochemical results are hydraulically meaningful, and has the added benefit of reducing the number of samples required to draw definitive conclusions. In order to fully characterize groundwater flow along these two main flow paths, detailed particle tracking was carried out by releasing closely-spaced particles at the top of the water table over the entire lengths of the two flow paths. Figure 4.3 shows a perspective view of particle tracking and Figure 4.5 shows vertical section views of particle tracking results. The particle tracking flow paths originate either near a groundwater divide (North Flow Path) or at the edge of the deltaic sediments at the border of the buried valley (South Flow Path). Both flow paths end at the Jacques-Cartier River, at their western end, where flow paths emerge in the river. The origin of a particle track corresponds to the water table, whose elevation decreases from east to west. Horizontal hydraulic gradients increase along flow paths, which is typical of unconfined aquifers. Besides indicating the paths of flow, particle tracking can also be used to

determine the advective time required for groundwater to flow from the point of origin to any location on the particle track, for a specified model porosity of the aquifer material.

Figure 4.5 shows that groundwater flow is mostly vertically downward at the origin of the flow paths (especially for the North Flow Path), due to the very slow horizontal velocity and the effect of the vertical stacking of groundwater recharge, which dominates over horizontal flow. Particle tracks get more and more horizontal going west, as groundwater velocity increases due to the cumulative effect of groundwater recharging the aquifer along flow lines. This recharge also causes the plunging of particle tracks, which get deeper within the saturated zone going west. Particle tracks also show the strong effect of variations in the deltaic aquifer base elevation and changes in saturated thickness along flow lines (especially on the South Flow Path). Tracks vary in elevation, and follow the ups and downs of the aquifer base topography. Tracks are squeezed together where the total saturated thickness decreases, and move apart where it increases, which has implications on mass dispersion. Tracks do not reach the aquifer base, due to groundwater inflow from upgradient of the flow path origins. This is more important on the South Flow Path, which receives a higher proportion of its groundwater from upgradient on Mount Rolland-Auger than the North Flow Path.

Figure 4.5 also shows color scales of simulated groundwater ages along particle tracks that were calculated by the simulator using a porosity of 0.35; particle tracking was also carried out for porosities of 0.30, 0.40 and 0.45. The particle tracking advective ages for the different porosities are compared to isotopic ages in Section 5 (Figures 4.7 and 4.8). On Figure 4.5, ages are shown using 5-year intervals which become thinner from east to west, indicating a progressive increase in velocity. Velocities are especially high close to the Jacques-Cartier River. Age patterns are quite different on the two sections: only the upper portion of the saturated section has ages less

than 20 years in the North Flow Path, whereas the South Flow Path has less than 20 years over most of the particle tracks.

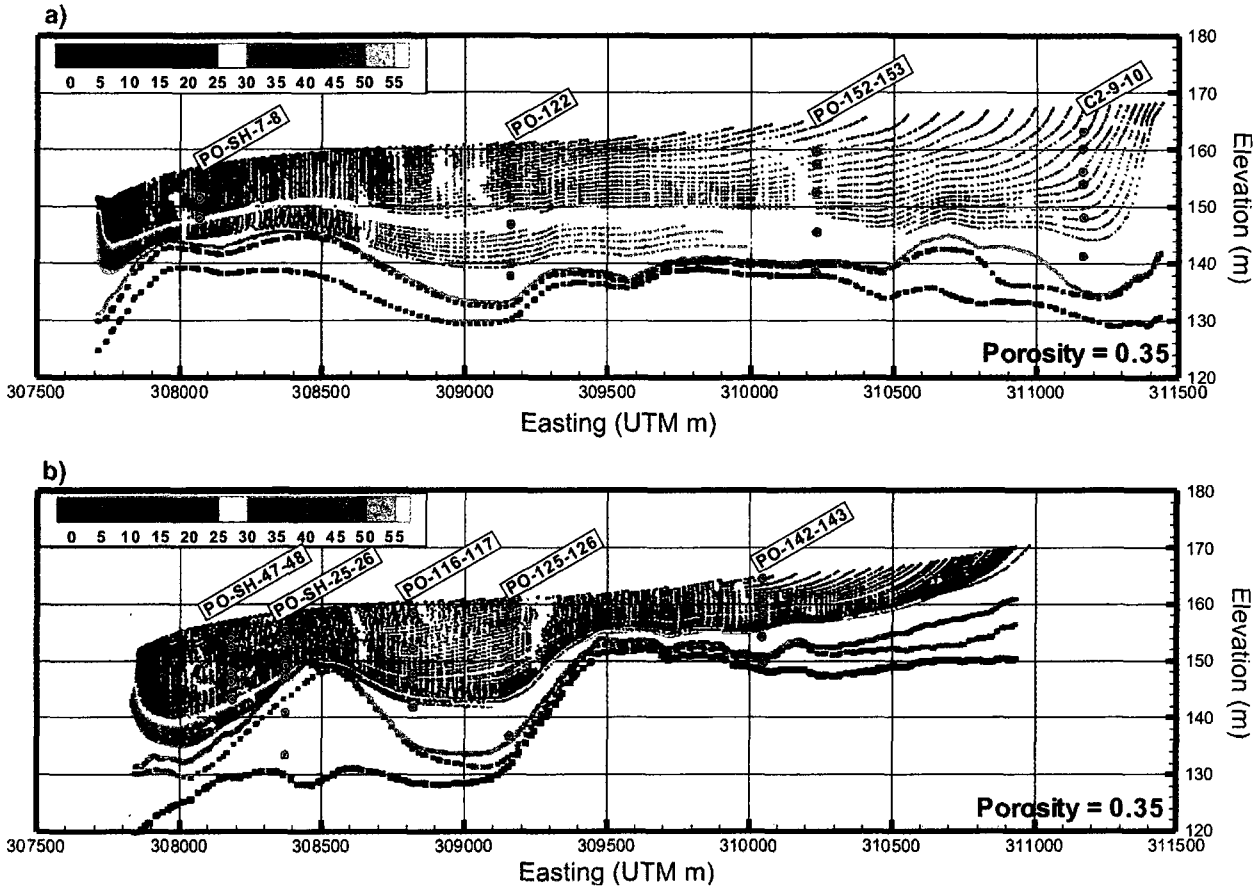


**Figure 4.5**. Detailed particle tracking along the a) North Flow Path and b) South Flow Path from closely spaced particles released at the water table along the two flow paths. The lines underlying particle tracks represent limits of units in the model: at bottom the base of the model (top of bedrock), then the proglacial aquifer top and the glaciomarine silt aquitard top. The color scale indicates advective ages obtained with a model porosity of 0.35. Groundwater sampling points at which $^{3}H$-$^{3}He$ groundwater ages were obtained were projected on the particle tracking sections.

## 4.5 $^3$H-$^3$He Dating Methodology

### 4.5.1 $^3$H-$^3$He Dating Principles

The $^3$H-$^3$He dating technique, first proposed by Tolsikhin and Kamenskiy (1969), is used to determine the residence times of groundwater in shallow aquifer systems. $^3$H decays to $^3$He, with a half-life of 12.32 years; if measurements can be obtained of both $^3$H in water molecules and tritiogenic $^3$He, the age of the groundwater can be determined. Many authors have addressed the theory and reliability of the technique and have outlined the steps to calculate $^3$H-$^3$He ages (Schlosser *et al.*, 1988; Schlosser *et al.*, 1989; Solomon and Sudicky, 1991; Reilly *et al.*, 1994; Solomon *et al.*, 1995; Labolle *et al.*, 2006). The important aspects of the technique are that $^3$H and $^3$He are conservative tracers, and the age obtained represents the groundwater transit time since entering the saturated zone.

Many hydrogeological studies have used $^3$H-$^3$He dating in a variety of applications. Groundwater recharge and velocities can be estimated using $^3$H-$^3$He ages along groundwater flow paths; the change in age with distance establishes a gradient that can be used to estimate the rate of groundwater movement (Solomon and Sudicky, 1991; Solomon *et al.*, 1992; Ekwurzel *et al.*, 1994; Reilly *et al.*, 1994; Dunkle-Shapiro *et al.*, 1998; Beyerle *et al.*, 1999; Price *et al.*, 2003; Moore *et al.*, 2006). This application of $^3$H-$^3$He ages as a method of estimating aquifer parameters has also been used to improve numerical groundwater models. The ages can be used as a calibration target by which to adjust model parameters such as recharge, hydraulic conductivity and porosity (Solomon *et al.*, 1992; Reilly *et al.*, 1994; Szabo *et al.*, 1996; Portniaguine and Solomon, 1998; Sheets *et al.*, 1998; Dunkle-Shapiro *et al.*, 1998; Zoellmann *et al.*, 2001). $^3$H-$^3$He ages are particularly valuable at sites with contaminated groundwater, as ages found in different parts of the contaminant plume can be related to the timing of its release and

migration (Solomon *et al.*, 1995; Bohlke and Denver, 1995; Dunkle-Shapiro *et al.*, 1999; Moore *et al.*, 2006).

The $^{3}H$-$^{3}He$ method is well suited for the Valcartier groundwater system. The unconsolidated sand aquifer is relatively homogenous, and groundwater recharge and velocities are sufficiently high so that differential diffusion of $^{3}He$ is not a concern, and $^{3}H$-$^{3}He$ ages can be considered equal to advective ages (Schlosser *et al.*, 1989; Labolle *et al.*, 2006). The record of $^{3}H$ in precipitation for Ottawa can be directly compared with Valcartier data as a consistency check on $^{3}H$-$^{3}He$ ages (Dunkle-Shapiro *et al.*, 1998). Ottawa is the nearest IAEA monitoring station to Valcartier (450 km away), and neither location is close enough to any nuclear facilities that would drastically change the $^{3}H$ profile in precipitation, so the Ottawa record is a reliable way to confirm the validity of $^{3}H$-$^{3}He$ ages. The availability of many wells at Valcartier (Table 4.1) provides the flexibility of selecting wells along flow paths and in other key areas to accommodate the goals of the study. Finally, the use of hydrosleeve water samplers (ITRC, 2006 and 2007) and gas diffusion samplers (Sanford *et al.*, 1996; Manning *et al.*, 2003) provides an efficient and reliable means of collecting spatially discrete samples for $^{3}H$ and $^{3}He$ analysis.

### 4.5.2 Sampling Design

The sampling program was designed to facilitate the comparison of $^{3}H$-$^{3}He$ ages directly with modeled ages and make estimates of aquifer parameters. The goal of the study is to compare $^{3}H$-$^{3}He$ ages with model ages in groundwater originating from TCE source zones, so sampling focused on groundwater flow paths stemming from two primary source zones; the flowlines were defined by the existing numerical model (Figure 4.2). The flow path originating from Lagoon C

is referred to as the South flow path (SFP), whereas the flow path located between Sector 214 and DRDC North is called the North flow path (NFP). Sector 214 and DRDC sources have been grouped into one flow path originating between the two sources as modeling has shown that flowlines originating from these sources are nearly parallel and have similar transit times (according to model simulations). Wells that lie on or close to the flow paths were chosen for sample collection. Table 4.3 lists the wells chosen to meet each of these objectives, and Figures 4.2 and 4.5 shows their locations in plan and section views, respectively. Those locations were selected to address specific objectives of the geochemical and isotopic age characterization program: 1) asses flow conditions, including recharge and transit time through the prodeltaic silty aquitard and in the aquifer along the two flow paths, and 2) help distinguish TCE plume origin on the basis of age gradients.

**Table 4.3**. Sampling locations chosen to meet the objectives of the groundwater $^{3}H$-$^{3}He$ dating program.

| Hydrogeological Context | Sampling locations | Sampling points | Location names |
|---|---|---|---|
| Silt aquitard | 3 | 6 | B69, B70, B98 |
| North Flow Path | 4 | 19 | C2-9-10, PO-152-153, PO-122, PO-SH-7-8 |
| South Flow Path | 5 | 25 | PO-142-143, PO-125-126, PO-116-117, PO-SH-26, PO-SH-47-48 |
| Downgradient section | 2 | 10 | PO-SH-21-22, PO-SH-5-6 |
| *Total* | 14 | 58 | |

## 4.6 Methods

### 4.6.1 Sample Collection

Sampling of groundwater was carried out from November 2007 to June 2008. A total of 58 samples were collected from 42 wells screened in the deltaic sand aquifer, with some wells having 2 or 3 samples collected in different locations along its screen; details are listed in Table 4.4. The screen lengths of available observation wells allowed sampling at more than one level within the screened interval. Within the high permeability deltaic unit (where no prodeltaic silt is present), insignificant vertical hydraulic gradients are assumed to prevail over the limited lengths of screened intervals, thus avoiding vertical groundwater circulation and mixing within the observation wells. The locations chosen for sampling are shown in Figure 4.2, and are either on or near one of the flow paths stemming from source zones (North Flow Path or South Flow Path), or constitute a transect through the western end of the TCE plume.

A multi-parameter TROLL 9500 – WQP-100 was used to measure field parameters (temperature, pH, dissolved oxygen, oxidation-reduction potential and electrical conductivity) in-situ prior to sample collection. The probe was lowered into the well to a depth corresponding with the location where samples were collected for $^{3}H$-$^{3}He$ dating, and a measurement was recorded once all parameters had stabilized.

Hydrasleeve bulk samplers were used to collect water samples for $^{3}H$ analysis from a discrete interval along the well screen (GeoInsight, 2006; ITRC 2006 and 2007). The disposable polyethylene 'sleeve' is slowly lowered into the well to the target sampling depth using a retaining cable with a weight attached to the sleeve base. They are left at the sampling depth for a minimum of 5 minutes to stabilize the water column, after which the sleeve is pulled in quick, short strokes up and down several times. Water enters the sleeve through a flexible check valve

at the top of the sleeve that is opened when pulled upward to collect a core of water roughly the length of the sampler (71 cm). The water-filled sleeve is then smoothly and rapidly pulled to the surface, where the sleeve is then punctured with a pointed tube to discharge the water into 500 mL sample bottles.

Gases collected for $^{3}H$-$^{3}He$ dating of groundwater (He and Ne) are collected using diffusion samplers, a method that allows for in-situ passive sampling of dissolved gases (Sanford *et al.*, 1996; Manning *et al.*, 2003). Two pieces of approximately 10 cm annealed copper tubing with 0.6 cm outer diameter are attached to silica tubing (also about 10 cm long) using stainless steel wire, to create a seal that will prevent water from entering the initially air-filled tubing; the outer ends of the copper tube are sealed. The silica tube acts as a semi-permeable membrane across which gases can diffuse, so that the partial pressures of gas components dissolved in the groundwater equilibrate with those of the gas components inside the diffusion sampler. The diffusion samplers were lowered into a well to the depth corresponding with the location of the top of the hydrasleeve sampler during water sample collection; the sampler was then left for a minimum of one week. Samples were collected by removing the diffusion sampler from the water column and immediately pinching off the copper tubes with a customized pinch-off tool, which creates a cold-weld seal that prevents escape of gases.

### 4.6.2 Laboratatory Analyses

Tritium analysis was carried out at the Environmental Isotope Laboratory at the University of Waterloo on 500 mL groundwater samples. Water samples were first deionized on a mixed bed ion exchange resin, and underwent electrolytic enrichment followed by liquid scintillation

counting (Heemskerk and Johnson, 1998). The average analytical precision is ±1.1 tritium unit (T.U.).

Helium isotope analysis was carried out at the Noble Gas Laboratory of the Department of Earth Sciences at the University of Ottawa; neon isotopes were also analyzed, which are required to quantify non-tritiogenic components of $^{3}He$ (Schlosser *et al.*, 1989). Samples were analyzed using a Mass Analyzer Products (MAP) 215-50 mass spectrometer connected to a stainless steel vacuum line for cryogenic processing and separation. $^{3}He$ was analyzed on a channel electron multiplier, and $^{4}He$, $^{20}Ne$, $^{21}Ne$ and $^{22}Ne$ were analyzed on a Faraday Cup. The average analytical precision for Ne and He concentrations is ±10%.

### 4.6.3 $^{3}H$-$^{3}He$ Data Processing and Age Calculation

Measured $^{3}He$ in groundwater is a combination of $^{3}He$ originating from 1) solubility equilibrium with the atmospheric concentration ($^{3}He_{eq}$), 2) excess air related to entrapment of air bubbles in groundwater ($^{3}He_{ex}$), 3) terrigenic production from radiogenic decay of elements in minerals ($^{3}He_{ter}$) and 4) decay of tritium in water molecules occurring as recharged precipitation flows in the aquifer ($^{3}He_{tri}$) (Tolstikhin and Kamenskiy, 1969; Schlosser *et al.*, 1988). To determine this last source of $^{3}He$ that is related to groundwater age, the other three sources of $^{3}He$ must be accounted for. The calculation procedure used for that purpose is described in Appendix B.

## 4.7 Results and Discussion

Results of the analyses of tritium, helium and neon isotopes and the computed groundwater ages are listed in Table 4.4. Successful analyses of gas samples for He and Ne was completed on 47 of the 55 samples collected for $^{3}H$-$^{3}He$ dating; 8 samples were not processed due to down time of the helium analytical equipment. The 47 samples on which groundwater dating was completed had $^{3}H$ concentrations ranging from 8.8 to 20.6 tritium units (T.U.) and tritiogenic $^{3}He$ concentrations are between 0.5 and 194.8 T.U. Calculated groundwater ages range from 0.6 years (PO-126-H) to 50.5 years (PO-142-B).

**Table 4.4**. Results of $^{3}H$-$^{3}He$ Groundwater Dating of the Valcartier Deltaic Aquifer

| Sample | Elev. W.T. | Elev. Sample | $^{3}H$ | Error (1σ) | $^{3}He$ | Error (1σ) | $^{4}He$ | Error (1σ) | Ne | Error (1σ) | $^{4}He_{ter}$ | $^{3}He_{tri}$ | $^{3}H + {}^{3}He_{tri}$ | Age | Error (1σ) |
|---|---|---|---|---|---|---|---|---|---|---|---|---|---|---|---|
| *units* | *m* | *m* | *T.U.* | *T.U.* | *cc/cc* | *cc/cc* | *cc/cc* | *cc/cc* | *cc/cc* | *cc/cc* | *cc/cc* | *T.U.* | *T.U.* | *yr* | *yr* |
| Silt Locations | | | | | | | | | | | | | | | |
| B69-2-6m | 170.94 | 168.577 | 12.3 | 0.9 | - | - | - | - | - | - | - | - | - | - | - |
| B69-2-23m | | 153.06 | 11.3 | 0.9 | 2.12E-13 | 2.12E-14 | 9.69E-08 | 9.69E-09 | 3.14E-07 | 3.14E-08 | 1.71E-08 | 40.9 | 52.2 | 27.2 | 3.1 |
| B70-1-10m | 171.05 | 165.00 | 12.3 | 0.9 | 1.22E-13 | 1.22E-14 | 8.26E-08 | 8.26E-09 | 2.50E-07 | 2.50E-08 | 2.09E-08 | 15.2 | 27.5 | 14.3 | 2.1 |
| B70-1-21m | | 154.14 | 10.5 | 1.0 | 3.34E-13 | 3.34E-14 | 1.57E-07 | 1.57E-08 | 6.33E-07 | 6.33E-08 | 0.00E+00 | 39.1 | 49.6 | 27.6 | 3.3 |
| B98-1-13m | 171.49 | 163.17 | 10.6 | 1.0 | 1.28E-13 | 1.28E-14 | 8.63E-08 | 8.63E-09 | 2.48E-07 | 2.48E-08 | 2.53E-08 | 17.7 | 28.3 | 17.4 | 2.6 |
| B98-1-22m | | 153.37 | 8.8 | 0.8 | 1.57E-13 | 1.57E-14 | 8.56E-08 | 8.56E-09 | 2.46E-07 | 2.46E-08 | 2.53E-08 | 29.7 | 38.5 | 26.2 | 3.2 |
| North Flow Path | | | | | | | | | | | | | | | |
| PO-SH-8H | 157.29 | 152.23 | 12.3 | 1.1 | - | - | - | - | - | - | - | - | - | - | - |
| PO-SH-7H | | 148.37 | 11.3 | 1.0 | 1.53E-13 | 1.53E-14 | 1.98E-07 | 1.98E-08 | 3.20E-07 | 3.20E-08 | 1.17E-07 | 15.6 | 26.9 | 15.4 | 1.9 |
| DP-PO-122-1 | 162.99 | 159.64 | 12.3 | 0.9 | 1.52E-13 | 1.52E-14 | 8.63E-08 | 8.63E-09 | 4.12E-07 | 4.12E-08 | 0.00E+00 | 1.4 | 13.7 | 2 | 0.4 |
| DP-PO-122-2 | | 155.64 | 13.8 | 1.0 | 1.51E-13 | 1.51E-14 | 6.74E-08 | 6.74E-09 | 3.06E-07 | 3.06E-08 | 0.00E+00 | 18.2 | 32.0 | 15 | 2.1 |
| DP-PO-122-3 | | 151.64 | 14.3 | 1.1 | 1.77E-13 | 1.77E-14 | 8.94E-08 | 8.94E-09 | 4.14E-07 | 4.14E-08 | 0.00E+00 | 11.3 | 25.6 | 10.3 | 1.7 |
| PO-122-H | | 146.73 | 12.9 | 1.2 | 1.62E-13 | 1.62E-14 | 8.61E-08 | 8.61E-09 | 3.58E-07 | 3.58E-08 | 0.00E+00 | 13.9 | 26.8 | 13.0 | 2.2 |
| PO-122-B-U | | 139.86 | 12.3 | 1.1 | 2.61E-13 | 2.61E-14 | 9.91E-08 | 9.91E-09 | 4.06E-07 | 4.06E-08 | 0.00E+00 | 45.9 | 58.2 | 27.6 | 3.2 |
| PO-122-B-L | | 137.66 | 11.9 | 1.0 | 2.86E-13 | 2.86E-14 | 1.28E-07 | 1.28E-08 | 3.70E-07 | 3.70E-08 | 3.19E-08 | 61.6 | 73.5 | 32.4 | 3.3 |
| PO-153-H-U | 165.71 | 159.69 | 17.2 | 1.4 | 1.23E-13 | 1.23E-14 | 1.03E-07 | 1.03E-08 | 2.96E-07 | 2.96E-08 | 2.80E-08 | 8.1 | 25.3 | 6.9 | 1.3 |
| PO-153-H-L | | 157.39 | 20.6 | 1.5 | 1.44E-13 | 1.44E-14 | 1.04E-07 | 1.04E-08 | 3.72E-07 | 3.72E-08 | 7.35E-09 | 4.6 | 25.2 | 3.6 | 0.7 |
| PO-152-H | | 152.51 | 18.5 | 1.4 | 1.16E-13 | 1.16E-14 | 8.59E-08 | 8.59E-09 | 2.99E-07 | 2.99E-08 | 1.01E-08 | 4.7 | 23.2 | 4.0 | 0.8 |
| PO-153-B | | 145.47 | 12.9 | 1.1 | 1.21E-13 | 1.21E-14 | 8.95E-08 | 8.95E-09 | 3.12E-07 | 3.12E-08 | 1.00E-08 | 4.6 | 17.5 | 5.5 | 1.1 |
| PO-152-B | | 138.32 | 10.5 | 1.0 | 2.90E-13 | 2.90E-14 | 2.81E-07 | 2.81E-08 | 4.14E-07 | 4.14E-08 | 1.72E-07 | 55.1 | 65.6 | 21.3 | 2.7 |
| DP-C2-10-1 | 167.00 | 164.70 | 14.3 | 1.1 | 1.30E-13 | 1.30E-14 | 7.14E-08 | 7.14E-09 | 3.44E-07 | 3.44E-08 | 0.00E+00 | 3.6 | 17.9 | 4.0 | 0.8 |
| DP-C2-10-2 | | 161.70 | 13.8 | 1.0 | 1.32E-13 | 1.32E-14 | 9.90E-08 | 9.90E-09 | 3.03E-07 | 3.03E-08 | 2.21E-08 | 10.6 | 24.4 | 10.1 | 1.6 |
| DP-C2-10-3 | | 157.70 | 12.3 | 0.9 | 1.94E-13 | 1.94E-14 | 1.54E-07 | 1.54E-08 | 4.44E-07 | 4.44E-08 | 3.65E-08 | 12.7 | 25.0 | 12.6 | 1.9 |
| C2-10-22m | | 153.97 | 13.1 | 1.0 | 1.23E-13 | 1.23E-14 | 8.55E-08 | 8.55E-09 | 2.41E-07 | 2.41E-08 | 2.64E-08 | 16.7 | 29.8 | 14.6 | 2.2 |
| C2-9-28m | | 148.11 | 13.7 | 1.0 | 1.32E-13 | 1.32E-14 | 9.13E-08 | 9.13E-09 | 2.59E-07 | 2.59E-08 | 2.71E-08 | 17.5 | 31.2 | 14.6 | 2.1 |
| C2-10-35m | | 141.27 | 15.0 | 1.1 | 3.80E-13 | 3.80E-14 | 1.75E-07 | 1.75E-08 | 2.85E-07 | 2.85E-08 | 1.03E-07 | 112.5 | 127.5 | 38 | 3.4 |

** Well locations and detailed results of $^{3}H$-$^{3}He$ dating are provided in Appendix A*

**Table 4.4**. Results of $^{3}H$-$^{3}He$ Groundwater Dating of the Valcartier Deltaic Aquifer (continued).

| SAMPLE | Elev. W.T. | Elev. Sample | $^{3}H$ | Error (1σ) | $^{3}He$ | Error (1σ) | $^{4}He$ | Error (1σ) | Ne | Error (1σ) | $^{4}He_{terrigenic}$ | $^{3}He_{tritiogenic}$ | $^{3}H + {}^{3}He_{tritiogenic}$ | Age | Error (1σ) |
|---|---|---|---|---|---|---|---|---|---|---|---|---|---|---|---|
| *units* | *m* | *m* | *T.U.* | *T.U.* | *cc/cc* | *cc/cc* | *cc/cc* | *cc/cc* | *cc/cc* | *cc/cc* | *cc/cc* | *T.U.* | *T.U.* | *years* | *years* |
| South Flow Path | | | | | | | | | | | | | | | |
| PO-SH-48H U | 156.77 | 153.88 | 12.9 | 1.2 | - | - | - | - | - | - | - | - | - | - | - |
| PO-SH-48H L | | 152.48 | 14.5 | 1.2 | 2.51E-13 | 2.51E-14 | 1.49E-07 | 1.49E-08 | 3.05E-07 | 3.05E-08 | 7.20E-08 | 57.8 | 72.3 | 28.6 | 3.2 |
| PO-SH-48B U | | 147.69 | 11.3 | 1.0 | 2.53E-13 | 2.53E-14 | 3.16E-07 | 3.16E-08 | 3.29E-07 | 3.29E-08 | 2.32E-07 | 53.3 | 64.6 | 31 | 3.4 |
| PO-SH-48B L | | 146.29 | 14.6 | 1.2 | 2.56E-13 | 2.56E-14 | 3.49E-07 | 3.49E-08 | 2.99E-07 | 2.99E-08 | 2.73E-07 | 59.2 | 73.8 | 28.8 | 3.2 |
| PO-SH-47H | | 143.29 | 15.0 | 1.2 | 2.65E-13 | - | 2.60E-07 | - | 2.99E-07 | - | 1.84E-07 | 63.2 | 78.2 | 29.4 | 3.2 |
| PO-SH-26H U | 158.39 | 155.57 | 16.5 | 1.4 | 1.71E-13 | 1.71E-14 | 7.08E-08 | 7.08E-09 | 3.80E-07 | 3.80E-08 | 0.00E+00 | 14.5 | 31.0 | 11.2 | 1.9 |
| PO-SH-26H L | | 153.57 | 15.2 | 1.3 | 2.08E-13 | 2.08E-14 | 1.34E-07 | 1.34E-08 | 4.17E-07 | 4.17E-08 | 2.40E-08 | 22.7 | 37.9 | 16.2 | 2.4 |
| PO-SH-26B U | | 149.07 | 12.5 | 1.1 | 1.93E-13 | 1.93E-14 | 8.27E-08 | 8.27E-09 | 3.95E-07 | 3.95E-08 | 0.00E+00 | 20.7 | 33.2 | 17.3 | 2.5 |
| PO-SH-26B L | | 148.42 | 14.6 | 1.1 | 2.17E-13 | 2.17E-14 | 1.40E-07 | 1.40E-08 | 4.93E-07 | 4.93E-08 | 8.37E-09 | 14.6 | 29.5 | 12.1 | 1.9 |
| PO-117-H | 161.86 | 158.09 | 12.2 | 1.0 | 1.63E-13 | 1.63E-14 | 8.78E-08 | 8.78E-09 | 4.14E-07 | 4.14E-08 | 0.00E+00 | 5.7 | 17.9 | 6.8 | 1.3 |
| PO-116-H | | 152.03 | 14.4 | 1.2 | 2.04E-13 | 2.04E-14 | 1.11E-07 | 1.11E-08 | 4.79E-07 | 4.79E-08 | 0.00E+00 | 11.7 | 26.1 | 10.6 | 1.8 |
| PO-117-B | | 146.86 | 17.3 | 1.4 | 3.37E-13 | 3.37E-14 | 3.12E-07 | 3.12E-08 | 2.54E-07 | 2.54E-08 | 2.49E-07 | 99.0 | 116.3 | 33.9 | 3.3 |
| PO-116-B | | 141.89 | 13.5 | 1.1 | 2.03E-13 | 2.03E-14 | 1.49E-07 | 1.49E-08 | 2.68E-07 | 2.68E-08 | 8.21E-08 | 44.1 | 57.6 | 25.8 | 3 |
| PO-126-H | 162.42 | 159.19 | 14.1 | 1.2 | 1.27E-13 | 1.27E-14 | 9.14E-08 | 9.14E-09 | 3.54E-07 | 3.54E-08 | 0.00E+00 | 0.5 | 14.6 | 0.6 | 0.1 |
| DP-PO-125 | | 156.34 | 13.5 | 1.1 | 1.31E-13 | 1.31E-14 | 9.52E-08 | 9.52E-09 | 3.44E-07 | 3.44E-08 | 6.56E-09 | 3.8 | 17.3 | 4.4 | 0.9 |
| PO-126-B-U | | 150.21 | 12.7 | 1.1 | 1.21E-13 | 1.21E-14 | 8.66E-08 | 8.66E-09 | 2.88E-07 | 2.88E-08 | 1.41E-08 | 8.7 | 21.4 | 9.2 | 1.6 |
| PO-126-B-L | | 148.01 | 14.5 | 1.2 | 1.27E-13 | 1.27E-14 | 8.91E-08 | 8.91E-09 | 3.65E-07 | 3.65E-08 | - | - | 13.2 | - | - |
| PO-125-H | | 136.68 | 11.7 | 1.1 | 1.26E-13 | 1.26E-14 | 1.34E-07 | 1.34E-08 | 2.77E-07 | 2.77E-08 | 6.43E-08 | 11.9 | 23.6 | 12.5 | 2.1 |
| PO-143-H | 166.50 | 164.34 | 13.8 | 1.1 | 5.28E-14 | 5.28E-15 | 4.08E-08 | 4.08E-09 | 1.94E-07 | 1.94E-08 | - | - | 10.3 | - | - |
| PO-142-H-U | | 160.28 | 12.9 | 1.1 | 1.21E-13 | 1.21E-14 | 8.77E-08 | 8.77E-09 | 3.36E-07 | 3.36E-08 | 1.30E-09 | 1.0 | 13.9 | 1.3 | 0.3 |
| PO-142-H-L | | 158.03 | 12.5 | 1.0 | 1.35E-13 | 1.35E-14 | 9.87E-08 | 9.87E-09 | 3.66E-07 | 3.66E-08 | 3.73E-09 | 2.0 | 14.5 | 2.7 | 0.5 |
| PO-143-B | | 154.13 | 13.4 | 1.2 | 1.22E-13 | 1.22E-14 | 8.87E-08 | 8.87E-09 | 3.31E-07 | 3.31E-08 | 3.90E-09 | 2.4 | 15.8 | 2.9 | 0.6 |
| PO-142-B | | 149.48 | 12.1 | 1.1 | 6.75E-13 | 6.75E-14 | 3.96E-06 | 3.96E-07 | 3.21E-07 | 3.21E-08 | 3.88E-06 | 194.8 | 206.9 | 50.5 | 3.9 |
| Downgradient | | | | | | | | | | | | | | | |
| PO-SH-22H U | 157.76 | 157.41 | 13.0 | 1.1 | 2.18E-13 | 2.18E-14 | 1.28E-07 | 1.28E-08 | 5.17E-07 | 5.17E-08 | 0.00E+00 | 11.2 | 24.2 | 11 | 1.8 |
| PO-SH-22B L | | 149.78 | 10.8 | 1.0 | 2.02E-13 | 2.02E-14 | 9.29E-08 | 9.29E-09 | 4.49E-07 | 4.49E-08 | 0.00E+00 | 15.6 | 27.5 | 14.9 | 2.3 |
| PO-SH-6B L | | 144.24 | 14.9 | 1.1 | 2.17E-13 | 2.17E-14 | 1.40E-07 | 1.40E-08 | 4.93E-07 | 4.93E-08 | 8.37E-09 | 14.6 | 29.5 | 12.1 | 1.9 |
| PO-SH-5H | | 137.03 | 9.9 | 0.8 | 2.56E-13 | 2.56E-14 | 2.27E-07 | 2.27E-08 | 5.35E-07 | 5.35E-08 | 8.33E-08 | 22.9 | 32.8 | 21.3 | 2.7 |

** Well locations and detailed results of $^{3}H$-$^{3}He$ dating are provided in Appendix A*

### 4.7.1 Coherence of Tritium and Helium Analyses

To evaluate the validity of $^3H$-$^3He$ Valcartier data, the consistency of the results with historical tritium input into the groundwater system can be checked. For this purpose, the present tritium ($^3H_{pre}$) and tritiogenic $^3He$ ($^3He_{tri}$) concentrations found in groundwater and the calculated groundwater ages obtained from these concentrations were used to reconstruct the initial concentration of tritium ($^3H_{ini}$) in precipitation for Valcartier (Dunkle-Shapiro *et al.*, 1998). On Figure 4.6, the reconstructed values are compared with the record of tritium in precipitation from Ottawa (IAEA/WMO, 2006), Ontario, which is the nearest IAEA monitoring station to Valcartier. There is an excellent match between the $^3H$ input history for Ottawa and the distribution reconstructed from $^3H$-$^3He$ data in groundwater at Valcartier. Taking into account that $^3H$-$^3He$ ages may be affected by dispersion, and that the $^3H$ input record for the study area is not precisely known, this close match is a strong indication that the $^3H$-$^3He$ results are meaningful in the context of the groundwater flow system.

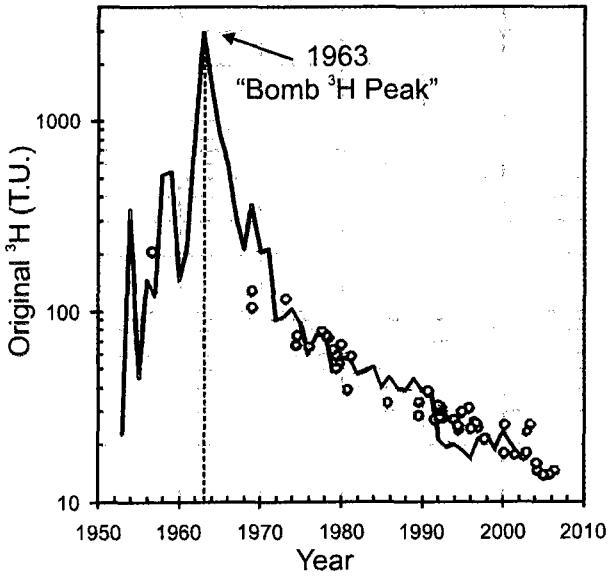


**Figure 4.6**. Comparison of $^3H$-$^3He$ Valcartier data (red dots) with the Ottawa record of $^3H$ in precipitation (black line) (IAEA/WMO, 2006).

### 4.7.2 Ages across the Prodeltaic Silty Unit

There are three well locations (B69, B70 and B98) where groundwater ages in the prodeltaic aquifer were obtained directly above and below the prodeltaic silty aquitard. These wells are in the eastern part of the study area on DRDC North property, and are shown in Figure 4.4. Results and their interpretation on the basis of local hydrogeological conditions are compiled in Table 4.5. The ages above the silty aquitard are between 14.3 and 17.5 years, and ages beneath the aquitard are between 26.2 and 27.6 years. The age above the aquitard at B69-2-6 could not be processed due to sampling problems, so this age was estimated for calculation purposes as being the average age from the two wells above the aquitard that were analyzed. The vertical transit time for groundwater across the aquitard is about 11 years, which corresponds to vertical velocities between 0.69 m/y and 0.85 m/y. The aquitard has a retardation factor of 1.7 for TCE estimated from a column test (Lefebvre *et al.*, 2003), which can be multiplied by the groundwater transit time to obtain a transit time for TCE of about 19 years.

The vertical hydraulic conductivity ($K_v$) of the aquitard is an important control on the migration of TCE into the deltaic aquifer. $K_v$ is a difficult parameter to measure in aquitards, so groundwater ages can be used to estimate this value. The effective porosity of the aquitard is 0.36, as determined by column testing on laboratory samples and cone penetration tests performed in the field (Lefebvre *et al.*, 2003; Fauveau *et al.*, 2005; Fauveau, 2006). The water flux through the aquitard can be calculated by finding the product of the effective porosity and groundwater velocity, which was estimated using groundwater ages (discussed later in this section). The vertical hydraulic gradient of the aquitard can be compared with the groundwater flux to estimate the $K_v$ of the aquitard. This was done for the three locations where $^{3}H$-$^{3}He$ ages were obtained (Table 4.5), and calculated $K_v$ values range from $1.3\text{-}3.1 \times 10^{-8}$ m/s. These values

are slightly lower than the $K_v$ used in the numerical model. These results lend credibility to the assumed vertical anisotropy of the finer grained hydrofacies defined by Ouellon *et al.* (2008a) as well as to their calculation of equivalent horizontal and vertical hydraulic conductivity on the basis of hydrofacies proportions using generalized means. Such independent supporting evidence provided by $^{3}H$-$^{3}He$ ages is quite important as there are no commonly used, practical and accepted methods of measuring vertical hydraulic conductivity.

**Table 4.5**. Groundwater and TCE transit time through the prodeltaic silty aquitard

| | Sampled boreholes | | | Global |
|---|---|---|---|---|
| | B69-2 | B-70-1 | B-98-1 | **Silt** |
| ***Measurements*** | | | | |
| Porosity | 0.36 | 0.36 | 0.36 | 0.36 |
| Retardation factor | 1.7 | 1.7 | 1.7 | 1.7 |
| Head above silt (m) | 170.94 | 171.05 | 171.49 | |
| Head under silt (m) | 167.92 | 168.06 | 167.90 | |
| Thickness of silt (m) | 9.62 | 9.76 | 6.10 | 8.0[a] |
| Age above silt (y) | 15.88[b] | 14.31 | 17.45 | 15.9 |
| Age under silt (y) | 27.21 | 27.60 | 26.23 | 27.0 |
| ***Calculations*** | | | | |
| Head difference (m) | 3.02 | 2.99 | 3.59 | |
| Vertical gradient (m/m) | 0.31 | 0.31 | 0.59 | 0.31 |
| **Water transit time (y)** | **11.3** | **13.3** | **8.8** | **11.1** |
| **TCE transit time (y)** | **19.3** | **22.6** | **14.9** | **18.9** |
| Water velocity (m/y) | 0.85 | 0.73 | 0.69 | 0.72 |
| Vertical flux (m/s) | 9.7E-09 | 8.4E-09 | 7.9E-09 | 8.2E-09 |
| Mean $K_v$ (m/s) | 3.1E-08 | 2.7E-08 | 1.3E-08 | 2.6E-08 |
| ***Comparison to numerical model $K_v$ distribution (Ouellon et al., 2008b)*** | | | | |
| Model $K_v$ (m/s) | 1.04E-07 | 2.91E-08 | 6.20E-08 | |

a: Representative thickness of silty prodeltaic aquitard based on isopach map (Ouellon et al., in prep.).
b: Age not available for that well – Used mean value of age above the silt for other two wells.

### 4.7.3 Groundwater Recharge Estimation

The average recharge rate estimated and used in the groundwater flow numerical model was 300 mm/y, which was based on estimates made from well hydrograph records (Maltais, 2006; Lefebvre *et al.*, 2009; Ouellon *et al.*, 2008b; Healy and Cook, 2002). However, as recharge is one of the most important parameters in groundwater models controlling circulation, this value can be further assessed using $^{3}H$-$^{3}He$ ages to evaluate its use in the Valcartier model. Groundwater ages were obtained in a vertical profile in the deltaic sand aquifer near the groundwater divide (C2-9-10). Groundwater flow at this location is predominantly downward, so the change in age with depth should reflect the vertical groundwater velocity at this location. The vertical velocity is proportional to recharge in an unconfined aquifer, and can be related by:

$$R = V * n$$

where R = Recharge, V = average vertical linear velocity and $n$ = effective porosity

The $^{3}H$-$^{3}He$ ages for C2-9-10 are shown along with the age profile obtained from numerical modelling that was reproduced at a porosity of 0.35 on an age versus depth graph in Figure 4.7. That porosity of 0.35 was found to be the one allowing the best match between model and $^{3}H$-$^{3}He$ ages (next section, Figure 4.8). The straight line represents the age profile with depth of uniform vertical recharge of 300 mm/y with no horizontal advection. Although this age profile does not provide enough detail to estimate recharge by itself using the method outlined in Solomon and Sudicky (1991) and Solomon *et al.* (1992), the close match between model ages and $^{3}H$-$^{3}He$ ages offers support for the use of 300 mm/y for an average recharge rate in the model. The recharge value used in the model is better validated by the general match established between model and $^{3}H$-$^{3}He$ ages presented in the next section.

### 4.7.4 Matching of Numerical Model Ages to Isotopic Ages

Groundwater ages from $^{3}H$-$^{3}He$ dating along the North Flow Path and South Flow Path generally increase with depth and are coherent with the pattern of ages obtained from numerical modelling. Graphs in Figure 4.7 show age versus depth to compare isotopic age results with model ages at the four model porosities between 0.30 and 0.45. The lines representing steady vertical recharge are shown to assess the effect of horizontal advection on groundwater ages at each well location. Ages are higher at depth than predicted by vertical recharge at most locations because horizontal groundwater flowing at depth, which has recharged upgradient, is older than groundwater that would have undergone vertical recharge. An important effect of the cumulative effect of recharge in unconfined aquifers is that groundwater velocity will increase away from the groundwater divide (Chesnaux *et al.*, 2005); this will be addressed later in this paper.

On the NFP, ages at PO-152-153 are less than predicted by the model. This could be related to the effects of nearby pumping wells, which can affect the $^{3}He$ dissolved in groundwater and change the groundwater age distribution even after operation has ceased (Dunkle-Shapiro *et al.*, 1998; Zinn and Konikow, 2007; see Figure 4.7). A production well that is currently inactive is located upgradient of PO-152-153, which may have impacted the groundwater age distribution resulting in low $^{3}H$-$^{3}He$ ages nearby at PO-152-153. However, the model represents present-day pumping conditions and does not account for the potential influence of pumping that occurred in the past. The modelled ages represent advective ages based on current flow conditions, whereas $^{3}H$-$^{3}He$ ages reflect the change in flow conditions over the past several years, so the isotopic ages

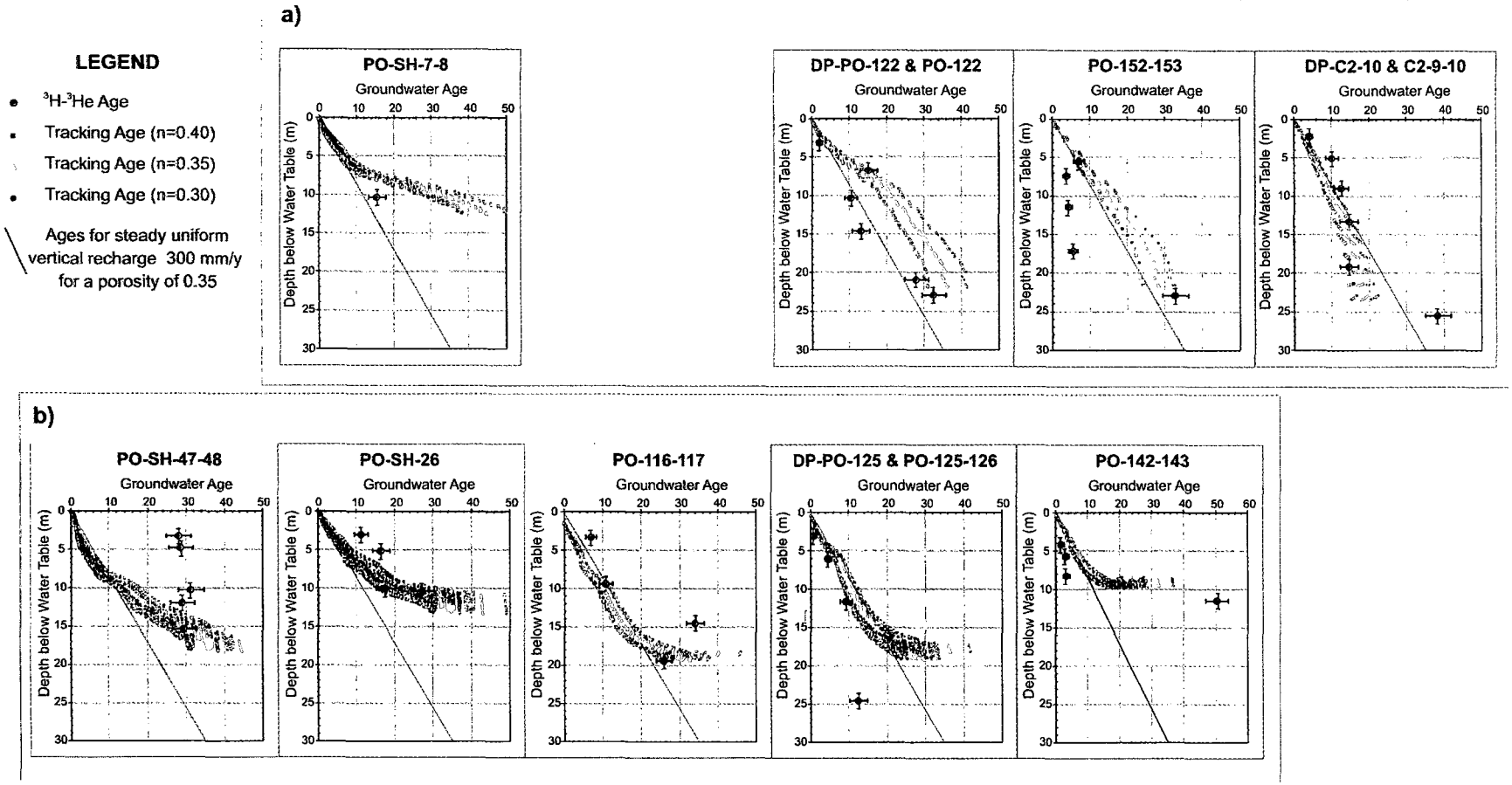


**Figure 4.7**. Comparison of $^3$H-$^3$He ages with particle tracking ages at effective porosities of 0.30, 0.35 and 0.40 for groundwater along a) the North Flow Path and b) the South Flow Path. The diagonal line represents steady vertical recharge at 300 mm/y.

at this location are anomalous in the context of interpreting groundwater transit time and velocities. On the South Flow Path, especially at its western end, several $^{3}H$-$^{3}He$ ages are older than predicted by the model, including one location (PO-117-B) where groundwater is older (33.9 years) than the underlying sample location (25.8 years at PO-116-B). This is especially prominent at well PO-SH-47-48, where ages are nearly uniform around 30 years even in the uppermost sample. This may relate to upflow of groundwater from the underlying proglacial aquifer that is mixing with water in the deltaic aquifer.

Proglacial aquifer groundwater is recharged further upgradient than groundwater in the adjacent deltaic aquifer, and travels slower through the proglacial aquifer due to its lower hydraulic conductivity (Ouellon *et al.*, 2008a, b). Groundwater in the proglacial aquifer is thus older than groundwater in the deltaic sand aquifer and contains a higher concentration of tritiogenic $^{3}He$. When the upflowing proglacial aquifer groundwater comes in contact with water in the deltaic unit that has lower $^{3}He$ concentrations, diffusion may occur to cause an increase in the $^{3}H$-$^{3}He$ age. This phenomenon has been observed in other investigations (Solomon *et al.*, 1992; Ekwurzel *et al.*, 1994; Dunkle-Shapiro *et al.*, 1998). High concentrations of dissolved terrigenic $^{4}He$ at these sample locations may also relate to the mineralogy of the proglacial aquifer and lower units, which contain minerals with radioactive isotopes of K, U and Th that decay to produce $^{4}He$ compared with the deltaic sand, which is primarily quartz. For this reason, samples affected by exchange with proglacial aquifer groundwater are not used for comparison with the tracking ages.

On the western transect across flow direction, four $^{3}H$-$^{3}He$ ages were obtained that are not compared with simulated model ages (PO-SH-22-H-U, PO-SH-22-B-L, PO-SH-6-B-L and PO-SH-5). However, they can provide insight on groundwater flow in Shannon. The groundwater in south Shannon (PO-SH-5-6) is relatively younger than ages in North Shannon. This may be due to groundwater flow from Mount Rolland-Auger to the south, which is under higher hydraulic gradient than groundwater flowing in the buried valley to the north. Another possible reason for young ages could be the expansion of the flow in south Shannon, as PO-SH-5-6 are located on a thicker part of the deltaic aquifer that has expanded compared with the upgradient section.

Isotopic ages are directly compared with model ages at porosities of 0.30, 0.35, 0.40 and 0.45, and are shown on Figure 4.8; the diagonal line through the graph represents a 1:1 match between ages. $^{3}H$-$^{3}He$ ages from groundwater that mixed with proglacial aquifer groundwater deviate from their corresponding tracking ages, and were omitted from the comparison along with outliers that have a disproportionately strong influence on the coefficient of determination ($R^2$) and root-mean-square (RMS) values. Appendix A lists the values for isotopic and model ages at the four porosities. The isotopic ages are most coherent with model results where a porosity of 0.35 is used. These results have the smallest RMS value (3.64), whereas $R^2$ values do no show significant variation (0.6873 to 0.6925). The slope of the regression between isotopic ages and model ages for porosity of 0.35 are also close to unity (0.92) compared to other porosities. The slope for porosity of 0.30 (0.79) indicates that ages predicted by the model are underestimated, whereas larger slopes at porosities of 0.40 and 0.45 (1.05 and 1.19) show that model ages at higher porosities are higher than isotopic ages. Since $^{3}H$-$^{3}He$ ages provide estimates of the minimum groundwater transit time (Schlosser *et al.*, 1989), the overestimation of ages by the

model at a porosity of 0.40 is probably too high. A porosity of 0.35 appears to be the most representative of the Valcartier groundwater system using the $^{3}H$-$^{3}He$ ages as a calibration target. This value is supports a porosity of 0.36 for the deltaic aquifer previously obtained from independent measurements (Table 4.2).

### 4.7.5 Model and Isotopic Velocity and Transit Time Comparison

Figure 4.9 shows the isotopic and particle tracking ages at a porosity of 0.35 reported on graphs of age as a function of the sampling point distance along the North and South Flow Paths. Age estimates are plotted along lines corresponding to the particle tracks that crossed sampling points used for isotopic age estimation. To do so, tracks intersecting a sampling point were followed up and down gradient and their intersections with other sampling locations were noted. At the upgradient location, the age corresponding to the intersecting track was estimated by linear interpolation between two adjacent sampling points where isotopic ages were available.

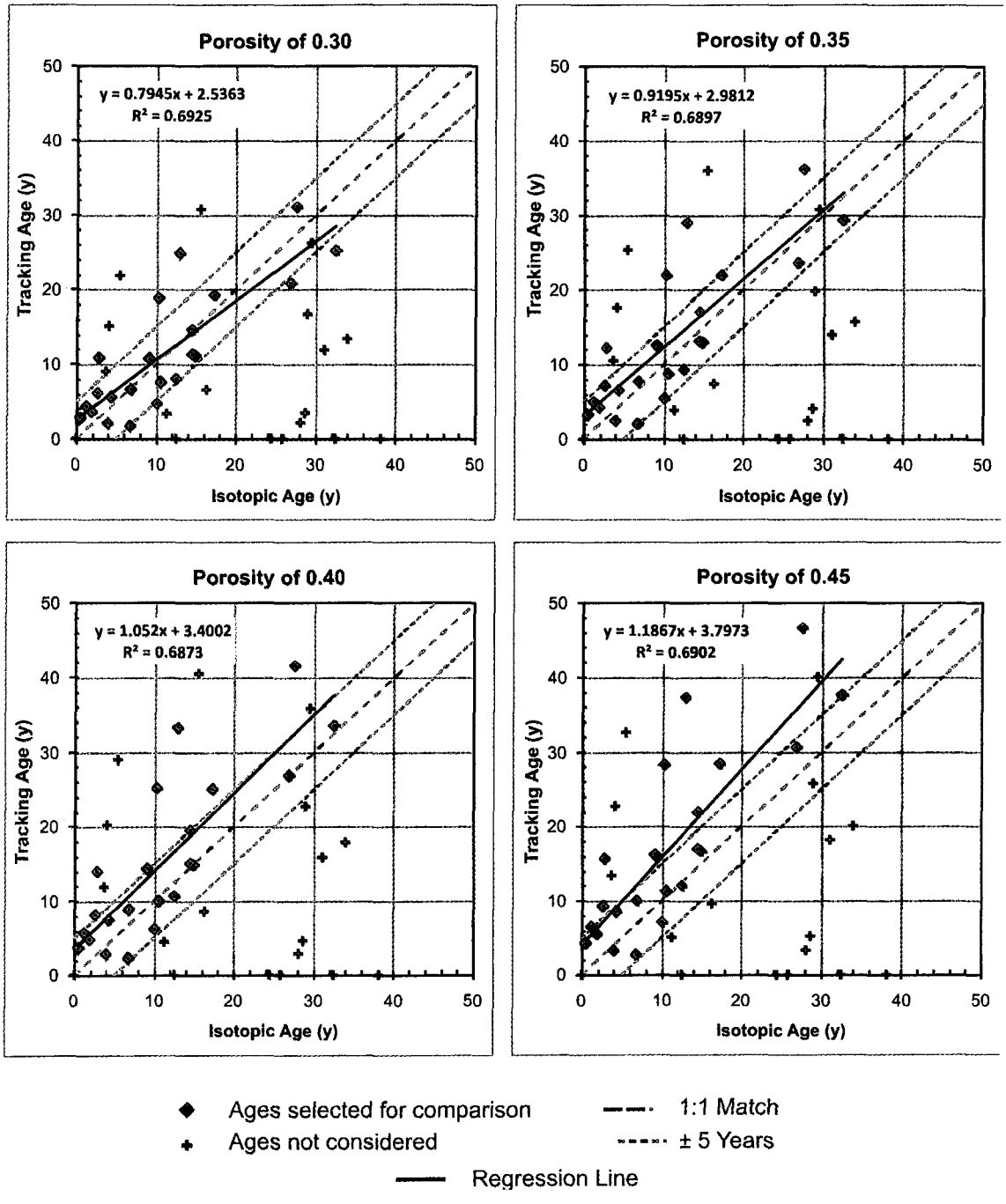


**Figure 4.8**. Correlation of particle tracking advective ages and $^{3}H$-$^{3}He$ ages at sampling locations projected on the tracking sections (Figure 4.5). Samples used in the regression are shown by lozenges whereas crosses indicate samples excluded for reasons explained in the text. Regression lines and their $R^2$ are indicated for the four model porosities used in particle tracking. The diagonal perfect fit line and parallel lines at ± 5 years are shown as references.

Upgradient, particle tracks were followed to their origin at the water table, where the age was presumed to be zero. Figure 4.9 shows only the isotopic ages that are representative of flow conditions in the deltaic unit, so relatively few pairs of ages, which form "tracks" between adjacent wells, are actually available for comparison. This is because each track requires a valid age at the sampling location as well as two valid ages at the upgradient location to be used for age interpolation where the track intersects the well. Several $^{3}H$-$^{3}He$ ages are not considered valid either due to the influence of proglacial aquifer groundwater or because they are outliers. Overall, the valid isotopic ages used for both North and South Flow Paths are coherent with the particle tracking ages at a porosity of 0.35.

The slope of a line joining a pair of ages on Figure 4.9 is inversely proportional to groundwater velocity; for example, a steeper slope indicates a higher age gradient over a given distance because of slower moving water. However, small changes in the hydraulic conductivity of the deltaic aquifer lead to relatively drastic changes in velocity over a short interval. The deltaic aquifer is heterogeneous in terms of hydraulic conductivity (Ouellon *et al.*, 2008a) and has a variable saturated thickness (Figure 4.5), resulting in variable groundwater velocity along the flow paths as indicated by the groundwater model, shown on Figure 4.10. $^{3}H$-$^{3}He$ ages can theoretically be used to estimate groundwater velocities if there is a steady increase along a flow path, which would result in a predictable increase in groundwater ages. However, the heterogeneity of the sediments, and therefore the groundwater velocities, at the scale of the Valcartier deltaic aquifercannot be resolved by $^{3}H$-$^{3}He$ ages, making them an unreliable means of independently estimating groundwater velocity.

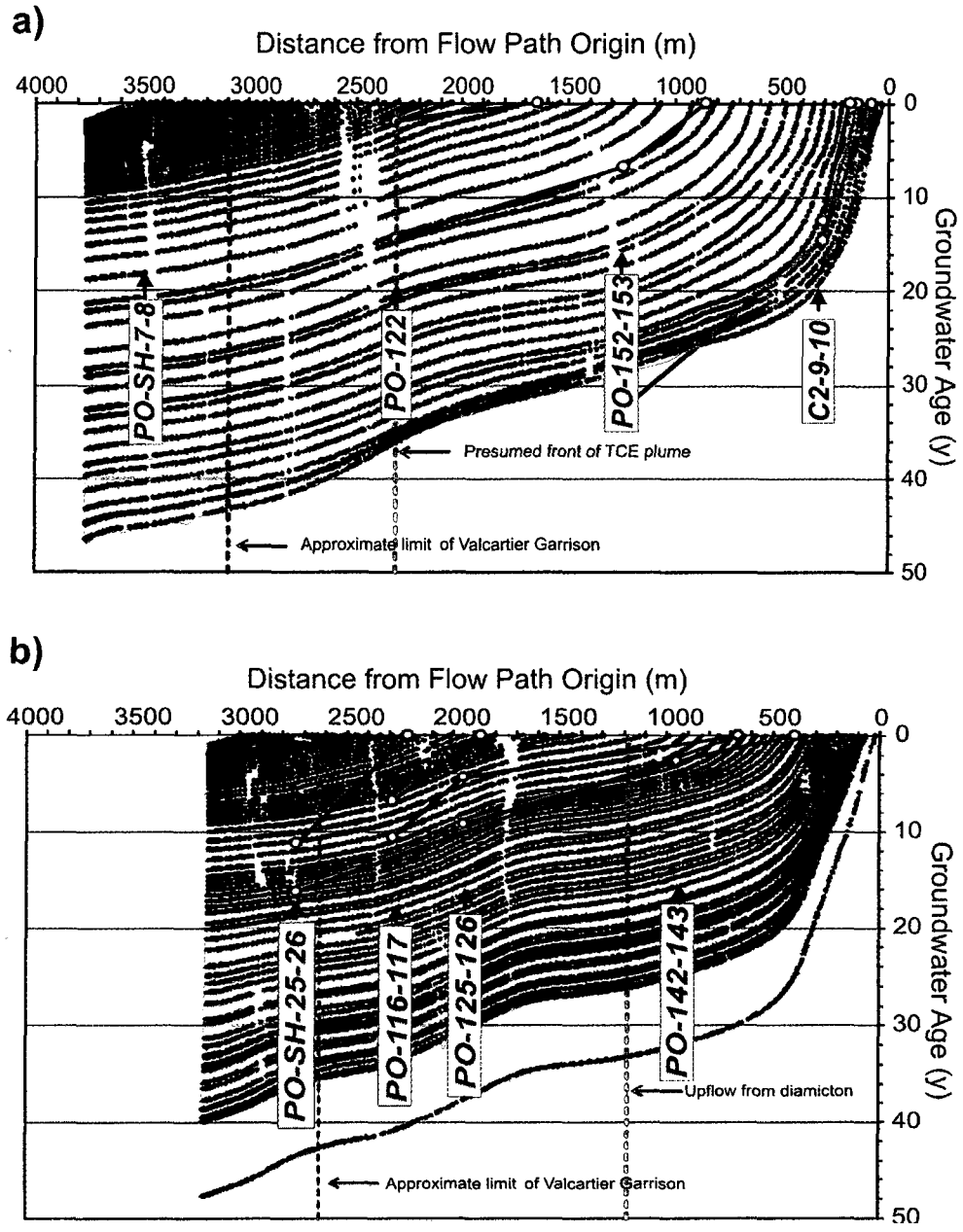


**Figure 4.9**. Graphs showing age versus distance from origin for the a) North and b) South Flow Paths for $^{3}H$-$^{3}He$ ages (in blue and yellow) compared with particle tracking results at an effective porosity of 0.35. The area shaded in orange indicates the range of ages considered for the calculation of groundwater transit time (Murphy et al., 2009).

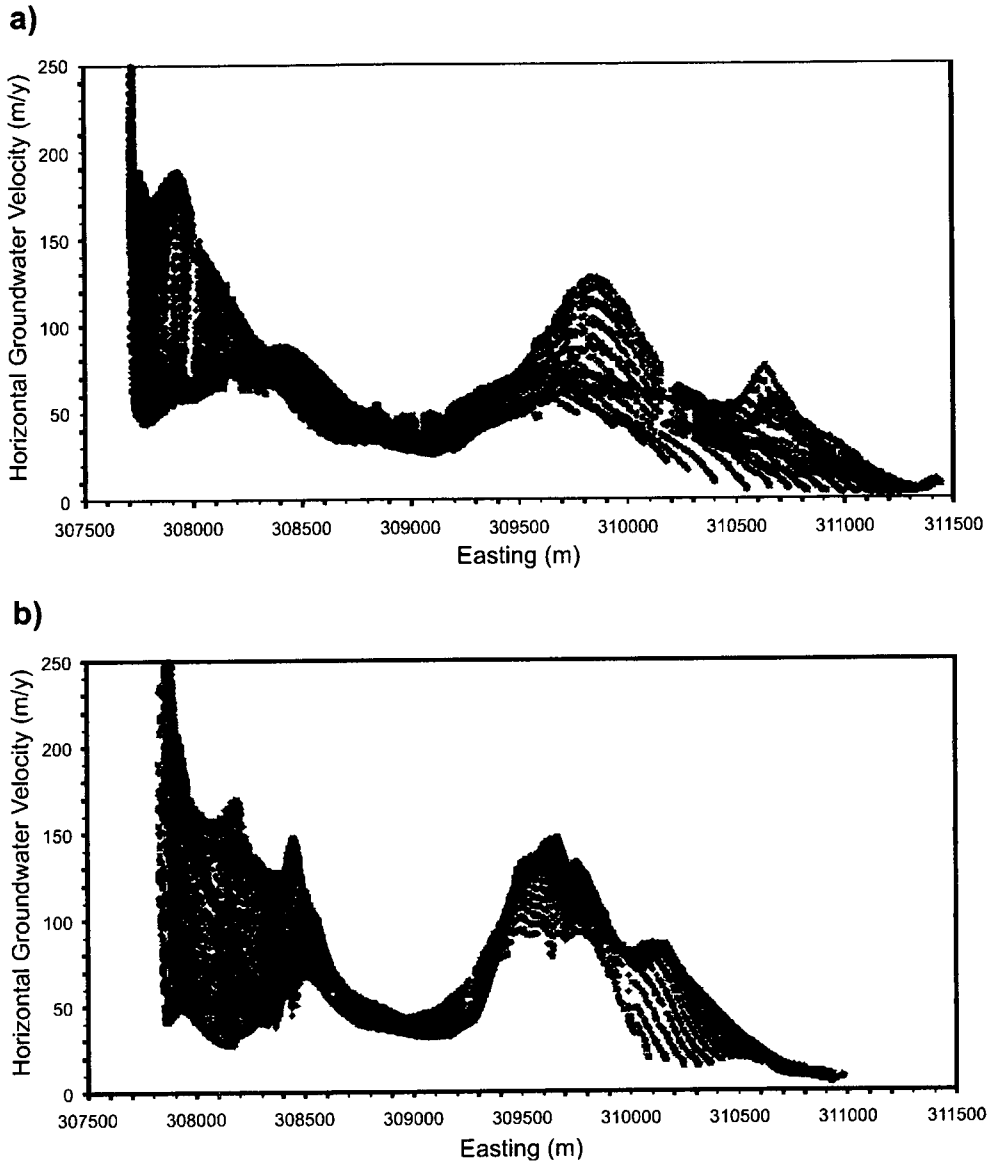


**Figure 4.10**. Velocities derived from particle tracking versus distance from tracking origin for the a) North and b) South Flow Paths (Murphy et al., 2009).

In spite of the inability of $^{3}H$-$^{3}He$ ages to provide direct estimates of groundwater velocity between sampling locations, there is strong coherence between the isotopic ages and model results which supports the use of parameters and boundary conditions currently used in the model. A model porosity to 0.35 produces the closest match between modeled and isotopic ages; this verifies previous estimates of porosity, so these ages can be used to estimate travel times from the TCE source zones to receptors. Groundwater velocities can be derived from the difference in transit time between sampling locations, which may be used to calculate the mean rate of groundwater flow from each source zone. The groundwater velocities can be related to the timing of TCE release to determine the history of TCE migration in the subsurface.

## 4.8 Conclusions

Tritium-helium ($^{3}H$-$^{3}He$) dating of groundwater was used to validate a numerical groundwater flow model developed to better define dissolved TCE transport and guide the implementation of plume control systems in a deltaic sand aquifer. This study closely integrates numerical modeling with the $^{3}H$-$^{3}He$ dating program to produce a framework for interpreting groundwater age distribution. The results offer unique information, requiring a minimal number of samples, which can be used for model calibration and validation. The approach used first involved detailed particle tracking along flow paths stemming from TCE source zones that were related to isotopic groundwater ages at sampling points projected on the particle tracking sections. $^{3}H$-$^{3}He$ ages were obtained and compared with advective tracking ages to assess the ability of the numerical model to reproduce the independently measured parameter of age. Results of the comparison reveal a good match between model ages and isotopic ages that further supports the use of a porosity of 0.36 and a recharge rate of 300 mm/y in the numerical model, which had been

measured independently of the $^3$H-$^3$He ages prior to this study. The match also corroborates the heterogeneous $K$ field defined by Ouellon *et al.* (2008a) that is currently being used in the numerical model. Furthermore, isotopic ages found across the prodeltaic silty aquitard provide a simple way to estimate $K_v$, a parameter that is difficult to calculate and rarely measured. The estimated value for $K_v$ is coherent with results of Ouellon *et al.* (2008a,b), which strongly supports the inferred anisotropy of the aquitard.

The ability to use groundwater ages to calibrate numerical models has some limitations. Advective travel times produced by the model do not correspond exactly with the ages measured by $^3$H-$^3$He dating at equivalent spatial positions. The effect of dispersion on concentrations of $^3$H and $^3$He in groundwater causes the measurement to represent an average age. Although this is minimal in the deltaic aquifer relative to other groundwater systems, heterogeneity in hydraulic conductivity at smaller scale than can be accounted for by the model will cause enough groundwater dispersion that $^3$H-$^3$He ages will depart from ages produced from model simulations. Small discrepancies in ages lead to large differences in the prediction of groundwater velocities between the model and calculations based on $^3$H-$^3$He ages. The use of groundwater ages to calibrate models should be restricted to a secondary independent means of calibrating the parameters used in a groundwater model, rather than an independent way of determining groundwater velocities.

Apart from serving as a target for validating the numerical model, the results of $^3$H-$^3$He dating play an important role as a groundwater tracer. Unexpectedly old ages and high concentrations of terrigenic helium indicate the upflow of TCE from a previously unrecognized source that migrates through units beneath the deltaic aquifer. These data are complementary to a geochemical tracing study by Murphy *et al.* (2009) that finds evidence for a distinct source of

TCE in the southwest portion of the study area. Further characterization of hydrogeological conditions in the underlying proglacial aquifer is required to ascertain the location of such a TCE source zone and the migration paths of emitted plumes.

Overall, this study further illustrates the important application of $^{3}H$-$^{3}He$ groundwater dating as an independent means of verifying numerical groundwater flow models. The constraints offered by isotopic ages are uniquely suited to the validation of groundwater velocity and transit times made by numerical models, which is commonly critically lacking. The study also provides an example of the integrated characterization and modeling of a complex heterogeneous system.

# 5.0 Geochemical tracers applied to the delineation of flow paths and the identification of TCE source zones in a valley fill aquifer system

## 5.1 Abstract

A geochemical characterization was carried out to better understand groundwater flow and TCE migration in a valley fill aquifer system. At 16 sampling locations, 63 discrete groundwater samples were obtained over the entire saturated thickness of an unconfined deltaic sand aquifer. At 5 locations, 6 samples were obtained from a proglacial aquifer separated from the deltaic aquifer by a locally discontinuous silty aquitard. Sampling was mostly carried out along two parallel flow paths (North and South), originating from two known TCE source zones, and on a downgradient section across the flow paths near receptors. These flow paths were defined by particle tracking with a numerical model and sampling points in monitoring wells were projected on particle tracking vertical sections along the two flow paths. In the deltaic aquifer, TCE plumes converge to form a single plume with an overall length and width of about 4 500 m by 500 m. The geochemical tracers considered include physicochemical parameters, major ions, stable isotopes $^{18}O$ and $^{2}H$, terrigenic $^{4}He$, perchlorate ($ClO_4$) and TCE. Geochemical patterns from individual parameters were contoured on the three vertical sections where the spatial distribution of hydrochemical facies was also shown. These contours show distinct patterns that are coherent with groundwater flow conditions. Geochemical facies were defined using multivariate statistical techniques, including principal component analysis (PCA) and cluster analysis carried out with two approaches that both defined 7 similar clusters. The two flow paths are characterized by distinct geochemical clusters related to water origins. A cluster on the South Flow Path has a distinct geochemical signature and originates from areas where groundwater from the underlying proglacial aquifer flows upward into the deltaic sand aquifer through aquitard windows. Upflow

locations correspond with increased TCE concentrations originating from a previously unrecognized TCE source zone in the southwest part of the study area. Clusters and specific tracers found at the downgradient section allow the zoning of the plume in three parts related to distinct TCE source zones. Geochemical tracers provided important insights on groundwater flow paths, exchanges between the two aquifers and definitive clues concerning the origin of TCE in a large "comingled" plume, which would be very difficult to obtain on the sole basis of hydraulic data or numerical modeling.

## 5.2 Introduction

The chemical and isotopic characteristics of groundwater are a function of its origin and flow history, which may lead to distinct spatial patterns in groundwater geochemistry. For instance, the stable isotope composition of groundwater ($^{18}O$ and $^{2}H$) reflects the conditions at the groundwater recharge location (Clark and Fritz, 1997). Inputs to the groundwater from anthropogenic activities at the surface that can affect groundwater chemistry by adding specific inorganic or organic components from point sources (landfills, lagoons, road salt, etc.) or diffuse sources (especially agricultural practices) (Hounslow, 1995; Domenico and Schwartz, 1998; Appelo and Postma, 2005). As groundwater flows away from its recharge location, there are processes occurring in the aquifer that cause its evolution towards a different composition, such as mixing, interaction with aquifer minerals, and microbiological activity. The original composition of recharging groundwater and its evolution along flow paths can impart geochemical characteristics to groundwater representing a distinct fingerprint that allows the tracing of flow paths from the recharge area, and the quantification of mixing between groundwaters of different origins (Keating and Bahr, 1998; Stuyfzand, 1999).

Groundwater sampled at any point in the flow system thus contains a hydrogeochemical signature that, integrated in the geological and hydrological contexts, may be used to interpret its origin, evolution and flow paths. The recognition of geochemical patterns in a groundwater system can greatly improve the understanding of groundwater flow at a variety of scales (Freeze and Cherry, 1979; Stuyfzand, 1999; Tóth, 1999; Glynn and Plummer, 2005). The use of geochemistry thus provides a powerful basis by which to conceptualize groundwater flow. Such a conceptual model deduced from isotopic and geochemical information is independent of hydraulic data and can thus be used to further constrain and validate numerical models (Reilly *et al.*, 1994). A combination of geochemical parameters offers a better possibility to distinguish groundwaters of distinct origins, since these parameters provide clues on either the conditions prevailing at their recharge point or along their flow paths. Since it cannot be known *a priori* which geochemical conditions or processes can lead to distinct signatures on groundwater, a range of geochemical parameters needs to be determined (Clark et al., 1998; Abbott et al., 2000; Cloutier et al., 2006; Koh et al., 2006; Moore et al., 2006; Bassett et al., 2008).

This paper reports on geochemical tracers that were used as part of an integrated study aiming to better represent groundwater flow and contaminant transport in a complex aquifer system where multiple TCE source zones are present. Understanding of the groundwater flow system and of the migration and fate of TCE will help provide independent constraints on the numerical model developed to represent groundwater flow in this system (Murphy *et al.,* 2009). This validation is important as the model is used to support environmental management decisions, including the implementation of plume control infrastructures. Geochemical sampling was designed with the help of the numerical model, which provided locations of likely flow paths originating from the two main known TCE source zone locations.

The classical approach to defining hydrochemical facies examines groundwater evolution in terms of the changes occurring over long timescales and wide areas, which involve significant reaction of groundwater with aquifer solids (Freeze and Cherry, 1979; Stuyfzand, 1999). In that perspective, most previous investigations that utilized statistical techniques to identify geochemical patterns were seeking to understand geochemical processes controlling groundwater evolution through time (Adar *et al.*, 1992; Melloul and Collin, 1992; Farnham *et al.*, 2000; Cloutier *et al.*, 2008). More local studies have focused on variations in geochemistry related to natural attenuation of contaminants (Weidmeyer *et al.*, 1998; Mayer *et al.*, 2001; Devlin *et al.*, 2002; Crowe *et al.*, 2004). First, the study site is small relative to other tracing studies, and focuses on local groundwater circulation and TCE transport over a longitudinal distance of about 3 km and a transverse distance of about 1 km. The aquifer of interest is a 20 to 30 m thick shallow unconfined sand within which groundwater has a residence time of less than 50 years (Chapter 4). Although TCE degradation products are observed in the system (Lefebvre *et al.*, 2003), degradation rates are relatively limited and the focus of the study is not natural attenuation since TCE plumes reach receptors. Given the context and objectives of the study, there is a greater impetus to identify differences in groundwater chemistry that can be related to its origin, rather than its evolution, to help identify flow patterns and TCE origins.

Since the geochemical characterization aims to validate the numerical groundwater flow model, especially with $^{3}H$-$^{3}He$ ages, sampling design and $^{3}H$-$^{3}He$ data interpretation were based on numerical modeling (Murphy *et al.*, 2009). The selection of samples in "meaningful" locations relative to flow conditions defined by the numerical model was paramount to facilitate the interpretation and minimize the number of samples required, as opposed to what would have been needed based on "random" sampling locations. Given the limited extent of the study area,

samples had to be collected in close proximity. Also in contrast to many other studies, samples had to be obtained across the entire saturated thickness in order to resolve from geochemical tracers the spatial distribution and provenance of TCE coming from the surface, laterally and from upflow through the basal aquitard. Rather than collecting many samples that only provide a two dimensional classification of hydrofacies, the 3-D distribution of groundwater geochemistry was established from two cross sections along groundwater flow paths originating from TCE source zones. These flow paths were defined on the basis of detailed particle tracking originating from the two main known source zones (Murphy *et al.,* 2009). Another cross section was located in a downgradient location, across the two flow paths, in an area just upgradient of receptors where plume control infrastructures could be installed.

The study reported in this paper thus provides an example of the practical application of geochemical tracers to the understanding of a complex flow system, and especially the complementary nature of independent geochemical and hydraulic data. Although the study site has relatively well defined geological and hydrogeological contexts, this geochemical investigation demonstrates the potential benefits of integrated multidisciplinary approaches to the characterization and interpretation of complex flow systems.

## 5.3 Study Site

The study area is the Valcartier sector, located 25 km northwest of central Quebec City (Figure 5.1). The area is at the margin of Laurentian Mountains and encompasses a relatively flat valley bounded by two large hills (Mount Rolland-Auger and Mount Brillant) and the Jacques-Cartier and Nelson Rivers. The area overlies a bedrock valley filled with up to 50 m of unconsolidated

Quaternary sediments including, from bottom to top, glacial and proglacial silty sand and gravel, glaciomarine silt, and deltaic sediments mostly made up of sand but including a wedge of prodeltaic silty sediments to the east of the area (Figure 5.2). The deltaic sand represents a high yield aquifer used for municipal and home water supply. Figure 5.1 shows the potentiometric surface of the regional deltaic sand aquifer, which is semi-confined under the prodeltaic silty aquitard in the eastern part of the study area. There is a groundwater divide to the east of the area and groundwater generally flows westward, except in the south where recharge from Mount Rolland Auger causes groundwater to flow northward. Vertical hydraulic gradients are very low in most of the study area so flow is predominantly horizontal, except near the groundwater divide where recharging groundwater has a greater vertical component. Vertical groundwater flow also occurs across the prodeltaic silty aquitard from the upper to the lower deltaic sand (Chapter 4).

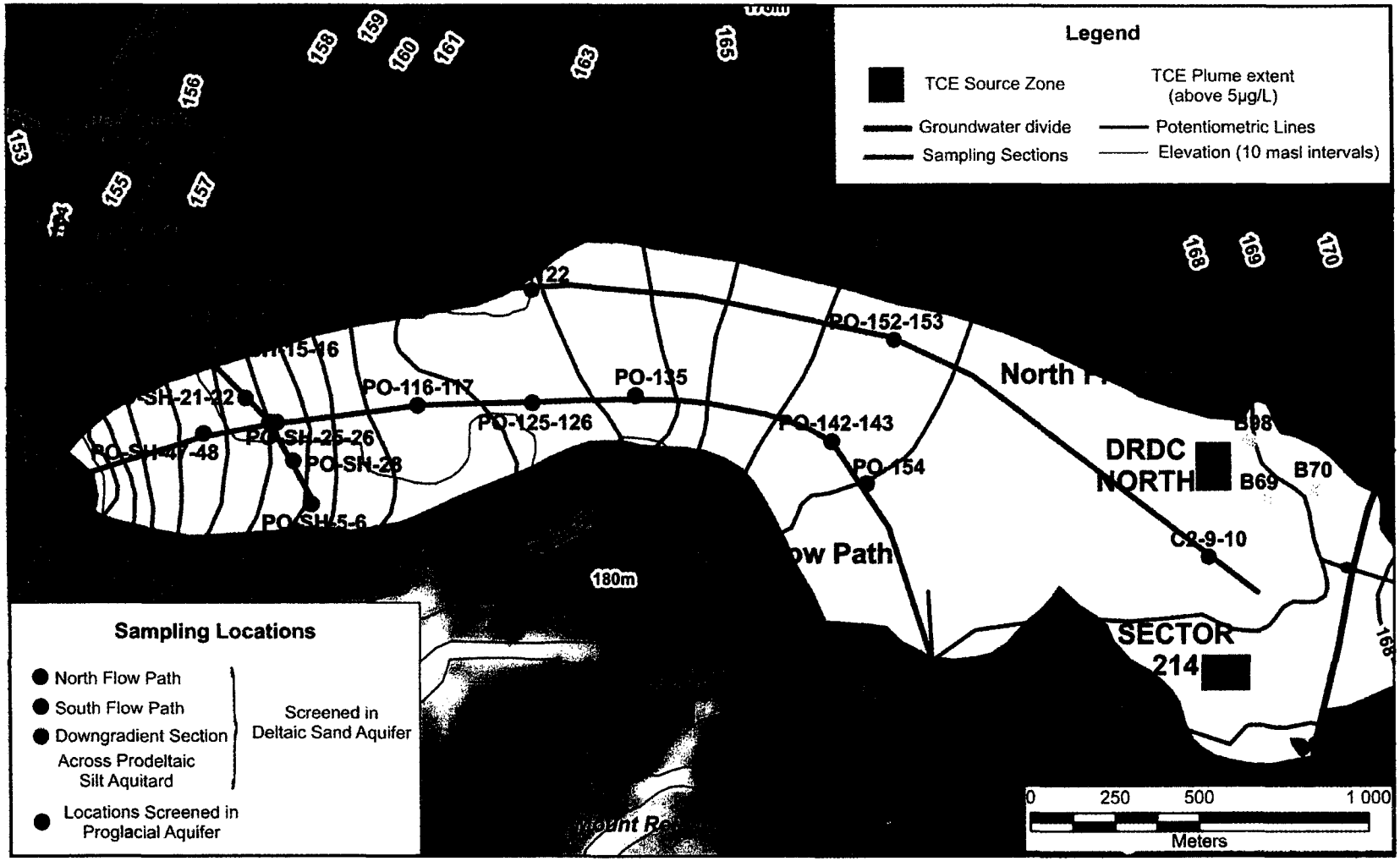


**Figure 5.1**. Location and physiography of study area (modified from Ouellon *et al.*, 2008b). The overall extent of the TCE plume in the deltaic aquifer is shown, as well as sampling locations along simulated flow paths originating from known source zones. Elevations are in meters above main sea level (MASL). The groundwater divide is for semi-confined conditions present to the east of the study area under a prodeltaic silty aquitard.

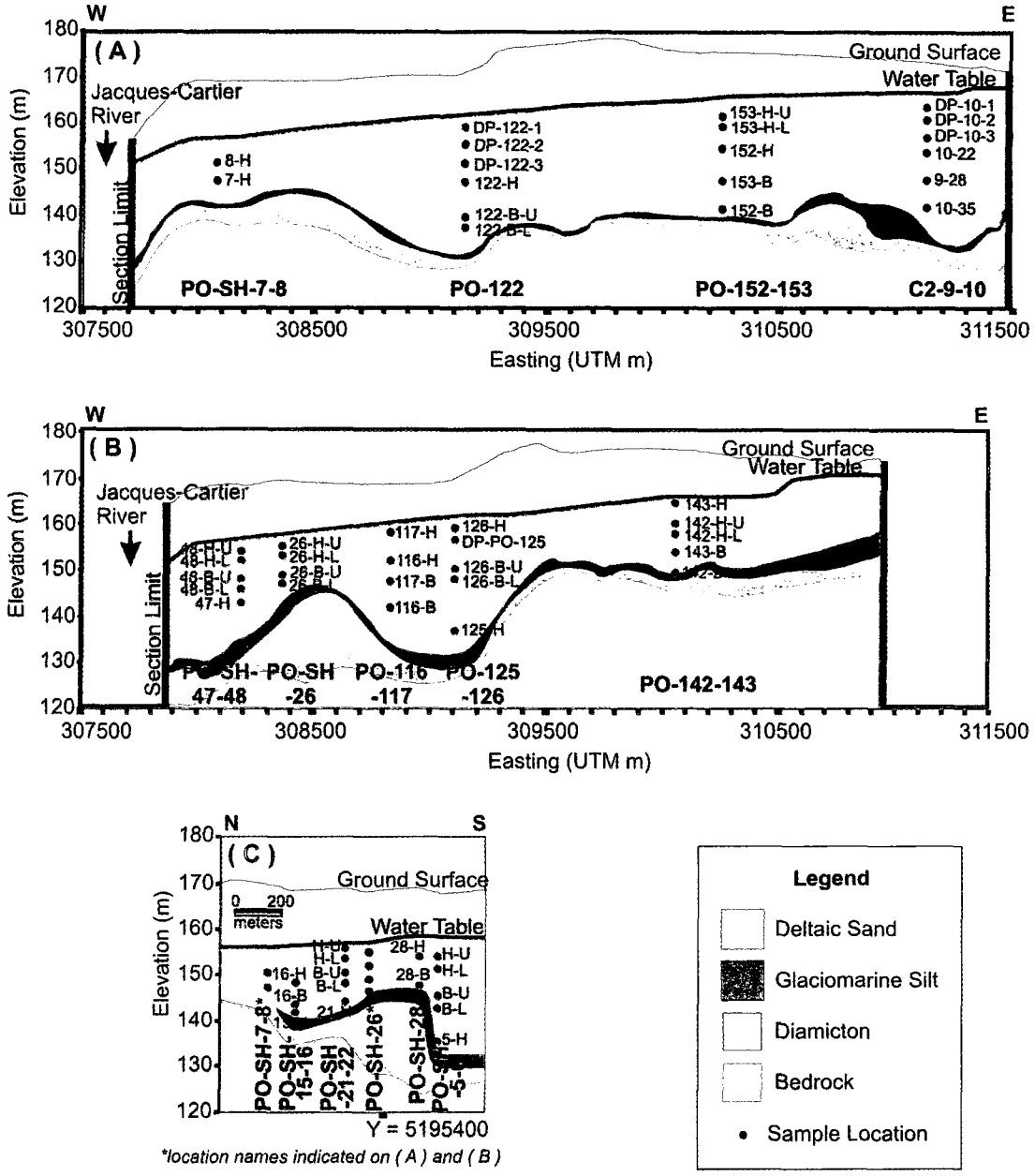


**Figure 5.2**. Sections showing hydrogeological context and sampling locations along and across flow paths (locations shown on Figure 5.1): a) North Flow Path, b) South Flow Path and c) Downgradient Section. From top to bottom, hydrogeological units include a deltaic unconfined aquifer separated from a semi-confined proglacial aquifer by a glaciomarine silty aquitard, which is locally absent.

Figure 5.1 shows the extent of trichloroethylene (TCE) in the deltaic sand aquifer with concentrations mostly between 5 and a few hundred μg/L with local highs above 590 μg/L, mostly near source zones. The TCE plume extends over a length of about 4.5 km by a width of about 500 m and originates from known source zones in the eastern part of the study area (Lefebvre *et al.*, 2003). Efforts to characterize the origin and migration of TCE are complicated by the coalescence of TCE plumes downgradient of source zones to form a larger plume. This plume integrates TCE-bearing groundwater from all sources, so it is difficult to distinguish TCE contributions from different source zones. TCE was released to Valcartier groundwater in waste that likely contained other substances and at locations under different conditions, so it is plausible that waste at each TCE source zone had different compositions. If these differences can be established and geochemical fingerprints are identified with each source zone, there is a way to relate the chemistry of groundwater in different parts of the TCE plume to its origin and thus verify groundwater flow paths.

## 5.4 Field and Laboratory Methods

Particle tracking with a steady-state numerical model of groundwater flow using FEFLOW was used to define two flow paths (North and South) related to groundwater flow and TCE migration from two groups of source zones. Figure 5.1 shows these flow paths from their origin to their end in the Jacques-Cartier River. The North Flow Path originates half way between two groups of source zones emitting TCE mostly from above the prodeltaic silty aquitard. A single flow path was defined from these source zones because the locations of paths originating from these sources were found to be very close a few hundred meters downgradient of their origin. The South Flow Path starts in deltaic sands downgradient of a source zone located on the southern

edge of the valley fill and laterally receiving groundwater recharging to the north of Mount Rolland-Auger.

The North and South Flow Paths were used to select monitoring wells to be used for groundwater sampling. A downgradient section oriented across the flow paths was also selected for sampling. Nearly 1000 observation wells have been installed in the study area and at most locations two boreholes with dual screen installations allow sampling over the entire saturated thickness in deltaic sands (Murphy *et al.*, 2009). Rather than randomly sampling a large number of wells, sampling locations were primarily located at wells allowing the sampling of groundwater flowing along two flow paths. Figure 5.2 shows hydrostratigraphic sections along the North and South Flow Paths and at the Downgradient Section. Well locations that lie on or close to both flow paths were chosen for sampling, where groundwater could be sampled at multiple depths in one location. Direct push well installations completed existing wells in three sampling locations.

Three locations located north of the origin of the North Flow Path were chosen to examine the effects of the prodeltaic silty aquitard on groundwater geochemistry. The prodeltaic silty aquitard extends under these locations where groundwater was sampled in the deltaic unit immediately above and below the aquitard. This was done because groundwater and TCE emitted from the source zones located above the aquitard must flow vertically downward before it enters the lower deltaic aquifer and migrates west. The unit contains finer grained material with some organic carbon (TOC = 0.16%) that may affect groundwater geochemistry (Lefebvre *et al.*, 2003).

Finally, wells screened in the proglacial aquifer were chosen to examine groundwater geochemistry as it may relate to TCE migration; TCE may have entered the proglacial aquifer in

Lagoon C, which was excavated into this unit, or in other locations where exchange occurs between the deltaic and proglacial aquifers. There are also some waste disposal locations excavated in the proglacial aquifer or bedrock on the northern flank of Mount Rolland-Auger that are also potential sources of TCE to the groundwater in the proglacial aquifer or possibly the bedrock. Sampling locations and sampling points used in the areas of interest are shown on Figures 5.1 and 5.2. A total of 69 samples were collected from 21 well locations between November 2007 and June 2008. The screen lengths of available observation wells allowed discrete sampling at two or three levels within the screened interval in some wells. Within the high permeability deltaic unit (where no prodeltaic silt is present), insignificant vertical hydraulic gradients have been measured between screened intervals. Vertical gradients are thus assumed to be insignificant over the limited lengths of screens, thus avoiding vertical groundwater circulation and mixing within the observation wells.

A multi-parameter TROLL 9500 – WQP-100 was used to measure field parameters (temperature, pH, dissolved oxygen, oxidation-reduction potential and electrical conductivity) in-situ prior to sample collection. The probe was lowered into the well to a depth corresponding with the location where samples were collected for laboratory analyses, and a measurement was recorded once all parameters had stabilized.

Hydrasleeve bulk samplers were used to collect water samples for analysis of major ion concentrations and stable isotope ratios from a discrete interval along the well screen (GeoInsight, 2006; ITRC 2006 and 2007). The disposable polyethylene 'sleeve' is slowly lowered into the well to the target sampling depth using a retaining cable with a weight attached to the sleeve base. They are left at the sampling depth for a minimum of 5 minutes to stabilize the water column, after which the sleeve is pulled in quick, short strokes up and down several

times. Water enters the sleeve through a flexible check valve at the top of the sleeve that is opened when pulled upward to collect a core of water roughly the length of the sampler (71 cm). The water-filled sleeve is then smoothly and rapidly pulled to the surface, where the sleeve is then punctured with a pointed tube to discharge the water into 500 mL sample bottles.

Major dissolved ions were analyzed by the Department of Earth Sciences Geochemistry Lab, University of Ottawa. All water samples collected in 60 mL bottles were filtered in the lab on 0.45 μm filter paper. DIC species ($H_2CO_3$, $HCO_3^-$, $CO_3^{2-}$) were determined by alkalinity titration on 25 mL samples with 1.0 M $HNO_3$ using a Hach® digital titrator. Major cations ($Ca^+$, $Mg^+$, $Na^+$, $K^+$, Fe (total), $Sr^{2+}$, $Si^{4+}$, $Al^{3+}$) in 15 mL aliquots acidified with 15 μL pure $HNO_3$ were analyzed by ICP-AES. Major anions ($Cl^-$, $SO_4^{2-}$, $NO_3^-$) in 15 mL aliquots were analyzed by ion chromatography.

Stable isotope ratios of hydrogen ($^2H/^1H$) and oxygen ($^{18}O/^{16}O$) in groundwater were determined by the G.G. Hatch Stable Isotope Laboratory at the University of Ottawa. Hydrogen isotopes are determined on a 200 μL aliquot that is equilibrated with a 2% hydrogen – 98% He gas mixture using Hoko beads as a catalyst, and the $H_2$ gas is analyzed on a Finnigan MAT Delta plus XP + Gasbench mass spectrometer. Oxygen isotopes are determined similarly using a 2% $CO_2$ – 98% He mixture, with the $CO_2$ being analyzed on the same mass spectrometer. Results for both hydrogen and oxygen are normalized to Vienna Standard Mean Ocean Water (V-SMOW).

Concentrations of TCE and perchlorate in Valcartier groundwater were obtained during groundwater monitoring in 2007 (B. Michaud, pers. comm, 2008). Perchlorate is a conservative tracer that is known to be present in Valcartier groundwater that can be used in addition to other geochemical parameters to help identify patterns and relate TCE with source zones (Motzer,

2001; Trumpolt *et al.*, 2005). Terrigenic $^4He$ concentrations were measured on a subgroup of samples that were analyzed in a study done in parallel with the present one where groundwater in Valcartier was dated using the $^3H$-$^3He$ method (Chapter 4). Terrigenic $^4He$ ($^4He_{terr}$) is derived from the radioactive decay of U and Th (Mamyrin & Tolstikhin, 1984) contained in minerals in the soil, the aquifer or underlying geologic units, and can be an indicator of lithology encountered or mixing between groundwater in different hydrogeologic units.

## 5.5 Multivariate Data Analysis

### 5.5.1 Data Selection and Preparation

Multivariate statistical techniques can be used to classify groundwater samples based on their geochemistry into groups of similar composition whose spatial distribution should help better understand the relation between water chemistry and the origin of groundwater in Valcartier (Davis, 2002; Güler *et al.*, 2002; Cloutier *et al.*, 2008). Principal components and hierarchical cluster analyses were selected to define groundwater geochemical facies.

The data set of geochemical parameters required some preparation before multivariate techniques could be applied. Descriptive statistics, histograms and bivariate graphs of geochemical parameters were used for the selection of parameters to be considered in the analyses. Certain variables were excluded from the analyses on the following basis: 1) parameters with additive characteristics (specific conductivity) and those with many samples below the detection limit (Fe, Al) were first dismissed, 2) parameters were also excluded if several samples were either missing the parameter or not analyzed (perchlorate, TCE, $^4He_{terr}$),

and 3) strongly correlated parameters (Mg, K) with other more significant ones were excluded to avoid redundant parameters providing the same information about groundwater origin.

Nitrate ($NO_3^-$) is a parameter that was included in the multivariate analyses despite some samples having concentrations below the detection limit; these are referred to as censored data. $NO_3^-$ is a valuable parameter for this study, for although it is not a conservative tracer, it does provide an indication of recharge near human activity (e.g. fertilizers or sewage). For samples below the detection limit for $NO_3^-$, the censored values had to be replaced by unqualified values (Güler *et al.*, 2002). For this study, the censored data was replaced with the value of the detection limit in the data set used for statistical analyses. The final data set was a matrix of 69 rows of samples by 13 columns of chemical parameters (variables).

The entire data set is available in Appendix A. Table 5.1 shows the descriptive statistics obtained for all parameters used in the multivariate analyses. Multivariate analyses were performed on standardized data to ensure that the data were homoscedastic, or equally weighted (Davis, 2002). Standardized values $Z_i$ were calculated for each variable $i$ by subtracting the mean $\bar{X}$ from each analytical value then dividing by the standard deviation $\sigma$ of the distribution:

$$Z_i = \frac{X_i - \bar{X}}{\sigma} \qquad 5.1$$

**Table 5.1**. Descriptive statistics of the geochemical tracers (highlighted parameters are those used in multivariate statistical analyses).

| | Parameter | Units | N | Mean | Median | Minimum | Maximum | Lower Quartile | Upper Quartile | Standard Deviation |
|---|---|---|---|---|---|---|---|---|---|---|
| Stable Isotopes | $\delta^{18}O$ | ‰ *VSMOW* | 69 | -12.06 | -12.00 | -12.72 | -11.45 | -12.24 | -11.92 | 0.27 |
| | $\delta^{2}H$ | ‰ *VSMOW* | 69 | -84.93 | -85.00 | -91.50 | -78.17 | -87.20 | -82.79 | 2.87 |
| Major Ions | $Ca^{2+}$ | *mg/L* | 69 | 15.50 | 11.19 | 1.11 | 52.09 | 7.96 | 22.25 | 12.07 |
| | $Mg^{2+}$ | *mg/L* | 69 | 3.73 | 2.14 | 0.30 | 18.88 | 1.10 | 5.37 | 4.05 |
| | $Sr^{2+}$ | *mg/L* | 69 | 0.102 | 0.090 | 0.010 | 0.277 | 0.045 | 0.141 | 0.067 |
| | $K^{+}$ | *mg/L* | 69 | 1.80 | 1.69 | 0.33 | 5.42 | 1.01 | 2.22 | 1.06 |
| | $Na^{+}$ | *mg/L* | 69 | 27.46 | 22.05 | 1.04 | 74.10 | 10.34 | 47.03 | 20.50 |
| | $SO_4^{2-}$ | *mg/L* | 69 | 13.13 | 11.24 | 3.70 | 52.09 | 7.74 | 16.72 | 8.68 |
| | $Cl^{-}$ | *mg/L* | 69 | 41.30 | 28.80 | 0.48 | 147.58 | 7.93 | 67.84 | 37.54 |
| | $NO_3^{-}$ | *mg/L* | 69 | 2.36 | 1.02 | 0.00 | 9.31 | 0.00 | 4.60 | 2.75 |
| | $HCO_3^{-}$ | *mg/L* | 69 | 44.13 | 35.58 | 0.01 | 156.86 | 22.47 | 54.66 | 32.91 |
| | Si | *mg/L* | 69 | 6.15 | 5.87 | 2.57 | 10.20 | 4.13 | 8.12 | 2.26 |
| Field Parameters | T | *°C* | 69 | 7.71 | 7.62 | 6.10 | 12.51 | 7.17 | 8.11 | 1.21 |
| | Dissolved $O_2$ | *% saturation* | 69 | 46.5 | 52.4 | 0.0 | 95.1 | 30.4 | 64.9 | 24.1 |
| | Conductivity | *µS/cm* | 68 | 272.9 | 266.7 | 25.4 | 675.7 | 140.0 | 365.3 | 174.4 |
| | pH | - | 69 | 6.24 | 6.20 | 5.23 | 7.59 | 5.79 | 6.62 | 0.55 |
| | ORP | *mV* | 69 | 171.6 | 184.0 | -113.5 | 311.4 | 124.0 | 236.0 | 88.6 |
| Supplementary Parameters | $^{4}He_{terrigenic}$ | *cc/cc* | 50 | 13.0 | 1.8 | 0.0 | 387.8 | 0.0 | 8.3 | 54.7 |
| | $ClO_4^{-}$ | *µg/L* | 57 | 1.67 | 0.05 | 0.00 | 73.00 | 0.00 | 0.14 | 9.69 |
| | TCE | *µg/L* | 60 | 74.09 | 8.30 | 0.00 | 1600.00 | 0.00 | 78.75 | 215.67 |

### 5.5.2 Principal Components Analysis (PCA)

Principal components analysis (PCA) is a technique that reduces the data to fewer dimensions to help reveal patterns in the data matrix. Variables are represented by principal components, which can be displayed for all data on a scatter plot. Each principal component, which usually stands for more than one of the original variables, accounts for a proportion of variance in the data; if that variance is greater than any individual original variable (i.e. the eigenvalue is greater than 1), the principal component is retained (Davis, 2002).

PCA was applied to the standardized geochemical data set from Valcartier groundwater. The analysis produced three components with eigenvalues greater than 1 that account for 70% of the total variance in the data (Table 5.2). The principal component loadings for geochemical parameter, which indicate the relative importance of each geochemical parameter for the three main principal components, are shown on Figure 5.3. Loadings greater than 0.60 or less than -0.60 are considered a very important contribution to a principal component; each of the three main components has two or more geochemical parameters related to it. Table 5.2. Eigenvalues and explained variance of Principal Components.

**Table 5.2**. Eigenvalues and Explained Variance of the Principal Components.

| | PC1 | PC2 | PC3 |
|---|---|---|---|
| Eigenvalue | 4.293 | 2.579 | 2.226 |
| Explained Variance (%) | 33.0 | 19.8 | 17.1 |
| Cumulative Variance (%) | 33.0 | 52.9 | 70.0 |

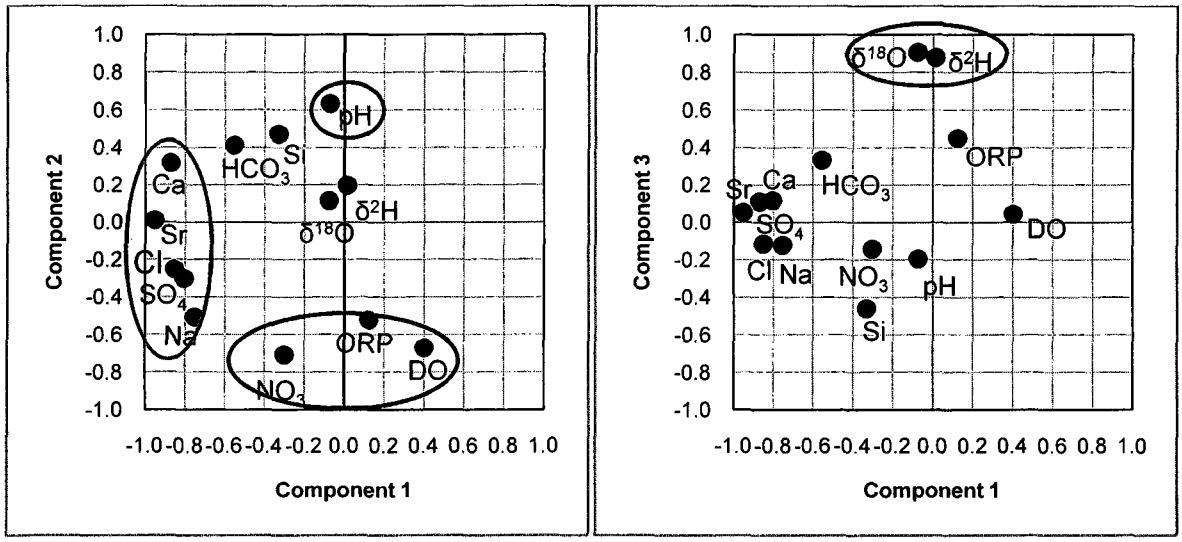


**Figure 5.3**. Loadings of geochemical parameters for the first three principal components.

Component 1 explains 33.0% of the total variance in the data set, and has high negative loadings for Cl, $SO_4$, Ca, Na, and Sr, which implies that Component 1 is related mostly to concentrations of major ions. Groundwater samples with high positive scores for principal component 1 therefore generally had low concentrations of these solutes, whereas samples with negative scores had higher concentrations. Component 2, which accounts for 19.8% of the variance, has negative loadings in $NO_3$, dissolved oxygen and ORP and a positive loading for pH, which relate Component 2 mostly to geochemical conditions. Higher scores for Component 2 therefore are usually either particularly low concentrations of $NO_3$ or dissolved oxygen and have higher pH. 17.1% of the total variance is represented by Component 3, which has very high positive loadings in $\delta^{18}O$ and $\delta^{2}H$, and samples with high positive scores are relatively enriched in heavy isotopes. Since stable isotopes are the geochemical parameters whose concentrations are the most strongly related to a specific flow path (North or South), this component can provide important clues regarding groundwater origin.

### 5.5.3 Cluster Analyses

*Hierarchical Cluster Analysis (HCA)*

Cluster analysis is a technique that classifies data into various groups based on their similarity (Davis, 2002). When hierarchical clustering is performed, a dendrogram is produced that shows the relative similarities of data points based on the selected variables. For the standardized Valcartier geochemical data set, hierarchical cluster analysis (HCA) was done using the Euclidean distance as a measure of similarity to group the data. Ward's method was chosen as a linkage rule, which combines clusters iteratively to minimize the sums of squares in the clusters at each step (Davis, 2002).

The clusters are branches of the dendrogram linked at a distance (called the phenon line) defined by the user, shown in Figure 5.4. In this study, four groups and seven subgroups were found at Euclidean linkage distances of 24 and 10, respectively. Each cluster contains samples that are more similar to each other geochemically than samples in other clusters, and will herein be referred to as groundwater facies and subfacies. Facies C and D are joined at a closer linkage distance than facies A and B, and samples in facies C are the most similar to each other. Of the subfacies, samples in A2 have the lowest linkage distance, and subfacies D1 and D2 are the least similar, as they have the highest linkage distance.

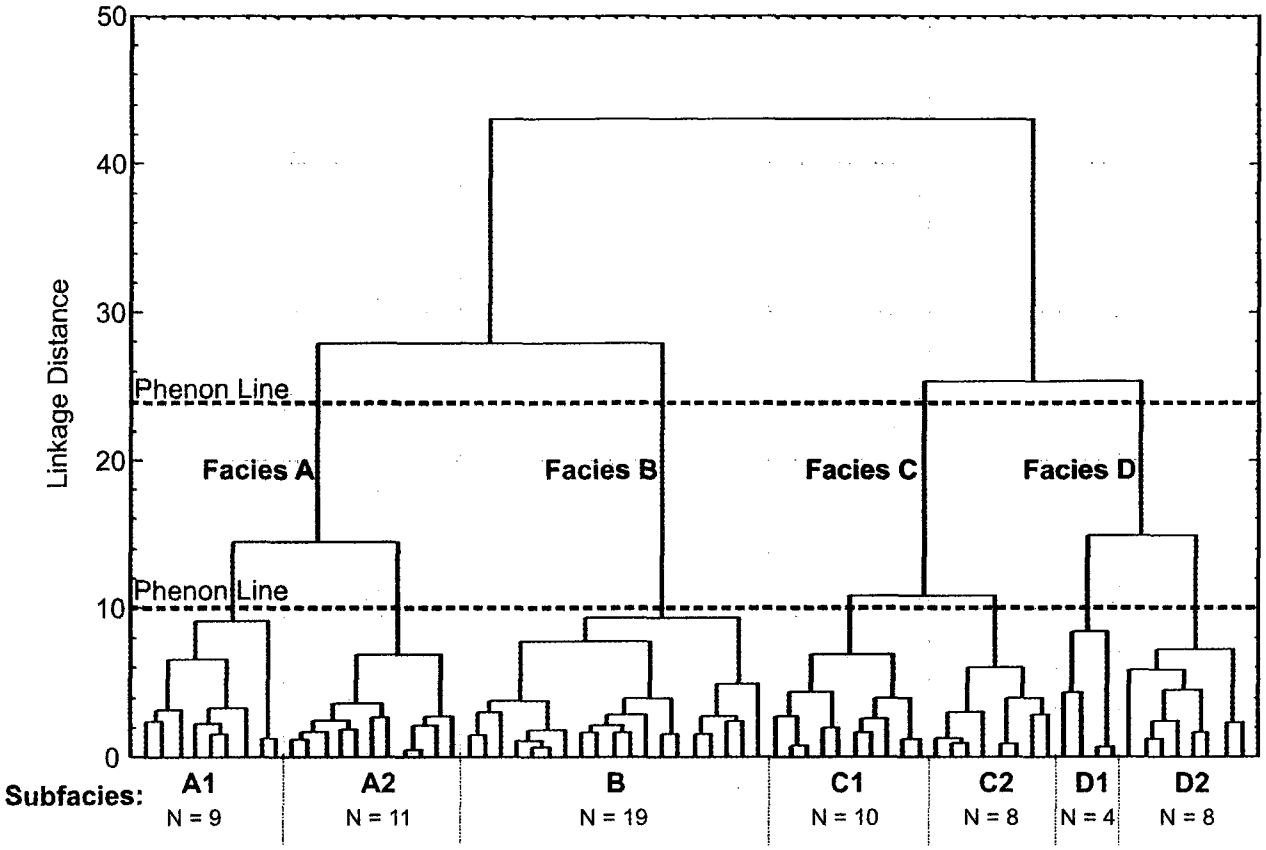


**Figure 5.4.** Dendrogram showing the linkage distances between 69 groundwater samples resulting from hierarchical cluster analysis done using Ward's Method as a linkage rule and using Euclidean distance as a measure of distance. The phenon lines represent the subdivision of clusters into facies (at a linkage distance of 24) and subfacies (at a linkage distance of 10).

*Agglomerative Model-based Clustering (AMBC)*

A second method of clustering was performed on the standardized data to compare with the HCA classification. The method used was agglomerative model-based clustering (AMBC) using an Expectation-Maximization algorithm to merge clusters in order to optimize the classification likelihood (Martinez and Martinez, 2005). An advantage of the output from AMCB is that in addition to classifying samples into discrete clusters, AMCB provides the uncertainty that each sample belongs to the group it is assigned to.

The classification results and associated uncertainties of the AMBC performed on the Valcartier data are provided in the supplementary electronic data along with the results from HCA. As with HCA classification, AMBC placed the data into 7 groups, many of which are nearly identical to the HCA clusters. Samples in clusters 1 and 2 correspond with HCA subfacies A1, and compared with the HCA results, represents a lower linkage distance from 10 down to 8. Cluster 3 is the same as HCA facies A2, Cluster 4 is the same as HCA facies D1 (but does not include sample C2-10-35), and Cluster D2 consists of HCA facies G (except sample PO-SH-48-H-L). Cluster 6 contains HCA facies C, which are linked at a Euclidean distance of about 11. Cluster 7 consists almost entirely of the HCA facies C, plus sample PO-128 which was classified with other proglacial aquifer groundwater samples in facies A by HCA. These results are presented in Appendix A.

## 5.6 Geochemical Patterns

### 5.6.1 Relationships between Geochemical Tracers

Table 5.2 shows the descriptive statistics of geochemical parameters for Valcartier groundwater samples. Samples have variable concentrations of all major ions, which all have positively skewed distributions due to some samples having very high concentrations. Cl, $HCO_3$, Na, Ca and $SO_4$ concentrations exceed 50 mg/L in some samples. Dissolved oxygen ranged between 0 and 95% saturation, and pH was between 5.23 and 7.56. Some samples contained perchlorate, though only a few exceeded 0.10 µg/L.

The relationships between some geochemical parameters are shown on Figure 5.5, which displays bivariate plots of selected parameters. Fig. 5.5a shows the stable isotope composition of

Valcartier groundwater, which plots just below the local meteoric water line for Ste. Agathe, Quebec. Groundwater on the South Flow Path is more enriched in heavy isotopes than groundwater on the North Flow Path. Of the downgradient samples, groundwater of facies B is also notably enriched relative to facies A and C. The reason for this enrichment is not currently understood. Within subfacies A1, groundwater in the proglacial aquifer is more enriched than groundwater above and below the prodeltaic silty unit, similar to NFP samples. On Fig. 5.5b, the distinction between sample locations is less clear, but there is a strong distinction between facies that can be identified. Subfacies A1 has low DO and relatively low conductivity, whereas facies D has high conductivity and low DO. Subfacies A2, B and C2 have a range in composition, subfacies C1 having slightly higher specific conductivity. Fig. 5.5c shows that Cl and Na are correlated, but different facies show distinct patterns in slope: for instance, subfacies D1 has a much higher Na:Cl ratio than D2. Groundwater in facies A has relatively low concentrations of both Na and Cl, whereas facies C has higher concentrations. Facies B has a range of concentrations that are close to a 1:1 ratio. Finally, Fig. 5.5d shows that although Ca and Na do not appear to be correlated, facies plot in distinct regions of the graph. There is very clear separation between subfacies, especially D1 with very high Na concentration, and D2, which is higher in Ca.

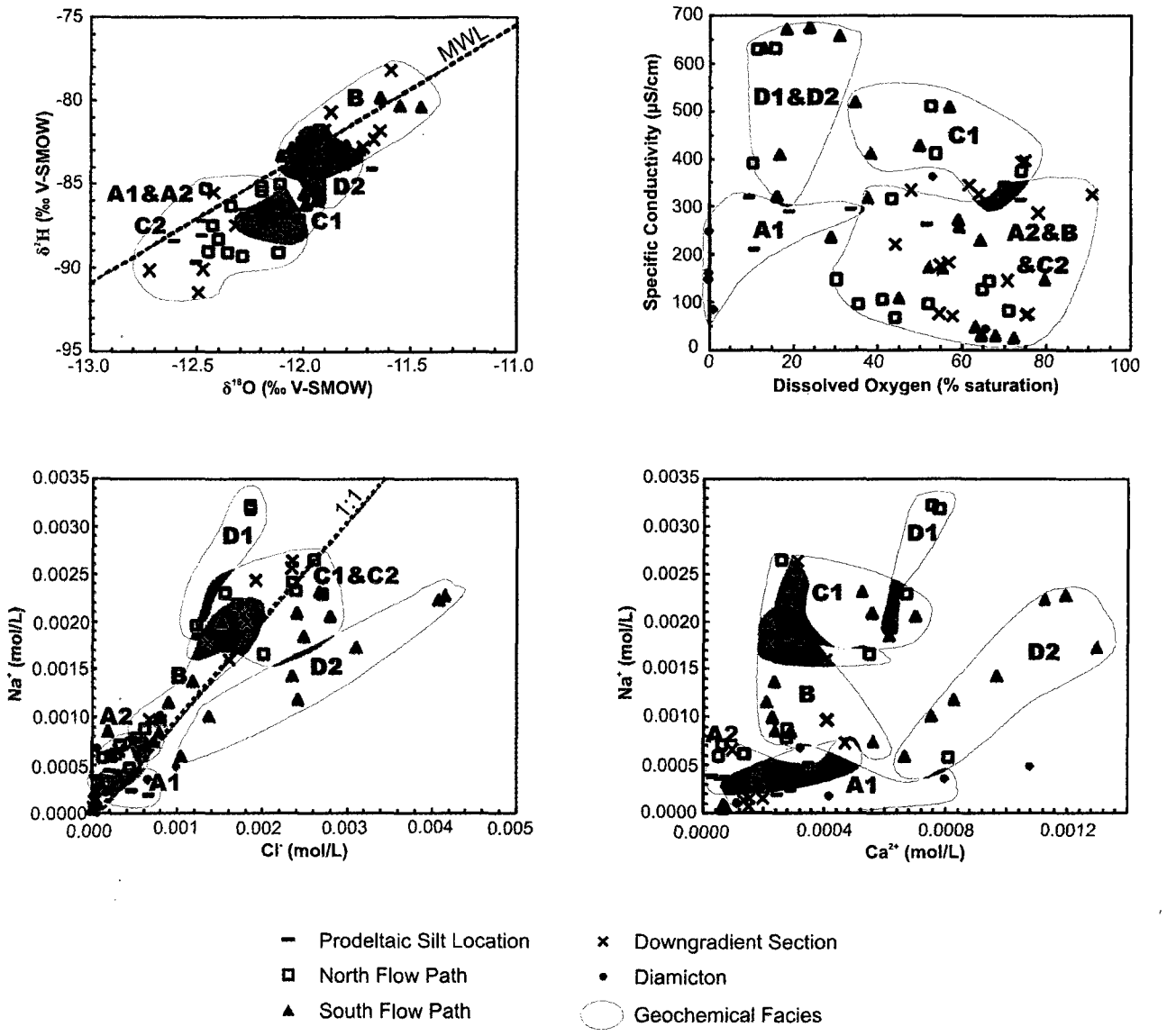


**Figure 5.5**. Relationships between geochemical tracers a) stable isotopes, b) dissolved oxygen and specific conductivity, c) Cl and Na and d) Ca and Na. Samples are displayed by facies as defined by HCA (symbols) and by location (colour). * MWL = Meteoric Water Line for Ste. Agathe (Fritz *et al.*, 1987)

### 5.6.2 Distribution of Clusters related to Principal Components

A weakness of cluster analysis is that no information is provided on the distribution of variables for each geochemical facies, so the mean and median values of variables for each subfacies found using HCA were calculated (Table 5.3). The principal component scores of samples

**Table 5.3**. Mean and median values of geochemical parameters and principal component loadings for HCA clusters (Bold values are highest values; underlined values are lowest values).

| Parameter | A1 | | A2 | | B | | C1 | | C2 | | D1 | | D2 | |
|---|---|---|---|---|---|---|---|---|---|---|---|---|---|---|
| | Mean | Median | Mean | Median | Mean | Median | Mean | Median | Mean | Median | Mean | Median | Mean | Median |
| $\delta^{18}O$ | -12.09 | -11.98 | -12.37 | -12.42 | **-11.80** | **-11.80** | -12.07 | -12.08 | -12.34 | -12.37 | -11.99 | -11.99 | -11.96 | -11.96 |
| $\delta^{2}H$ | -85.28 | -84.50 | -87.68 | -87.62 | **-82.01** | **-82.47** | -85.25 | -85.73 | -88.13 | -88.07 | -85.22 | -85.56 | -83.92 | -83.65 |
| $Ca^{2+}$ | 11.71 | 9.77 | 6.15 | 5.30 | 9.65 | 9.12 | 18.15 | 16.71 | 12.09 | 11.07 | 32.24 | 30.58 | **38.27** | **35.99** |
| $Mg^{2+}$ | 2.94 | 3.37 | 1.53 | 1.09 | 1.76 | 1.27 | 5.73 | 5.91 | 2.00 | 1.41 | 2.55 | 1.87 | **12.11** | **12.82** |
| $Sr^{2+}$ | 0.062 | 0.046 | 0.042 | 0.033 | 0.069 | 0.077 | 0.143 | 0.149 | 0.108 | 0.102 | 0.186 | 0.187 | **0.205** | **0.206** |
| $K^{+}$ | 1.47 | 1.27 | 1.10 | 0.92 | 1.35 | 1.37 | 1.92 | 1.90 | 1.66 | 1.60 | 4.41 | 5.02 | 2.87 | 2.67 |
| $Na^{+}$ | 7.09 | 5.71 | 11.53 | 13.76 | 20.73 | 22.05 | 51.52 | 51.49 | 42.49 | 46.67 | **50.85** | **59.15** | 31.50 | 29.84 |
| $SO_4^{2-}$ | 8.66 | 8.70 | 6.26 | 5.66 | 9.57 | 9.10 | 18.38 | 19.35 | 15.17 | 15.10 | **35.76** | **37.47** | 16.13 | 16.01 |
| $Cl^{-}$ | 9.64 | 7.49 | 8.53 | 9.42 | 26.11 | 27.87 | **82.32** | **84.59** | 59.50 | 63.22 | 52.44 | 54.43 | **82.98** | **84.95** |
| $NO_3^{-}$ | 0.60 | 0.40 | 0.51 | 0.00 | 1.49 | 1.20 | 4.24 | 4.62 | 6.46 | **6.60** | **6.83** | **6.60** | 0.23 | 0.00 |
| $HCO_3^{-}$ | 26.36 | 30.50 | 29.31 | 26.10 | 41.51 | 36.60 | 34.64 | 32.81 | 25.18 | 25.42 | 90.12 | **94.97** | **98.56** | 84.38 |
| Si | 5.56 | 5.24 | 7.48 | 8.12 | 4.51 | 4.23 | 8.09 | 7.78 | 5.03 | 5.21 | 3.14 | 2.90 | **9.10** | **9.55** |
| T | 7.56 | 7.50 | 7.55 | 7.61 | 6.89 | 6.55 | 7.81 | 7.89 | 8.62 | 8.53 | **10.60** | **11.35** | 7.58 | 7.60 |
| Dissolved $O_2$ | 15.6 | 9.6 | 53.1 | 51.9 | 61.7 | 59.4 | 56.2 | 55.5 | **63.8** | **67.8** | 22.7 | 13.6 | 18.7 | 17.8 |
| Conductivity | 199.6 | 210.0 | 142.9 | 107.1 | 162.5 | 169.7 | 424.4 | 411.2 | 279.9 | 319.1 | 503.2 | 509.6 | **514.5** | **632.0** |
| pH | 6.39 | 6.37 | **6.76** | **6.82** | 5.97 | 5.85 | 6.16 | 6.07 | 5.78 | 5.77 | 6.49 | 6.29 | 6.45 | 6.47 |
| ORP | 45.0 | 92.7 | 198.9 | 190.5 | **232.8** | 236.0 | 144.4 | 156.0 | 208.7 | 202.3 | 225.2 | **256.2** | 101.1 | 135.0 |
| $^{4}He_{ter}$ | 6.0 | 8.3 | 5.0 | 2.1 | **29.0** | 0.4 | 3.9 | 2.4 | 1.3 | 0.7 | 2.0 | 2.2 | 18.3 | **20.8** |
| $ClO_4^{-}$ | **10.44** | 0.00 | 0.11 | 0.05 | 0.06 | 0.00 | 1.36 | **0.49** | 1.22 | 0.09 | 0.10 | 0.10 | 0.02 | 0.00 |
| TCE | **273.90** | 4.10 | 41.27 | 9.00 | 30.47 | 4.40 | 44.66 | 60.00 | 0.30 | 0.00 | 0.00 | 0.00 | 80.38 | **87.50** |
| PC1 | 1.253 | 1.256 | **1.880** | **1.964** | 1.207 | 0.961 | -1.577 | -1.545 | -0.249 | -0.442 | **-3.288** | **-3.500** | -2.999 | -2.718 |
| PC2 | 1.630 | 1.950 | 0.679 | 0.722 | -0.434 | -0.729 | -0.874 | -0.840 | -2.331 | -2.481 | -0.972 | -1.301 | **2.174** | **2.119** |
| PC3 | -0.549 | 0.268 | -1.516 | -1.481 | **1.681** | **1.436** | -0.649 | -0.873 | -1.230 | -1.260 | 0.986 | 0.820 | 0.256 | 0.299 |

distinguished by geochemical facies are presented on scatter plots in Figure 5.6. Samples in facies A generally have positive scores for PC1 and PC2 because they have low concentrations of major ions and high pH, but many have negative scores for PC3 because samples are relatively depleted in heavy stable isotopes. Facies A1 samples differ from A2 samples in that they have slightly higher concentrations of most major ions, less dissolved oxygen (DO) and lower oxidation-reduction potential (ORP); there is also terrigenic $^4He$ present in many samples in A that were analysed for He and Ne. Facies C has positive scores for PC1 and PC3, being relatively low in solutes and isotopically enriched, and has varying scores for PC2. These samples also have high ORP, low pH and low temperature.

Facies C has negative or low positive scores for PC1, PC2 and PC3, with C1 having higher solute concentrations, less dissolved oxygen, and a higher degree of isotopic enrichment than facies C2, which also has a higher average ORP and lower pH. All samples of facies D have negative scores for PC1, but subfacies D1 has negative scores for PC2 and positive score for PC3.However, subfacies D2 shows the opposite pattern: low DO and high solute concentrations The pattern of solute concentrations differs from between D1 and D2 as well, with D1 having more $SO_4$, K, and $NO_3$, and D2 with higher concentrations of Cl, Ca, Sr and Mg, as well as high concentrations of $^4He_{terr}$.

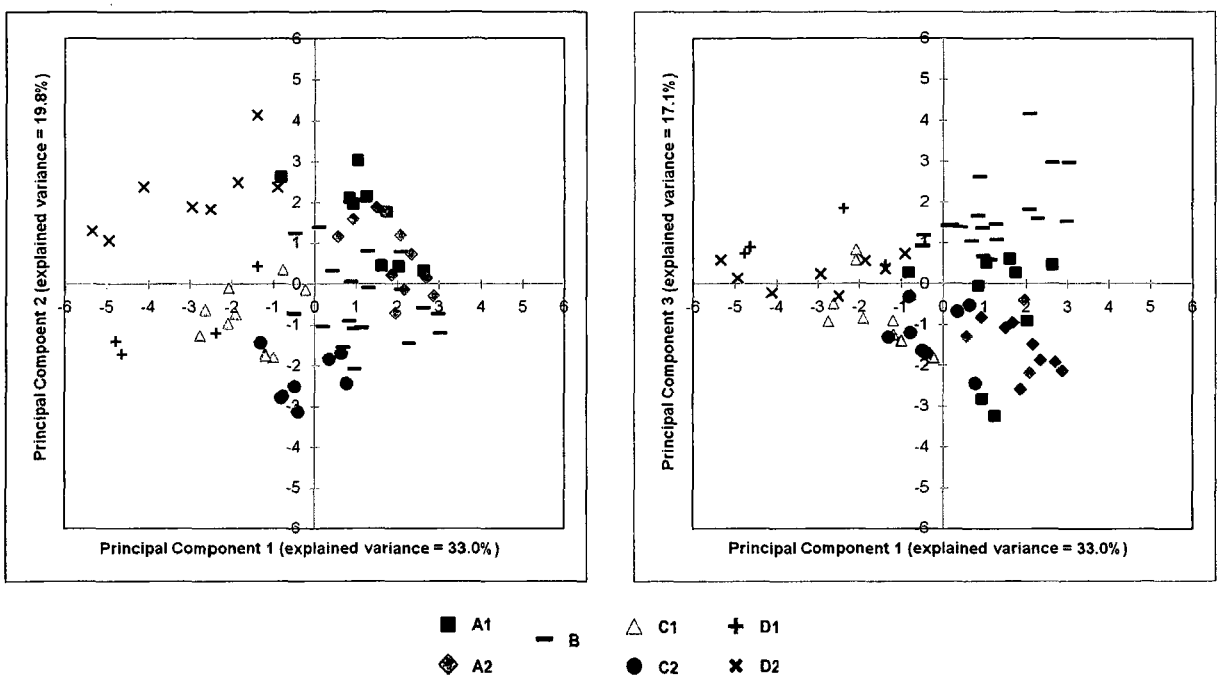


**Figure 5.6**. Loadings of samples in the 7 groundwater subfacies defined by HCA grouped by clusters for the first three principal components.

## 5.7 Spatial Geochemical Patterns

### 5.7.1 Spatial Distribution of Geochemical Tracers

Geochemical parameter values were plotted on cross sections so they could be manually contoured to examine their spatial distribution along the North and South flow paths and across flow paths at the downgradient section. Only a limited representative subset of the cross sections is presented in this paper. Figure 5.7 shows patterns of TCE and chloride concentrations on the North and South Flow Paths. Along the North Flow Path (NFP), elevated concentrations of all solutes (notably Na, $SO_4$ and perchlorate) and low dissolved oxygen form a distinct solute plume in the eastern part in samples from the easternmost sampling location, which coincide roughly with the distribution of high TCE concentration. In the center of the NFP, there is another plume of solutes originating from the surface, mostly restricted to high Na and Cl concentrations, but

not associated with an input of TCE or low dissolved oxygen. Groundwater geochemistry of the NFP is also characterized along the base of the deltaic aquifer by higher concentrations of $^4He_{terr}$ than at higher elevations and groundwater is found to be more depleted in stable isotopes in the NFP than elsewhere.

At the start of the South Flow Path (SFP), groundwater is relatively dilute and high in dissolved oxygen except for the base of the easternmost sampling location, where there are higher concentrations of major ions (excluding perchlorate), low dissolved oxygen and very high $^4He_{terr}$. This anomaly corresponds with high TCE concentrations that seem to flow upward from the proglacial aquifer into the deltaic aquifer at this location. In the western part of the flow path, very high concentrations of all solutes, especially Ca, Sr, and Cl, appear in the lower part of the saturated zone, as well as very low dissolved oxygen and elevated $^4He_{terr}$. A significant increase in TCE concentration also occurs at this location, which, like upgradient, appears to be coming from the underlying proglacial aquifer rather than from the surface.

Groundwater in the proglacial aquifer is generally low in dissolved oxygen with intermediate to low concentrations of solutes, with a single location having detectable perchlorate concentrations. Samples from PO-135 and PO-154 also contain high concentrations of TCE, but there is no distinct geochemistry associated with these wells.

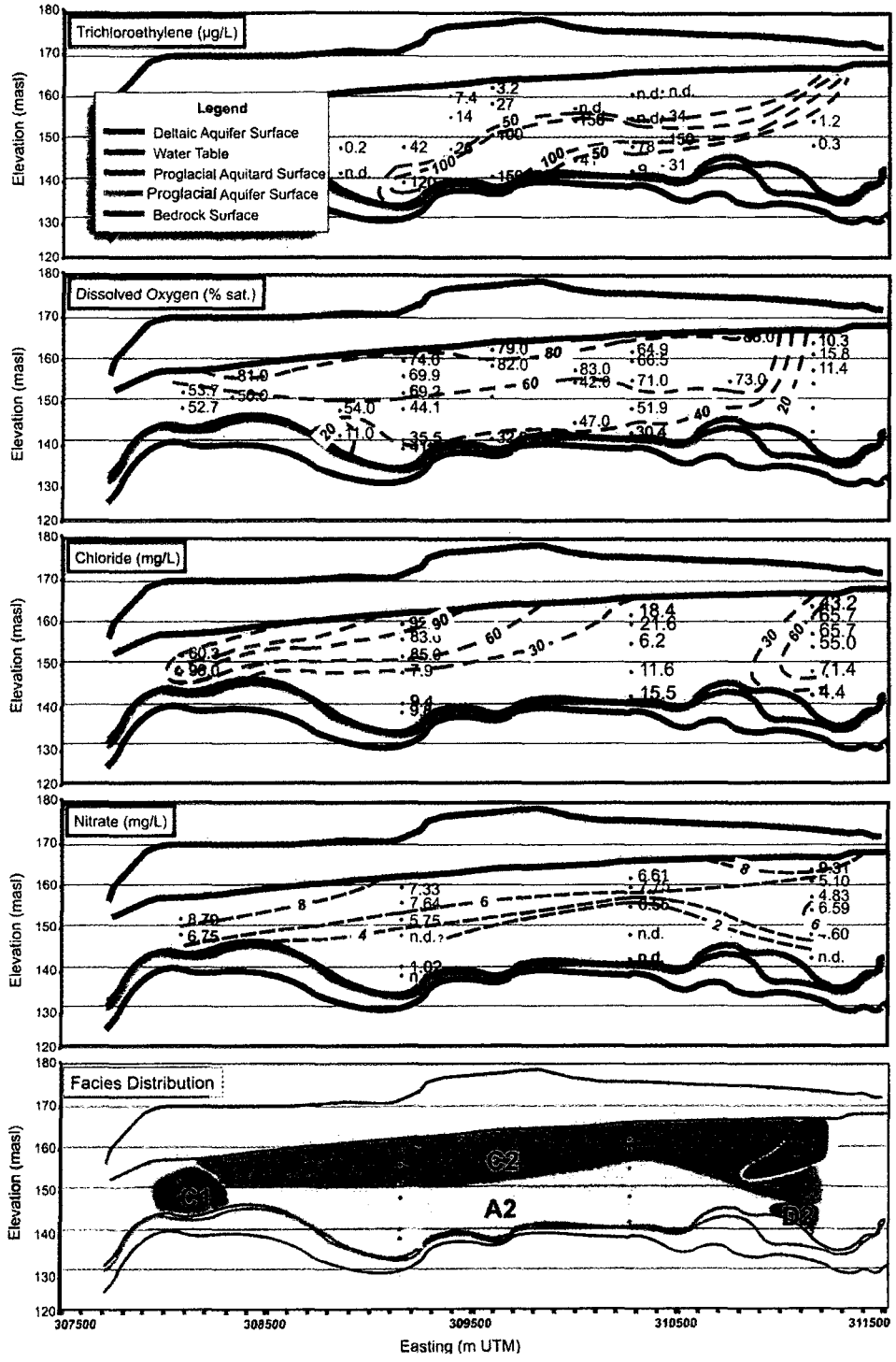


**Figure 5.7a**. Cross sections showing the spatial distribution of selected geochemical tracers on the North Flow Path: TCE (µg/L), dissolved oxygen (% saturation), Cl (mg/L), nitrate (mg/L as $NO_3$), and groundwater facies as defined by HCA. Concentration contours were hand-drawn to facilitate visualization.

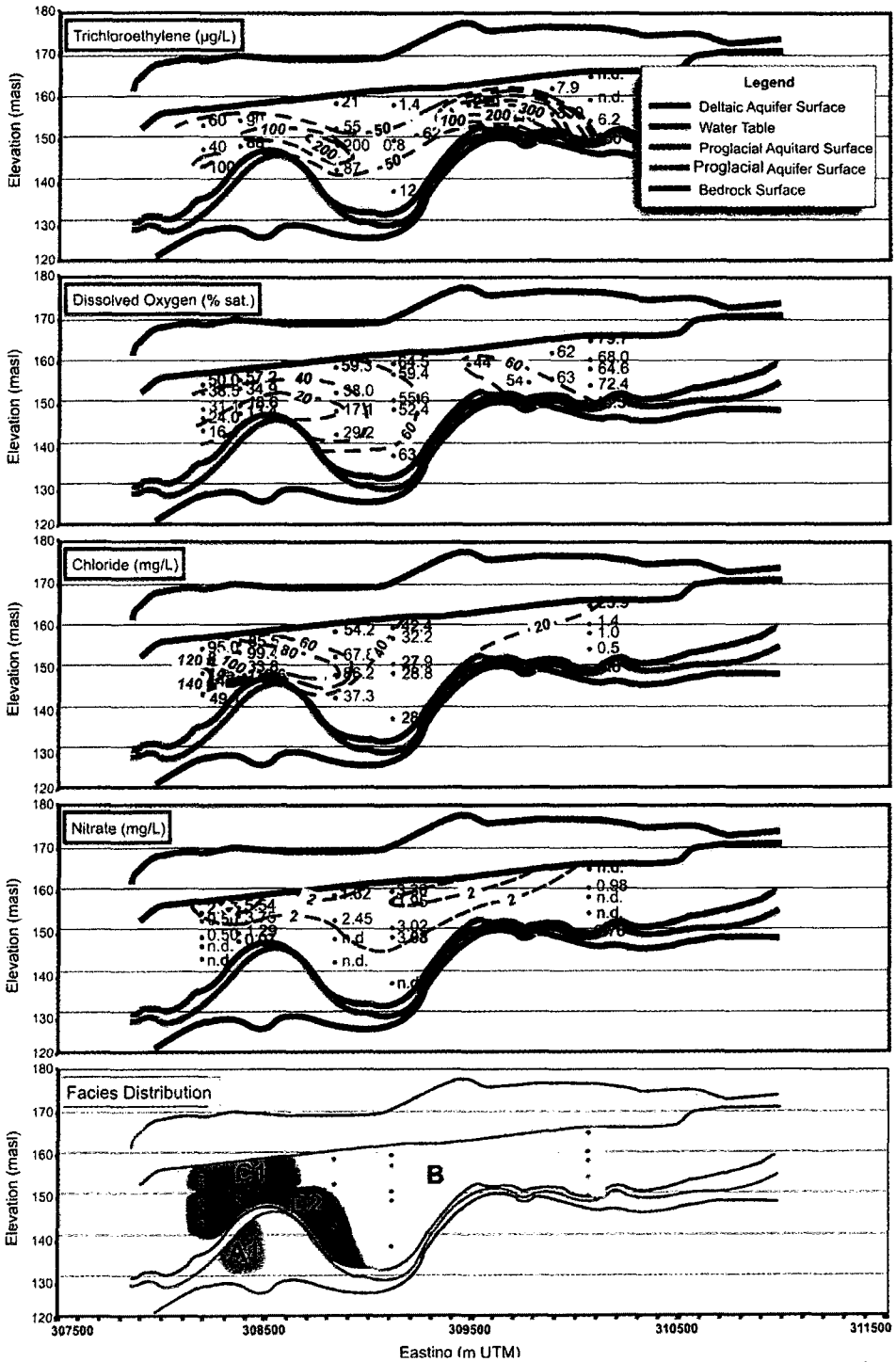


**Figure 5.7b**. Cross sections showing the spatial distribution of selected geochemical tracers on the South Flow Path: TCE (µg/L), dissolved oxygen (% saturation), Cl (mg/L), nitrate (mg/L as NO3), and groundwater facies as defined by HCA. Concentration contours were hand-drawn to facilitate visualization.

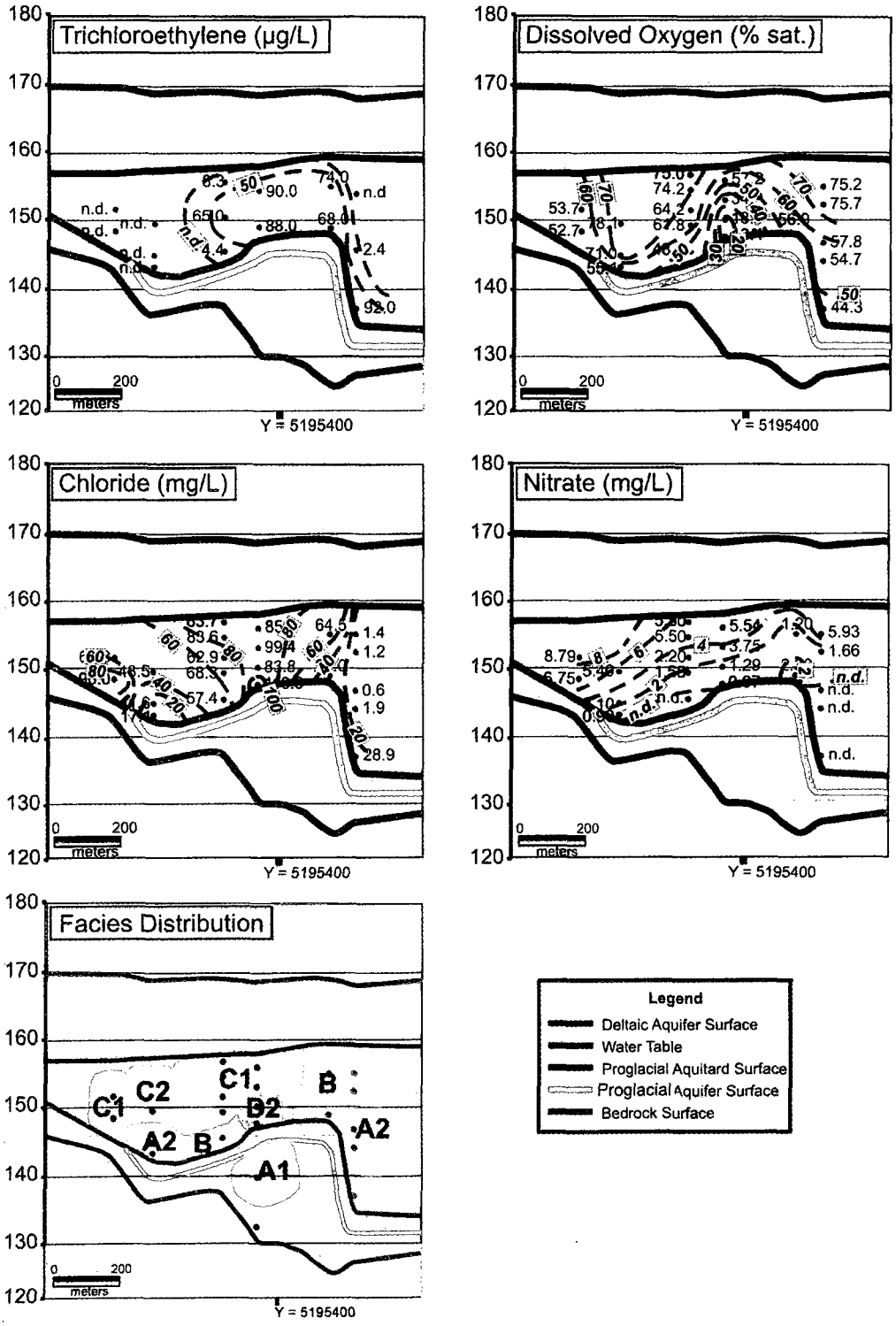


Legend
- Deltaic Aquifer Surface
- Water Table
- Proglacial Aquitard Surface
- Proglacial Aquifer Surface
- Bedrock Surface

**Figure 5.7c**. Cross sections showing the spatial distribution of selected geochemical tracers on the Downgradient Section looking east:TCE (µg/L),) dissolved oxygen (% saturation), Cl (mg/L), nitrate (mg/L as NO3), and groundwater facies as defined by HCA. Concentration contours were hand-drawn to facilitate visualization.

The bottom of Figure 5.7 also shows TCE and dissolved oxygen (DO) concentrations on the downgradient section. High solute concentrations are associated with the low DO at the center of the TCE plume near the base of the deltaic aquifer. This part of the TCE plume is in continuity with the high solutes, low DO and high TCE concentrations noted on the western part of the SFP. On the contrary, groundwater in the southern part of the downgradient section, even within the TCE plume, is very low in dissolved ions and has high dissolved oxygen and an enriched stable isotope composition. In the northernmost sampling location of the downgradient section, there is a local increase in solute concentrations and a decrease in dissolved oxygen where the silty aquitard is absent.

### 5.7.2 Spatial Distribution of Clusters

Figure 5.7 shows the distribution of samples belonging to the different facies on cross sections of the NFP, the SFP, and the downgradient section as classified by HCA at a linkage distance of 10. Facies are spatially coherent, and several trends can be deciphered.

Subfacies A1 consists of groundwater found in the proglacial aquifer and above and below the prodeltaic silty aquitard to the east of the NFP (not shown). D1 is in the upper east part of the NFP; one D1 sample is located in the proglacial aquifer in the western section (not shown). For most of the NFP, groundwater found in the lower half of the deltaic aquifer is facies A2, which can also be seen at the base of the downgradient section at the northernmost sampling location where the silty aquitard is still present. Subfacies C2 makes up the entire upper portion of the deltaic aquifer along the NFP. Although A2 and C2 are found at the downgradient section, they

seem to transition into subfacies C1 whose spatial distribution is restricted to the western ends of the NFP and SFP and in the downgradient section, mostly in the upper portions of these sections.

Groundwater of facies B dominates the eastern and central portions of the South Flow Path and is found mostly in the southern part of downgradient section. Laterally, to the west of the SFP and in the downgradient section, C1 is found laterally at the upper portion of the NFP. In the lower part of the NFP, facies D2 groundwater is found concentrated in the lower half of the deltaic aquifer on the SFP. There is also only one sample assigned to D2 at the east end of the NFP.

Most facies are represented in the downgradient section. The upper portion of the deltaic aquifer in that section is occupied by groundwater of facies C1. The southern part of the section consists of facies B. Subfacies D2 is found near the base of the deltaic aquifer at the center of the section. Groundwater of subfacies A2 and C2 groundwater are found on the north side of the section.

## 5.8 Implications on Groundwater Flow Paths and TCE Migration

The discussion presented in this section aims to use the results obtained from geochemical tracers to draw conclusions regarding the objectives for which the geochemical characterization was carried out. First, the groundwater geochemical groups obtained from cluster analysis are interpreted in the hydrogeological context of the study area to infer their respective origins. Afterward, implications on groundwater flow paths are derived from the spatial distribution of geochemical subgroups as well as concentration patterns of specific geochemical tracers. Finally, having established a firmer conceptual model of groundwater origins and flow paths in the

aquifer system, geochemical subgroups and individual tracers are used to infer the provenance of the TCE found in different parts of the plume delineated at the downgradient section.

### 5.8.1 Groundwater Types and Origins

The spatial distribution of groundwater types recognized by cluster analysis of geochemical tracers, placed in the hydrogeological context of the study area, can be used to infer the origins of these groundwaters. For this purpose, facies defined by HCA are used because HCA classification discriminates between the origin of groundwater in the eastern and western portion of the study area (subfacies C1 and C2) more clearly than AMBC which groups these into one category. On Figures 5.7, the spatial distribution of HCA geochemical subgroups is shown alongside concentration contours of specific tracers for the NFP and SFP and for the downgradient section. Table 5.4 summarizes the characteristics and spatial distribution of these groundwater clusters, along with an interpretation on the possible origins of the groundwater.

Facies A1 is groundwater in the proglacial aquifer and around the prodeltaic silt aquitard, and was recharged in the valley east of the study area through the prodeltaic silty aquitard. The low ORP and DO in these samples are likely caused by aerobic microbial activity, which is high because of organic carbon in the aquitard (Lefebvre *et al.*, 2003) and probably in the proglacial aquifer relative to the deltaic aquifer. Terrigenic $^4He$ in samples adjacent to the silty aquitard derives from the decay of radioactive isotopes from minerals in the silt. Although there are no measurements of $^4He_{terr}$ in proglacial aquifer groundwater, both the prodeltaic silt and the proglacial aquifer contain less quartz and a higher proportion of fine-grained material than the deltaic aquifer, and likley contain minerals such as clays or feldspars that contain radioactive isotopes that produce $^4He$ (Lefebvre *et al.*, 2003).

Subfacies A2 is similar to A1 but has higher DO; it is in the lower part of the deltaic unit along the North Flow Path and represents laterally equivalent groundwater to facies A1 that recharged the deltaic unit east of the study area. The similarity of samples in facies A may be related to the prodeltaic silty unit: groundwater in both categories would have traversed the aquitard in the east before reaching the deltaic aquifer and migrating westward to the study area. Diffusive or slow advective exchange between the proglacial and deltaic aquifers may also affect the composition of subfacies A2 in the lower part of the deltaic aquifer, and could also explain its similarity with facies A1. High Sr and terrigenic $^{4}He$ coupled to low DO and temperature near the base of the deltaic aquifer, more apparent on the NFP, are considered evidence of this upward input from the proglacial aquifer into the deltaic aquifer. The relatively depleted isotopic composition of both groundwater types further suggests a common recharge origin east of the study area in the buried valley.

**Table 5.4**. Geochemical characteristics and origin of groundwater facies.

| Group | Characteristics | Subgroup | Characteristics | TCE Concentration | Location | Origin |
|---|---|---|---|---|---|---|
| A | • isotopically depleted, • low solute concentrations, • moderate-low DO • high pH and terrigenic $^4He$ | A1 | low DO | high in some | deltaic aquifer near prodeltaic silt and in proglacial aquifer | GW that recharged through silt aquitard in east part of valley, influenced by contact with silt or by flow through proglacial aquifer[ |
| | | A2 | moderate DO | moderate-high in some | eastern North Flow Path, lower part of deltaic aquifer | GW that recharged through silt aquitard and flowed through deltaic aquifer in east part of the valley, in contact with proglacial aquifer |
| B | • isotopically enriched • moderate-low solute conc. • low T, high DO, high ORP, low pH | - | - | moderate-high in some | eastern part of South Flow Path and southern Shannon | GW that recharged on slopes of Mount Rolland-Auger |
| C | • moderate solute concentrations • moderate-high DO | C1 | high Na-Cl | moderate in most | central Shannon and north Shannon | mixture of water types (probably D2 and A2, B and C2) |
| | | C2 | isotopically depleted, high $NO_3$, high DO, low pH, high ORP | low in a few | upper part of North Flow Path | GW that recharged recently through deltaic aquifer, influenced by anthropogenic inputs |
| D | • very high solute concentrations, • low DO | D1 | high $SO_4$, K, Na, $NO_3$, high ORP | unknown | upper part of C2-9-10 wells on North Flow Path | North of NFP origin, strongly influenced by anthropogenic inputs |
| | | D2 | high Cl, Ca, Sr, Mg, Si, high pH, terrigenic $^4He$, low ORP | high in most | central Shannon, bottom part of deltaic aquifer | GW upflowing from proglacial aquifer into deltaic aquifer coming from western (dump) source zone |

Geochemical facies B is found along the South Flow Path to the east of the downgradient section. The characteristics of this groundwater – low solute concentrations, high DO and ORP, low temperature, and low pH – suggest that it recharged recently and was not significantly affected by anthropogenic inputs. This groundwater originated mostly from lateral inflow of groundwater that recharged on the slopes of Mount Roland-Auger to the south of the South Flow Path. The lateral inflow is influenced by the strong hydraulic gradient generated by the topography. Facies B groundwater is isotopically enriched compared with samples along the North Flow Path, reflecting a distinct recharge origin from groundwater found in the North Flow Path. This groundwater includes the TCE plume that emanates from the central source zone (Lagoon C) as well as TCE-free groundwater in the upper east portion of the aquifer (Figure 5.7b).

Subfacies C2 groundwater is only in the upper part of the deltaic aquifer along the North Flow Path. It is characterized by high DO and ORP and low pH, suggesting recently recharged groundwater, but it has significant $NO_3$ and moderate to high concentrations of solutes in some parts, notably Cl and Na. This groundwater is influenced by the anthropogenic activities on the Valcartier Garrison, which contributes solutes to the subsurface. High concentrations of $NO_3$ probably come from the application of fertilizer or leaky sewage pipes. Cl and Na (Fig. 5.5c) could originate from de-icing road salt applied to the main road and numerous streets found in the area. There is a location above the central part of the NFP that is used for snow storage in the winter, which would contain NaCl from road salt; when it melted, there would be a high concentration of salty water recharging the water table at this location, which can be seen clearly in Figure 5.7a.

Facies D groundwater has high concentrations of solutes and low DO, but subfacies have distinct geochemical characteristics and are found in separate areas. D1 has higher concentrations of $SO_4$, K and Na and is warmer than D2 groundwater. Referring to Figure 5.7a, it appears that this groundwater type recharged immediately upgradient of the start of the North Flow Path, and may be related to waste from DRDC source zones or the Sector 214 source zone. This groundwater represents the composition of waste from these source zones, which is clearly different from subfacies D2 groundwater found only in the lower part of the deltaic aquifer in Shannon along the South Flow Path.

Groundwater of the D2 geochemical facies has higher Ca, Mg, Sr, Cl and dissolved silica than D1, as well as high concentrations of terrigenic $^4He$; this groundwater also corresponds with very high concentrations of TCE. D2 only appears at the bottom of the deltaic aquifer on the SFP, as shown in Figure 5.7b, because it flows upward from the underlying proglacial aquifer near this location. The proglacial silt aquitard between the deltaic and proglacial aquifers is thin at this location (Figure 5.2), where there is also greater hydraulic head in the proglacial aquifer than in the deltaic aquifer, creating the conditions for upward groundwater flow and exchange between aquifers. Certain characteristics of this groundwater are similar to samples taken directly from the proglacial aquifer: low ORP and DO, high concentrations of Mg, and terrigenic $^4He$ derived from minerals in the proglacial aquifer. Significant concentrations of Sr in D2 could also indicate groundwater interaction with the bedrock. This could be evidence for the source of this groundwater from a former dump that was excavated down to bedrock to the south of the upflow location (Figure 5.1).

C1 groundwater occurs only at the western ends of the NFP and SFP, near the downgradient section (Figures 5.7a and b). On the NFP, facies C1 is laterally equivalent to A2 and C2

groundwater, which are also found all the way to the downgradient section (Figure 5.7c). On the SFP B groundwater (Figure 5.7b) is dominant in the eastern portion, as well as in the southern part of the downgradient section (Figure 5.7c). On the downgradient section, C1 surrounds D1 groundwater. The geochemical composition of C1 is intermediate between D2 groundwater and other facies, which is probably the result of mixing groundwater of different origins. There is evidence of strong mixing at the western ends of the NFP and especially the SFP based on individual tracers and tritium-helium ages (Chapter 4). This mixing is inferred to be caused by a sequence in the flow direction of a wide increase followed by an important decrease in the saturated thickness of the deltaic aquifer (Figures 5.2 and 5.7), and second by the convergence of groundwater flow into the western end of NFP and SFP from the valley in the north (A2 and C2), from Mount Rolland-Auger in the south (B), and from the proglacial aquifer (D2).

Groundwater found in the northernmost sampling location on the downgradient section is also classified as subfacies C1, even though it is separated from C1 groundwater in the center of the section by A2 and C2 related to the NFP (Figure 5.7c). The geochemistry and isotopic composition of these samples are very similar to groundwater on the South Flow Path, and may have a common origin. Similar to subfacies D2 groundwater (an "end-member" of the mixture that constitutes C1), this groundwater may flow upward from the proglacial aquifer into the deltaic aquifer due to the disappearance of the proglacial aquitard between the deltaic and proglacial aquifer near this location (Figures 5.2 and 5.7c). Although there is no detectable TCE at this location presently, low concentrations of TCE under 5 μg/L persisted there in the past (Lefebvre et al., 2003). The TCE in that location could have multiple origins but there is presently no definitive evidence to sort out which one is the more likely cause.

### 5.8.2 Groundwater Flow Paths

The spatial distributions of individual geochemical tracers and HCA-derived facies have provided independent evidence confirming previously inferred groundwater flow conditions based on conceptual and numerical models of groundwater flow in the aquifer system. These data have also shown flow processes that could not be identified on the sole basis of hydraulic data.

Important features of groundwater flow patterns in the aquifer systems were further validated by geochemical tracers. Tracers first demonstrate that the NFP and SFP are geochemically distinct from one another, even though they are distant by only a few hundred meters. On the basis of tritium-helium dating, Murphy *et al.* (Chapter 4) further show that groundwater ages are different on these paths. The lateral continuity in individual tracers and HCA subgroups along flow paths also validate the definition of these flow paths that were derived from particle tracking with a numerical model, thus also supporting modeling results. Since these flow paths represent the migration routes of TCE from different source zones, this validation has implications on the transit time and exposure period at receptors related to TCE release from these source zones. Besides validating the plan-view patterns of groundwater flow, geochemical tracers also provide evidence for the vertical components of groundwater flow. Although this was postulated long ago based on numerical modeling and TCE occurrence just under the prodeltaic silty aquitard (Lefebvre *et al.*, 2003), HCA facies provide direct evidence of the presence in the deltaic aquifer of groundwater that has recharged through the aquitard (subfacies A2 at the base of the aquifer, Figure 5.7a). In a parallel study, groundwater dating using tritium-helium ages has provided an estimated TCE transit time through the prodeltaic aquitard of 19 years. Geochemical tracers also show that near the origin of the NFP, groundwater flows steeply downward, which is coherent

with very low horizontal velocity and a relatively large estimated recharge rate of 300 mm/y (Chapter 4). This flow pattern implies that TCE originating from source zones related to the NFP should be found near the base of deltaic aquifer, as observed on Figure 5.7a. On the contrary, TCE entering the SFP along its course is found both at the base of the deltaic aquifer and within the aquifer itself due to the location and effect of groundwater upflow with TCE into the SFP. Further downstream on the NFP, a Cl plume shows that groundwater flow paths are not sinking as fast, due to the increased groundwater velocity. The flow patterns at the origin and along the NFP indicated by geochemical tracers are very coherent with particle tracking derived from the numerical model (Chapter 4).

Geochemical tracers also provided evidence of features of the groundwater flow system that had not been defined before. Tracers provide indications about the nature of groundwater exchanges between the proglacial aquifer and the overlying deltaic aquifer. Where the glaciomarine silty aquitard separating the proglacial aquifer from the deltaic aquifer is continuous, there is evidence of diffusive water mixing at the deltaic aquifer base. Where the aquitard is locally absent, important upflow can occur, in the deltaic sand, as seen near the beginning and at the center of the SFP (Figure 5.7b). This upflow is important as it carries TCE from different source zones that geochemical tracers can distinguish. The occurrence of TCE in the proglacial aquifer and deltaic aquifer in the downgradient part of the flow system has important implications on potential plume control infrastructures. Geochemical tracers also provided evidence of the complex flow paths present at the western end of the flow system. The upflow of proglacial aquifer groundwater with TCE indicated by tracers has led to a shift of the SFP TCE plume to the south. The "comingled" plume seen at the downgradient section thus shows geochemical evidence of provenance from three distinct source zones. This situation is made even more

complex by the important mixing occurring in the downgradient section, as described in the previous section, and that was again made evident by geochemical patterns and tritium-helium groundwater ages (Chapter 4)

### 5.8.3 TCE Origins at Downgradient Section

Previous sections have shown that geochemical tracers, placed in their hydrogeological context, have provided indications of groundwater types, their provenance and how they help define groundwater flow paths in the aquifer system. Table 5.4 summarizes the implications of these findings on the origins, migration paths and occurrence of TCE at the downgradient section where TCE from all sources converges. Since TCE migration paths follow groundwater flow paths already described, their description is kept very brief.

The source zones found to the east of the NFP origin emit TCE above the prodeltaic silty aquitard, and then migrate downward through the aquitard to emerge in the regional deltaic aquifer. The slow groundwater velocity and important recharge in the area near the groundwater divide leads to the sinking of the TCE plume to the base of the deltaic aquifer where it migrates to the west. At the downgradient section, TCE from the NFP appears on the north side of the plume in a groundwater type related to mixing, so its provenance from the NFP is partly inferred from the presence of high perchlorate concentrations.

The central source zone (Lagoon C) found upgradient of the SFP first migrates rapidly northward in the proglacial aquifer and deltaic aquifer due to the high hydraulic gradient on the slope of Mount Rolland-Auger. The flow path turns west as groundwater emerges in the thick main portion of the deltaic aquifer in the buried valley. Important groundwater upflow from the proglacial aquifer and the presence of a thicker saturated zone on the south side of the SFP lead

to preferential migration in that location, where TCE originating from the SFP is found at the downgradient section.

TCE presumed to originate from the previously unrecognized west source zone (dump in bedrock on Mount Rolland-Auger) first migrates northward through bedrock and proglacial aquifer. The TCE emerges within the SFP through a window in the glaciomarine silty aquitard and then migrates west to emerge at the base of the deltaic aquifer at the downgradient section.

**Table 5.5**. Origins, migration paths and occurrence of TCE at the downgradient section inferred from geochemical tracers and hydrogeological conditions.

| Source Zones | Conditions at source | Migration Paths | Conditions at Downgradient Section |
|---|---|---|---|
| **East** (3 at DRDC North and Sector 214) | • Variety of source zones to the north (3) and south of the flow path origin in research and industrial facilities<br>• All sources but one above prodeltaic aquitard<br>• Near groundwater divide in regional deltaic aquifer<br>• Very low horizontal hydraulic gradient and velocity<br>• Important downward flow due to recharge | • North Flow Path:<br>• At origin of NFP, flow through prodeltaic silty aquitard in regional deltaic sand aquifer<br>• Rapidly sinking plume near NFP origin due to flow pattern<br>• Westward migration at base of deltaic sand | • C2 and A2 subgroups related to NFP has no TCE associated to it past the northern limit of TCE plume<br>• Northern part of plume has high perchlorate and C1 subgroup groundwater that could be a transition from NFP C2 and A2 subgroups (A1 at source zones transition to A2) |
| **Central** (Lagoon C) | • Unlined excavation in deltaic sand and proglacial aquifer serving as fluid disposal "lagoon"<br>• Edge of deltaic sand extent<br>• Mountain side<br>• High horizontal hydraulic gradient and groundwater velocity | • South Flow Path:<br>• Upgradient of SFP origin, northward flow through proglacial aquifer and deltaic sand on slope of mount<br>• Flow turning west when plume enters main buried valley<br>• Proglacial aquifer upflow and thick sand lead to flow on SFP south side | • B subgroup groundwater associated to SFP found in southern part of TCE plume indicates central source zone origin<br>• C1 subgroup groundwater above D2 at center of TCE plume could also be related to SFP and central source zone |
| **West** (Dump) | • Unlined excavation in thin proglacial aquifer and bedrock serving as dry material dump<br>• High on mountain side<br>• High horizontal hydraulic gradient<br>• Unknown velocity for uncertain flow path in thin proglacial aquifer and bedrock | • Northward through bedrock and proglacial aquifer<br>• On SFP, emerges in deltaic sand through glaciomarine aquitard windows on edge of slope on aquifer base | • D2 subgroup groundwater at center of TCE plume at base of deltaic sand is related to the west source zone<br>• Individual tracers such as Sr and terrigenic $^{4}He$ have the unique signature of the west source zone |

## 5.9 Conclusions

The objective of the study is to distinguish flow paths related to different TCE source zones based on geochemical patterns in groundwater. The geochemistry of TCE origins can then be related to TCE found in a plume that integrates TCE contributions from all sources along the migration paths from source zones to receptors. An interpretation of groundwater flow based on the results of the study, which are independent of hydraulic data, can be used to constrain a numerical model that is being developed to aid in the design of plume control measures.

The Valcartier site is generally smaller and requires higher resolution in three dimensions than other areas that have been characterized based on groundwater geochemistry using multivariate statistical techniques. Spatial changes in groundwater chemistry relate more to groundwater origin and anthropogenic inputs than to groundwater evolution or the attenuation of contaminant species. In this context, it was important to collect data in closely spaced intervals to identify the geochemical changes necessary for distinguishing flow patterns and TCE origins.

The existing numerical model was used to identify two flow paths originating from TCE source zones (North and South Flow Paths) in order to select sample locations; samples were also collected along a downgradient section across the flow paths near receptors. Geochemical patterns were initially examined by plotting parameters on bivariate plots and on cross sections of the flow paths and of the downgradient section that were then contoured. Multivariate statistical techniques were then applied to the data to classify groundwater into geochemical facies that could be related to groundwater origin.

PCA was performed on the standardized data, which reduced the data to three Principal Components (PC) that account for 70% of the total variation. The distribution of principal

component loadings distinguished groundwater with similar geochemical characteristics, and allowed easy recognition of related geochemical parameters. Following this, clustering techniques were applied to the data to classify groundwater samples into groups with similar geochemical characteristics. Seven groups of samples, or geochemical facies, were identified by both HCA and AMBC methods, which are spatially coherent and show significant differences between groundwater on the North and South Flow Paths. The different facies are influenced by recharge location, contact with different lithologies, and proximity to anthropogenic activities.

The distinct geochemical groundwater facies identified through multivariate statistics lends confidence to the ability of the numerical model to identify flow paths for groundwater in Valcartier. Migration patterns predicted by the model are supported by the distribution of geochemical facies, which validates the existing values used for parameters and boundary conditions. Moreover, the geochemical facies linked to TCE source zones can be used to interpret TCE provenance in the plume downgradient. There is evidence of TCE origin from both known source zones (East and Central), as well as for a previously unknown third source (West) that appears to initially flow northward through the proglacial aquifer or the bedrock before emerging in the deltaic aquifer near the SFP.

Differences in groundwater geochemistry allowed the recognition of discrete flow paths and locations of groundwater exchange between aquifers in Valcartier. Geochemical characterization on such a small scale provides the resolution required to identify subtle but important changes in groundwater composition that cannot be derived from hydraulic data alone. Once identified, the groundwater facies can then be related to groundwater origin and migration history to improve the understanding of groundwater flow. This study demonstrates the need for an integrated

approach to groundwater studies that utilizes both hydraulic and geochemical data to characterize complex flow systems such as Valcartier.

# 6.0 Conclusion

The aquifer supplying groundwater for the Valcartier Garrison municipal wells and private wells in the neighboring town of Shannon was found to be contaminated with TCE, and can no longer be used for the drinking water. There are multiple locations from which the TCE derives, and contributions from all sources coalesce in a large dissolved TCE plume that spans about 4.5 km. Predominantly westward groundwater flow transports TCE from sources in Valcartier towards Shannon, where plume control measures are being planned to stop the migration of the TCE plume. Extensive characterization of the TCE plume and the groundwater system has led to the development of a numerical groundwater model using a finite-element grid in Feflow, which has been calibrated to match hydraulic heads. The results of model simulations will be used to guide decisions regarding remediation measures, so it is important for the model to replicate groundwater flow in Valcartier as accurately as possible. The purpose of this study was to verify the model using independent data, and to improve the understanding of TCE origin and migration in Valcartier.

An important aspect of the model verification is examining the validity of parameter values, namely recharge rate and porosity, as well as the hydraulic conductivity of the prodeltaic silty aquitard. The accurate estimation of these parameters is crucial to replicating groundwater travel times and velocities from TCE source zones. The model's ability to delineate flow paths should also be supported by independent data; because TCE from the various source zones merges into one large plume in downgradient areas, it is important to be able to distinguish TCE contributions from each source. It is especially important to understand the migration of TCE into Shannon, where TCE control technology will be employed and needs to be placed in areas where plume controlwill be maximized.

With these objectives in mind, a geochemical characterization program was designed to obtain samples from the deltaic aquifer along flow paths stemming from two main source zones (North and South Flow Paths) and from a transect in the downgradient portion of the study area in Shannon. Flow paths were identified using the numerical model to select appropriate wells; sample locations were also chosen above and below the aquitard in the east, and in the proglacial aquifer beneath the deltaic aquifer. The distribution of sampling locations provided coverage of the deltaic aquifer that targets groundwater flow paths for $^{3}H$-$^{3}He$ dating, as well as other important areas in Shannon and in the proglacial aquifer to carry out a detailed geochemical investigation.

$^{3}H$-$^{3}He$ ages were obtained from groundwater along the North and South Flow Paths and across the flow paths along the Shannon transect to establish cross sections of groundwater ages in the deltaic aquifer. The ability of the model to reproduce the ages was evaluated by comparing the $^{3}H$-$^{3}He$ ages, which are an independently measured parameter of the groundwater system, with advective particle tracking ages. All ages that were not affected by helium diffusion or mixing were used to compare with the model. The model ages were coherent with measured $^{3}H$-$^{3}He$ ages, producing the best match using a porosity of 0.35 and a recharge rate of 300 mm/y. Patterns in groundwater age that indicate dispersion also verify the heterogeneous $K$ field defined by Ouellon *et al.* (2008a). The ages obtained above and below the prodeltaic silty aquitard were used to calculate its $K_v$, found to be between 1.3-3.1x$10^{-8}$ m/s, similar though slightly lower than the values previously used in the model. It is difficult to get a direct measurement that can be used to calculate $K_v$, so the availability of $^{3}H$-$^{3}He$ ages along with other hydraulic data offers a unique way to estimate this parameter for use in the model. Although ages could not be used to independently estimate groundwater velocity due to heterogeneities in the aquifer, their use as an

independent calibration target lends confidence to predictions on groundwater flow and TCE transport made by the model.

In addition to groundwater ages, the $^{3}H$-$^{3}He$ technique offers information that can be used to trace groundwater. Discrete zones in the deltaic aquifer with high concentrations of terrigenic $^{4}He$ and old groundwater ages indicate locations where there is upward groundwater flow from the proglacial aquifer to the deltaic aquifer through windows in the proglacial aquitard. This process transports TCE that initially migrated through the proglacial aquifer into the deltaic aquifer, and its importance had not been previously recognized and only approximately included in the model. The association of this upflowing groundwater with high concentrations of TCE in Shannon suggests the presence of another location where TCE was released in addition to the known source zones that were the focus of this study. Although more detailed characterization of this area is required to draw firm conclusions about this potential source, the most likely source of this TCE is an abandoned dump to the south on the SIVI property west of Lagoon C. $^{3}H$-$^{3}He$ ages are a useful independent measurement of the groundwater system that gives insight on the groundwater flow and contaminant transport in Valcartier, providing important constraints on the groundwater model.

Results of the geochemical and isotopic investigation of Valcartier groundwater were used to make interpretations on TCE origin and groundwater flow. The spatial coherence of geochemical parameters of groundwater along the North and South Flow Paths validates the accuracy of flow paths identified by the numerical model, and supports the use of geochemical and isotopic parameters to categorize groundwater into types that can be associated with their location of origin. Statistical methods were applied to a standardized subset of the data to aid in the recognition of patterns. This approach is unique compared with other geochemical studies of

groundwater in that the distribution of geochemical characteristics needs to be known in three dimensions in a relatively small area. As well, the study focuses on how the groundwater geochemistry relates to its origin rather than evolution, particularly in relation to TCE source zones.

Principal components analysis reduced the data to three principal components that account for 70% of the total variance in the data, where the value of each principal component loading represents more than one aspect of a sample's geochemical composition. Clustering techniques were also performed on the data to group groundwater samples with similar characteristics. Both hierarchical clustering analysis and agglomerative model-based clustering produced seven clusters of groundwater with distinct geochemical and isotopic composition that are spatially coherent. The clusters defined by HCA distinguished groups that could be related to groundwater provenance more clearly than AMBC, and were therefore used to classify groundwater in Valcartier into distinct geochemical facies. The distribution of groundwater facies strongly indicates an association between groundwater geochemistry and the TCE source zones, for example subfacies D1 which seems to be linked to TCE source zones at the start of the North Flow Path. Subfacies D2 is closely related to increased TCE concentrations in Shannon on the South Flow Path, and likely represents groundwater from the suspected TCE source (the dump) that was recognized by terrigenic $^{4}He$ and old groundwater ages measured through $^{3}H$-$^{3}He$ dating. The classification of geochemical groundwater facies provides an effective way of assessing groundwater origins and flow paths at the scale of Valcartier as a complement to hydraulic measurements that cannot provide incatiosn of groundwater provenance.

The results from $^{3}H$-$^{3}He$ dating and the geochemical characterization have led to new interpretations about groundwater flow and the migration of TCE in Valcartier. By integrating

information previously obtained on the hydraulic properties of the system, groundwater ages were able to optimize the parameters used in the numerical model, and improve its predictive capabilities. Categorizing groundwater samples into facies based on their geochemical composition independently distinguished groundwater on the North and South flow paths, which also validates the model's reproduction of groundwater flow paths.

Tracers of groundwater flow such as major ion composition, dissolved terrigenic $^{4}He$ as well as groundwater age that correspond to high TCE concentrations in Shannon have led to the recognition that there may be significant TCE originating from a former dump that was not previously recognized. Upflow of TCE-bearing groundwater from the proglacial aquifer is also apparent in the east part of the South Flow Path, which indicates that TCE originating from Lagoon C currently comes from beneath the proglacial aquifer, rather than only directly from the deltaic aquifer. Patterns in groundwater composition suggest there may be significant groundwater exchange between the proglacial and deltaic aquifers that is not yet fully understood, but may play an important role in the transport of TCE from the Lagoon C and possibly the dump source zones.

Groundwater ages and geochemical facies along the North Flow Path represent groundwater flow from both DRDC North and Sector 214; because the flow path originates between the two TCE source zones, it is impossible to separate the geochemical characteristics of each source. However, modelled groundwater velocities validated by $^{3}H$-$^{3}He$ ages (Murphy *et al.*, 2009) and geochemical characteristics associated with these source zones provide some indication of their contribution to the dissolved TCE plume in Shannon. The TCE released from these source zones has likely reached Shannon by now, especially from Building B67 and the Blue Lagoon in DRDC North where the prodeltaic silty aquifer is absent. However, the dilution of TCE and

major ions, which are characteristic of groundwater subfacies D1, that occurs along the North Flow Path suggests that the TCE contributions from these source zones to groundwater in Shannon is minor relative to other TCE sources. The majority of TCE in Shannon probably consists of contributions from Lagoon C and, if it is the source, the dump on SIVI property.

This study was part of an integrated approach to the hydrogeological characterization at Valcartier, and has led to new interpretations about groundwater flow and TCE transport. The data obtained were successfully used to constrain the numerical groundwater model, with the help of a sampling program designed to meet specific objectives. Defining groundwater facies based on geochemical, isotopic and age data allowed the recognition of TCE input from the proglacial aquifer to the deltaic aquifer, and draws attention to the dump on SIVI property as being a potential significant source of TCE in Shannon groundwater. This possibility highlights the need to better resolve groundwater flow in the proglacial aquifer. More detailed characterization of the stratigraphy, vertical hydraulic gradients and groundwater geochemistry in all hydrogeologic units, especially in the southwest part of the study area, is recommended to determine if the dump is the source of TCE in Shannon associated with groundwater subfacies D2 and identify migration paths. The results of such characterization would further improve predictions made by the model and help ensure successful implementation of TCE plume control strategies in the Valcartier sector.

## References


Abbott, M.D., Lini, A., and Bierman, P.R., 2000. $\delta^{18}0$, $\delta D$ and $^{3}H$ measurements constrain groundwater recharge patterns in an upland fractured bedrock aquifer, Vermont, USA. *Journal of Hydrology*, 228, 101-112.

Adar, E.M., Rosenthal, E., Issar, A.S., and Batelaan, O. 1992. Quantitative assessment of the flow pattern in the southern Arava Valley (Israel) by environmental tracers and a mixing cell model., *Journal of Hydrology*, 136, 333-352.

Aeschbach-Hertig, W., Schlosser, P., Stute, M., Simpson, H.J., Ludin, A. And Clark, J.F., 1998. A $^{3}H/^{3}He$ Study of Ground Water Flow in a Fractured Bedrock Aquifer. *Ground Water*, 36 (4), 661-670.

Appelo, C.A.J., Postma, D., 2005. Geochemistry, groundwater and pollution, 2nd ed.. A.A. Balkema Publishers, Leiden (3rd corrected reprint 2007).

Baalousha, H., 2005. Using CRD method for quantification of groundwater recharge in the Gaza Strip, Palestine. *Environmental Geology,* 48, 889–900.

Bassett, R.L., Steinwand, A., Jorat, S., Petersen, C., and Jackson, R., 2008. Forensic isotope analysis to refine a hydrologic conceptual model. *Ground Water*, doi: 10.1111/j.1745-6584.2007.00421.x, 12 p.

Bauer, S., Fulda, C., and Schäfer, W., 2001. A multi-tracer study in a shallow aquifer using age dating tracers $^{3}H$, $^{85}Kr$, CFC-113 and $SF_6$ – indication for retarded transport of CFC-113. *Journal of Hydrology*, 248, 14-34.

Beyerle, U., Aeschbach-Hertig, W., Hofer, M., Imboden, D.M., Baur, H. and Kipfer, R., 1999. Infiltration of river water to a shallow aquifer investigated with 3H/3He, noble gases and CFCs. *Journal of Hydrology*, 220, 169-185.

Blais, V., 2006. Caractérisation et modélisation de l'écoulement et du transport de TCE en relation avec la rivière Jacques-Cartier à Shannon, Québec, Canada. M.Sc. Thesis, INRS-Eau Terre Environnement, February 2006.

Bohlke, J.K., and Denver, J.M., 1995, Combined use of groundwater dating, chemical, and isotopic analyses to resolve the history and fate of nitrate contamination in two agricultural watersheds, Atlantic coastal plain, Maryland. *Water Resources Research*, 31 (9), 2319-2339.

Bottomley, D.J., Ross, J.D. and Clarke, W.B., 1984. Helium and neon isotope geochemistry of some ground waters from the Canadian Precambrian Shield. *Geochimica et Cosmochimica Acta*, 48, 1973-1985.

Boutin, A., Lefebvre, R., Blais, V., Martel, R., Therrien, R. Parent, M., 2004. Modeling of groundwater flow and TCE transport in the Valcartier area aquifer system. In D. Demers, D. Leahy, R. Lefebvre, S. Leroueil et R. Martel, ed., Proceedings, *57th Canadian Geotechnical Conference and 5th Joint CGS/IAH Conference*, October 24-27, 2004, Quebec City, Canada, ISBN 0-920505-29-5, Session 4B, 36-43.

Brenot, A., Baran, N., Petelet-Giraud, E., and Négrel, P., 2008. Interaction between different water bodies in a small catchment in the Paris basin (Brévilles, France): Tracing of multiple Sr sources through Sr isotopes coupled with Mg/Sr and Ca/Sr ratios. *Applied Geochemistry* 23, p. 58-75.

Chesneaux, R., Molson, J.W., and Chapuis, R.P., 2005, An Analytical Solution for Ground Water Transit Time through Unconfined Aquifers. *Ground Water*, 43 (4), 511-517.

Clark, I.D. and Fritz, P., 1997. Environmental Isotopes in Geochemistry. Environmental Isotopes in Hydrogeology. CRC Press. Boca Raton, FL.

Clark, J.F., Davisson, M.L., Hudson, G.B., Macfarlane, P.A., 1998. Noble gases, stable isotopes, and radiocarbon as tracers of flow in the Dakota aquifer, Colorado and Kansas. *Journal of Hydrology*, 211, 151-167

Cloutier, V., Lefebvre, R., Savard, M.M., Bourque, E., and Therrien, R., 2006, Hydrogeochemistry and groundwater origin of the Basses-Laurentides sedimentary rock aquifer

system, St. Lawrence Lowlands, Québec, Canada. *Hydrogeology Journal* 14: 573-590. doi: 10.1007/s10040-005-0002-3.

Cloutier, V., Lefebvre, R., Therrien, R., and Savard, M.M., 2008. Multivariate statistical analysis of geochemical data as indicative of the hydrogeochemical evolution of groundwater in a sedimentary rock aquifer system. *Journal of Hydrology*, 353, 294-313.

Cook, P.G., and Solomon, D.K., 1997. Recent advances in dating young groundwater: chlorofluorocarbons, $^{3}H/^{3}He$ and $^{85}Kr$. *Journal of Hydrology*, 191, 245-265.

Crowe, A.S., Shikaze, S.G., Ptacek, C.J., 2004. Numerical modelling of groundwater flow and contaminant transport to the Point Pelee marsh, Ontario, Canada. *Hydrological Processes*, 18, 293-314.

Davis, J.C. 2002. Statistics and Data Analysis in Geology, third edition. John Wiley & Sons, Inc. New York, NY.

Devlin, J.F., McMaster, M. and Barker J.F., 2002. Hydrogeologic assessment of in situ natural attenuation in a controlled field experiment. *Water Resources Research*, 38(1) 10.1029/2000 WR000148: 3-1 - 3-11.

Domenico, P.A., Schwartz. F.W., 1998. Physical and Chemical Hydrogeology ($2^{nd}$ ed.). John Wiley and Sons, New York, NY, 506 p.

Dunkle-Shapiro, S., Rowe, G., Schlosser, P., Ludin, A. and Stute, M., 1998. Tritium-helium 3 dating under complex conditions in hydraulically stressed areas of a buried aquifer. *Water Resources Research,* 34, 1165-1180.

Dunkle-Shapiro, S., LeBlanc, D., Schlosser, P., and Ludin, A., 1999, Characterizing a Sewage Plume Using the 3H-3He Dating Technique. *Ground Water*, 37 (6), 861-878.

Environment Canada, 2008. Climate Normals and Averages 1971-2000 – Quebec City. National Climate Data and Information Archive. http://climate.weatheroffice.ec.gc.ca/climate_normals/

Ekwurzel, B., Schlosser, P., Smethie, W.M., Plummer, L.N., Busenberg, E., Michel, R.L., Weppernig, R., Stute, M., 1994. Dating of shallow groundwater: Comparison of the transient tracers $^{3}H/^{3}He$, chlorofluorocarbons, and $^{85}Kr$. *Water Resources Research*, 30 (6), 1693-1708.

Fagnan, N., Bourque, É., Michaud, Y., Lefebvre, R., Boisvert, É., Parent, M., Martel, R., 1999. Hydrogeology of the deltaic complexes along the north short of the Champlain Sea, Quebec. *Hydrogéologie*, no. 4, 9-22. [In French]

Farnham, I.M., Stetzenbach, K.J., Singh, A.K., and Johannesson, K.H., 2000. Deciphering Groundwater Flow Systems in Oasis Valley, Nevada, Using Trace Element Chemistry, Multivariate Statistics, and Geographical Information System. *Mathematical Geology*, 32 (8), 943-968.

Fauveau, É., Lefebvre, R., Ballard, J.-M., Fortier, R., and Martel, R., 2005. Examples of hydrogeological characterization of unconsolidated sediments with direct push and rotopercussion technologies. Proceedings, *58th Canadian Geotechnical Conference and 6th Joint CGS/IAH Conference*, Saskatoon, Canada, October 2005, Session 11EA, Paper 565, 8 p.

Fauveau, É., 2006. Caractérisation hydrogéologique et reconnaissance des faciès des dépôts meubles avec les sondages par enfoncement et par rotopercussion. Mémoire de maîtrise, INRS-Eau, Terre et Environnement, Juillet 2006.

Fisher, R.S., and Mullican, W.F., 1997. Hydrochemical Evolution of Sodium-Sulfate and Sodium-Chloride Groundwater Beneath the Northern Chihuahuan Desert, Trans-Pecos, Texas, USA. *Hydrogeology Journal*, 5 (2), 4-16.

Freeze, R.A. and Cherry, J.A., 1979. Groundwater. Prentice Hall. Englewood Cliffs, NJ.

Fritz, P., Drimmie, R.J., Frape, S.K., and O'Shea, O., 1987. The isotopic composition of precipitation and groundwater in Canada. In: *Isotope Techniques in Water Resources Development*, IAEA Symposium 299, March 1987, Vienna, 539-550.

GeoInsight, 2006. HydraSleeve Field Manual. GeoInsight, 1680 Hickory Loop, Suite B, Las Cruces, NM 88005, U.S.A., www.geoinsightonline.com, 8 p.

Glynn, P.D. and Plummer, L.N., 2005, Geochemistry and the understanding of ground-water systems. *Hydrogeology Journal*, 13, 263-286.

Güler, C., Thyne, G.D., McCray, J.E., and Turner, A.K., 2002. Evaluation of graphical and multivariate statistical methods for classification of water chemistry data. *Hydrogeology Journal*, 10, 455-474.

Healy, R.W., and Cook, P.G., 2002. Using groundwater levels to estimate recharge. *Hydrogeology Journal*, 10, 91–109.

Health Canada, 2008. Guidelines for Canadian Drinking Water Quality - Summary Table. www.hc-sc.gc.ca/ewh-semt/alt_formats/hecs-sesc/pdf/pubs/water-eau/sum_guide-res_recom/summary-sommaire-eng.pdf

Heaton, T.H.E., and Vogel, J.C., 1981. "Excess air" in groundwater. *Journal of Hydrology*, 50, 201-216.

Heemskerk, A.R. and Johnson, J., 1998. Tritium Analysis – Technical Procedure 1.0. Environmental Isotope Laboratory, Department of Earth Sciences, University of Waterloo. Waterloo, ON.

Hounslow, A.W., 1995. Water quality data: analysis and interpretation. Lewis Publisher, CRC Press, Boca Raton, Florida, 397 p.

IAEA/WMO, 2006. Global Network of Isotopes in Precipitation. The GNIP Database. isohis.iaea.org

ITRC (Interstate Technology & Regulatory Council), 2007. *Protocol for Use of Five Passive Samplers to Sample for a Variety of Contaminants in Groundwater*. DSP-5. Washington, D.C.: Interstate Technology & Regulatory Council, Diffusion/Passive Sampler Team. February 2007, www.itrcweb.org, 88 p. and appendices.

ITRC (Interstate Technology & Regulatory Council). 2006. *Technology Overview of Passive Sampler Technologies*. DSP-4. Washington, D.C.: Interstate Technology & Regulatory Council, Diffusion Sampler Team, March 2006. www.itrcweb.org, 94 p. and appendices.

Kipfer, R., Aeschback-Hertig, W., Peeters, F. and Stute, M., 2002. Noble Gases in Lakes and Groundwaters. In: D. Porcelli, C.J. Ballentine, and R Wieler, ed., Noble Gases in Geochemistry and Cosmochemistry. Reviews in Mineralogy and Geochemistry Vol. 47. The Mineralogical Society of America. Washington, D.C.

Keating, E.H., and Bahr, J.M., 1998, Using reactive solutes to constrain groundwater flow models at a site in northern Wisconsin. *Water Resources Research*, 34 (12), 3561-3571.

Koh, D.-C., Plummer, N., Solomon, K., Busenberg, E., Kim, Y.-J., and Chang, H.-W., 2006. Application of environmental tracers to mixing, evolution, and nitrate contamination of ground water in Jeju Island, Korea. *Journal of Hydrology,* 327, 258-275.

Konikow, L.F. and Bredehoeft, J.D., 1992. Ground-water models cannot be validated. *Advances in Water Resources*, 15, 75-83.

Labolle, E.M., Fogg, G.E. and. Eweis, J.B., 2006. Diffusive fractionation of $^{3}H$ and $^{3}He$ in groundwater and its impact on groundwater age estimates. *Water Resources Research,* 42, doi:10.1029/2005WR004756.

Landon, M.K., Delin, G.N., Komon, S.C., and Regan, C.P., 2000. Relation of Pathways and Transit Times of Recharge Water to Nitrate Concentrations Using Stable Isotopes. *Ground Water*, 38 (3), 381-395.

Lee, K., Wenner, D.B., and Lee, I., 1999. Using H- and O-isotopic data for estimating the relative contributions of rainy and dry season precipitation to groundwater: example from Cheju Island, Korea. *Journal of Hydrology*, 222, 65-74.

Lefebvre, R., Maltais, I., Paradis, D., and Michaud, Y., 2009. Recharge assessment using daily soil moisture balance and well hydrographs in deltaic unconfined aquifers. Paper 1147, *AGU 2009 Joint Assembly*, 24-27 May, 2009, Toronto, Ontario, Canada.

Lefebvre, R., Boutin, A., Blais, V., Martel, R., Therrien, R. Parent, M., Ouellon, T., Roy, N., and Lapointe, M., 2004. Characterization of the hydrogeological context and dissolved TCE plume in the granular aquifer system of the Valcartier area, Quebec, Canada. In D. Demers, D. Leahy, R.

Lefebvre, S. Leroueil et R. Martel, ed., Proceedings, *57th Canadian Geotechnical Conference and 5th Joint CGS/IAH Conference*, October 24-27, 2004, Quebec City, Canada, ISBN 0-920505-29-5, Session 4B, 28-35.

Lefebvre, R., Boutin, A., Martel, R., Therrien, R., Parent, M., and Blais, V., 2003. Caractérisation et modélisation numérique de l'écoulement et de la migration de la contamination en TCE dans l'eau souterraine du secteur Valcartier, Québec, Canada. Research Report R-631 submitted to the Ministry of National Defense, May 2003, 99 p., 28 plates and separate appendix volume. http://www.ete.inrs.ca/index.jsp?page=5_1

Maltais, I., 2006. Estimation de la recharge par le bilan hydrologique quotidien dans la région de Portneuf. Projet de fin d'étude, Département de géologie et de génie géologique, Université Laval.

Mamyrin, B.A. and Tolstikhin, I.N., 1984, Helium Isotopes in Nature. Developments in Geochemistry 3. Elsevier, Amsterdam. 273 p.

Manning, A.H., Solomon, D.K., and Sheldon, A.L., 2003. Applications of a Total Dissolved Gas Pressure Probe in Ground Water Studies. *Ground Water*, 41(4), 440-448.

Marsily, G., de, Delay, F., Gonçalves, J., Renard, Ph., Teles, V., and Violette, S., 2005. Dealing with spatial heterogeneity. Hydrogeology Journal, Vol. 13, p. 161-183.

Martel, R., Parent, M., Lefebvre, R., Carrier, M-A., Paradis, D., Mailloux, M., Hardy, F., Michaud, Y., and Boutin, A., 2000. *Caractérisation complémentaire des contextes géologique et hydrogéologique du secteur Valcartier* [In French], 115 p.

Martinez, W., and Martinez, A.R., 2005. Exploratory Data Analysis with MATLAB®. Chapman & Hall / CRC Press. Boca Raton, FL.

Mayer, K. U., Benner, S. G., Frind, E. O., Thornton, S. F., and Lerner, D. L., 2001. Reactive transport modeling of processes controlling the distribution and natural attenuation of phenolic compounds in a deep sandstone aquifer. *Journal of Contaminant Hydrol*ogy, 53, 341-368.

Melloul, A., and Collin, M. 1992. The 'principal components' statistical method as a complementary approach to geochemical methods in water quality factor identification; application to the Coastal Plain aquifer of Israel. *Journal of Hydrology*, 140, 49-73.

Michaud, Y., Parent, M., Mailloux, M., Boisvert, É., Lefebvre, R., Martel, R., Boivin, R., Roy, N., and Hains, S., 1999. *Cartographie des formations superficielles et cartographie hydrogéologique de la base des forces canadiennes Valcartier* [In French], Report submitted to the USS Valcartier, 1 CD-Rom, 2 maps.

Motzer, W.E., 2001. Perchlorate: Problems, Detection, and Solutions. *Environmental Forensics,* 2, 301-311.

Moore, K.B., Ekwurzel, B., Esser, B.K., Hudson, G.B., and Moran, J.E., 2006. Sources of groundwater nitrate revealed using residence time and isotope methods. *Applied Geochemistry,* 21, 1016–1029.

Murphy, S., Ouellon, T., Lefebvre, R., Clark, I.D., and Ballard, J.-M., 2009. Tritium-Helium dating and geochemical characterization of groundwater in the Valcartier deltaic aquifer system. INRS, Centre-Eau Terre Environnement, Research report R-960, March 2009, ISBN 978-2-89146-558-8, 75 p. and 21 plates.

Natural Resources Canada. 2008. Geoscape Quebec – An Extraordinary Geological Heritage. http://geoscape.nrcan.gc.ca/quebec/heritage_e.php

Neumann, R.B., Labolle, E.M. and Harvey, C.F., 2008. The Effects of Dual-Domain Mass Transfer on the Tritium-Helium-3 Dating Method. *Environmental Science and Technology,* 42, 4837-4843.

Oreskes, N., Shrader-Frechette, K., and Belitz, K., 1994, Verification, Validation, and Confirmation of Numerical Models in Earth Sciences. *Science,* 263, 641-646.

Ouellon, T., Lefebvre, R., and Blais, V., 2008b. Synthèse du contexte hydrogéologique et de la problématique du TCE dans le secteur Valcartier, Québec, Canada. INRS-Eau, Terre et Environnement, Research Report R-961, ISBN 978-2-89146-560-1. [In French]

Ouellon, T., Blais, V., Lefebvre, R., Ballard, and J.-M., 2008c. Contexte hydrogéologique et modélisation de l'écoulement de l'eau souterraine dans la vallée de Val-Bélair en relation avec la présence de TCE dans le secteur Valcartier, Ville de Québec, Québec, Canada. INRS, Centre-Eau Terre Environnement, Research Report R-962, December 2008, 81 p., 30 map plates and appedix, ISBN 978-2-89146-557-1. [In French]

Ouellon, T., Lefebvre, R., Marcotte, D., Boutin, A., Blais, V., Parent, M., 2008a. Hydraulic conductivity heterogeneity of a local deltaic aquifer system from the kriged 3D distribution of hydrofacies from borehole logs, Valcatier, Canada. *Journal of Hydrology*, 351 (1-2), 71-86.

Pankow, J.F. and Cherry, J.A., 1996. Dense chlorinated solvents and other DNAPLs in groundwater: history, behavior, and remediation. Waterloo Press – Portland, Oregon.

Paradis, D., Martel, R., Karanta, G., Lefebvre, R., Michaud, Y., Therrien, R., and Nastev, M., 2007. Comparative study of methods for wellhead protection area delineation. *Ground Water*, 45 (2), 158-167.

Parent, M., Girard, F., Fagnan, N., Michaud, Y., Boisvert, É. and Fortier, R., 2008. Caractérisation géologique des formations superficielles enfouies. *In* Michaud et al. ed., *Guide méthodologique pour la cartographie hydrogéologique régionale des aquifères granulaires.* Dépôt légal - Bibliothèque et Archives nationales du Québec, ISBN 978-2-550-51189-2 (pdf), 23-40. [In French]

Portniaguine, O., and Solomon, D.K., 1998. Parameter estimation using groundwater age and head data, Cape Cod, Massachusetts. *Water Resources Research,* 44 (4), 637-645.

Price, R.M., Top, Z., Happell, J.D., and Swart, P.K., 2003. Use of tritium and helium to define groundwater flow conditions in Everglades National Park. *Water Resources Research,* 39 (9), 1267-1278.

Reilly, T.E., Plummer, L.N., Phillips, P.J. and Busenberg, E., 1994. The use of simulation and multiple environmental tracers to quantify groundwater flow in a shallow aquifer. *Water Resources Research,* 30 (2), 421-433.

Rubin, Y., and Hubbard, S.S., 2005. Introduction to hydrogeophysics, in Rubin, Y. and Hubbard, S.S., ed., Hydrogeophysics. Springer, p. 3-21.

Salem, Z.E., Sakura, Y., and Mohammed Aslam, M.A., 2004. The use of temperature, stable isotopes and water quality to determine the pattern and spatial extend of groundwater flow: Nagaoka area, Japan. *Hydrogeology Journal*, 12, 563-575.

Sanford, W.E., Shropshire, R.G., and Solomon, D.K., 1996. Dissolved Gas Tracers in Groundwater: Simplified Injection, Sampling, and Analysis. *Water Resources Research*, 32 (6), 1635-1642.

Scanlon, B.R., Healy, R.W., and Cook, P.G., 2002. Choosing appropriate techniques for quantifying groundwater recharge. *Hydrogeology Journal,* 10, 18–39

Schlosser, P., Stute, M., Dorr, H., Sonntag, C. and Munnich, K.O., 1988. Tritium/3He dating of shallow groundwater. *Earth and Planetary Science Letters,* 89, 353-362.

Schlosser, P., Stute, M., Sonntag, C., and Munnich, K.O., 1989. Tritiogenic 3He in shallow groundwater. *Earth and Planetary Science Letters,* 94, 245-256.

Sheets, R.A., Bain, E.S. and Rowe, G.L., 1998. Use of $^{3}H/^{3}He$ ages to evaluate and improve groundwater flow models in a complex buried-valley aquifer. *Water Resources Research,* 34, 1077-1089.

Shinn, J.D., Timian, D.A., Morey, R.M., Mitchell, G., Antle, C.L., and Hull, R., 1998. Development of a CPT deployed probe for in situ measurement of volumetric soil moisture content and electrical resistivity. *Field Analytical Chemistry and Technology*, 2(2), 103-110.

Solomon, D.K., and Sudicky, E.A., 1991, Tritium and Helium 3 Isotope Ratios for Direct Estimation of Spatial Variations in Groundwater Recharge. *Water Resources Research*, 27(9), 2309-2319.

Solomon, D.K., Podera, R.J., Schiff, S.L., and Cherry, J.A., 1992. Tritium and helium 3 as groundwater age tracers in the Borden aquifer. *Water Resources Research*, 28 (3), 741-755.

Solomon, D.K., Schiff, S.L., Podera, R.J., and Clarke, W.B., 1993. A validation of the $^{3}H/^{3}He$ method of determining groundwater recharge. *Water Resources Research*, 29 (9), 2951-2962.

Solomon, D.K., Poreda, R.J., Cook, P.G., and Hunt, A., 1995, Site Characterzation Using 3H/3He Ground-Water Ages, Cape Cod, MA. *Ground Water*, 33 (6), 988-996.

Sracek, O., and Hirata, R., 2002, Geochemical and stable isotopic evolution of the Guarani Aquifer System in the state of São Paulo, Brazil. *Hydrogeology Journal,* 10, 643-655. doi:10.1007/s10040-002-0222-8.

Steinhorst, R.K., and Williams, R.E. 1985. Discrimination of Groundwater Sources Using Cluster Analysis, MANOVA, Canonical Analysis and Discriminant Analysis. *Water Resources Research*, 21 (8), 1149-1156.

Stimson, J., Frape, S., Drimmie, R., and Rudolph, D., 2001. Isotopic and geochemical evidence of regional-scale anisotropy and interconnectivity of an alluvial fan system, Cochabamba Valley, Bolivia. *Applied Geochemistry*, 16, 1097-1114.

Stute, M., Clark, J.F., Schlosser, P., Broecker, S., and Bonani, G., 1995. A 30,000 yr continental palaeotemperature record derived from noble gases dissolved in groundwater from the San Juan Basin, New Mexico. *Quaternary Research*, 43, 209-220.

Stuyfzand, P.J., 1999. Patterns in groundwater chemistry resulting from groundwater flow. *Hydrogeology Journal*, 7 (1), 15-27.

Szabo, Z., Rice, D.E., Plummer, L.N., Busenberg, E., Drenkard, S., and Schlosser, P., 1996, Age dating of shallow groundwater with chlorofluorocarbons, tritium/helium 3, and flow path analysis, southern New Jersey coastal plain. *Water Resources Research*, 32 (4), 1023-1038.

Tolstikhin, I.N. and Kamenskiy, I.L., 1969. Determination of ground-water ages by the $T-^{3}He$ Method. *Geochemistry International,* 6, 810-811.

Tompson, A.F.B., Carle, S.F., Rosenberg, N.D., and Maxwell, R.M., 1999. Analysis of groundwater migration from artificial recharge in a large urban aquifer: A simulation perspective. *Water Resources Research,* 35 (10), 2981-2998.

Tóth, J., 1999. Groundwater as a geologic agent: An overview of the causes, processes, and manifestations. *Hydrogeology Journal*, 7, 1-14.

Trumpolt, C.W., Crain, M., Cullison, G.D., Flanagan, S.J., Siegel, L., and Lathrop, S., 2005, Perchlorate: Sources, Uses, and Occurrences in the Environment. *Remediation*, Winter 2005, 65-89.

WASY Software, 2005, Feflow 5.2 Finite Element Subsurface Flow and Transport Simulation System – User's Manual. WASY Institute, 192 p.

Weidmeyer, T.H., Swanson, M.A., Moutoux, D.E., Gordon, E.K., Wilson, J.T., Wilson, B.H., Kampbell, D.H., Hass, P.E., Miller, R.N., Hansen, J.E., and Chapelle, F.H., 1998. Technical protocol for evaluating natural attenuation of chlorinated solvents in ground water. U.S. EPA - Report EPA/600/R-98/128, September 1998, 78 p. and appendices.

Weiss, R.F., 1971. Solubility of Helium and Neon in Water and Seawater. *Journal of Chemical and Engineering Data*, 16 (2), 235-241.

Weissmann, G.S., Zhang, Y., Labolle, E.M., and Fogg, G.E., 2002. Dispersion of groundwater age in an alluvial aquifer system. *Water Resources Research* 38 (10), doi: 10.1029/2001WR000907.

Zinn, B.A., and Konikow, L.F., 2007, Effects of intraborehole flow on groundwater age distribution. *Hydrogeology Journal*, 15, 633-643. DOI: 10.1007/s10040-006-0139-8

Zoellmann, K., Kinzelbach, W., and Fulda, C., 2001, Environmental tracer transport ($^3H$ and $SF_6$) in the saturated and unsaturated zones and its use in nitrate pollution management. *Journal of Hydrology*, 240, 187-205.

# Appendix A: Complete Data Set

**Table A1.** Sample Locations

| Sample | Objective | X | Y | Ground Elevation | Unit | Water Table Elevation | Elevation Top of Screen | Elevation Bottom of Screen | Sample Elevation |
|---|---|---|---|---|---|---|---|---|---|
| | | UTM m | UTM m | m | | m | m | m | m |
| *Prodeltaic Silt* | | | | | | | | | |
| B69-2-6m | Prodeltaic Silty Aquitard | 311336 | 5195271 | 173.73 | Deltaic Aquifer | 170.94 | 169.16 | 167.63 | 168.58 |
| B69-2-23m | Prodeltaic Silty Aquitard | 311336 | 5195271 | 173.73 | Deltaic Aquifer | 167.92 | 155.44 | 150.87 | 153.06 |
| B70-1-10m | Prodeltaic Silty Aquitard | 311479 | 5195301 | 173.68 | Deltaic Aquifer | 171.05 | 166.22 | 162.81 | 165.00 |
| B70-1-21m | Prodeltaic Silty Aquitard | 311479 | 5195301 | 173.68 | Deltaic Aquifer | 168.06 | 155.68 | 152.68 | 154.14 |
| B98-1-13m | Prodeltaic Silty Aquitard | 311284 | 5195446 | 174.02 | Deltaic Aquifer | 171.49 | 163.99 | 160.99 | 163.17 |
| B98-1-22m | Prodeltaic Silty Aquitard | 311283 | 5195446 | 174.02 | Deltaic Aquifer | 167.90 | 154.97 | 151.67 | 153.37 |
| *North Flow Path* | | | | | | | | | |
| PO-SH-8-H | North Flow Path + Shannon Transect | 308069 | 5195814 | 169.60 | Deltaic Aquifer | 157.29 | 152.20 | 150.70 | 152.23 |
| PO-SH-7-H | North Flow Path + Shannon Transect | 308068 | 5195815 | 169.39 | Deltaic Aquifer | 157.23 | 148.69 | 147.19 | 148.37 |
| DP-PO-122-1 | North Flow Path | 309159 | 5195894 | 170.60 | Deltaic Aquifer | 162.99 | 160.91 | 148.71 | 159.64 |
| DP-PO-122-2 | North Flow Path | 309159 | 5195894 | 170.60 | Deltaic Aquifer | 162.99 | 160.91 | 148.71 | 155.64 |
| DP-PO-122-3 | North Flow Path | 309159 | 5195894 | 170.60 | Deltaic Aquifer | 162.99 | 160.91 | 148.71 | 151.64 |
| PO-122-H | North Flow Path | 309159 | 5195894 | 170.60 | Deltaic Aquifer | 162.85 | 149.03 | 144.53 | 146.73 |
| PO-122-B-U | North Flow Path | 309159 | 5195894 | 170.60 | Deltaic Aquifer | 162.84 | 141.07 | 136.57 | 139.85 |
| PO-122-B-L | North Flow Path | 309159 | 5195894 | 170.60 | Deltaic Aquifer | 162.84 | 141.07 | 136.57 | 137.65 |
| PO-153-H-U | North Flow Path | 310231 | 5195745 | 176.29 | Deltaic Aquifer | 166.46 | 160.82 | 156.32 | 159.69 |
| PO-153-H-L | North Flow Path | 310231 | 5195745 | 176.29 | Deltaic Aquifer | 166.46 | 160.82 | 156.32 | 157.39 |
| PO-152-H | North Flow Path | 310229 | 5195748 | 176.30 | Deltaic Aquifer | 166.58 | 154.79 | 150.24 | 152.51 |
| PO-153-B | North Flow Path | 310231 | 5195745 | 176.29 | Deltaic Aquifer | 166.46 | 147.77 | 143.27 | 145.47 |
| PO-152-B | North Flow Path | 310229 | 5195748 | 176.30 | Deltaic Aquifer | 166.42 | 140.67 | 136.17 | 138.32 |
| DP-C2-10-1 | North Flow Path + Recharge | 311163 | 5195105 | 172.80 | Deltaic Aquifer | 166.95 | 166.96 | 154.77 | 164.70 |
| DP-C2-10-2 | North Flow Path + Recharge | 311163 | 5195105 | 172.80 | Deltaic Aquifer | 166.95 | 166.96 | 154.77 | 161.70 |
| DP-C2-10-3 | North Flow Path + Recharge | 311163 | 5195105 | 172.80 | Deltaic Aquifer | 166.95 | 166.96 | 154.77 | 157.70 |
| C2-10-22m | North Flow Path + Recharge | 311163 | 5195105 | 172.71 | Deltaic Aquifer | 167.70 | 155.22 | 150.72 | 153.97 |
| C2-9-28m | North Flow Path + Recharge | 311164 | 5195104 | 172.91 | Deltaic Aquifer | 167.96 | 149.38 | 144.88 | 148.11 |
| C2-10-35m | North Flow Path + Recharge | 311163 | 5195105 | 172.71 | Deltaic Aquifer | 167.74 | 142.19 | 137.69 | 141.27 |

| Sample | Objective | X | Y | Ground Elevation | Unit | Water Table Elevation | Elevation Top of Screen | Elevation Bottom of Screen | Sample Elevation |
|---|---|---|---|---|---|---|---|---|---|
| | | UTM m | UTM m | m | | m | m | m | m |
| *South Flow Path* | | | | | | | | | |
| PO-SH-48-H-U | South Flow Path | 308183 | 5195471 | 168.42 | Deltaic Aquifer | 156.77 | 154.72 | 151.72 | 153.88 |
| PO-SH-48-H-L | South Flow Path | 308183 | 5195471 | 168.42 | Deltaic Aquifer | 156.77 | 154.72 | 151.72 | 152.48 |
| PO-SH-48-B-U | South Flow Path | 308182 | 5195471 | 168.42 | Deltaic Aquifer | 156.78 | 148.52 | 145.52 | 147.69 |
| PO-SH-48-B-L | South Flow Path | 308182 | 5195471 | 168.42 | Deltaic Aquifer | 156.78 | 148.52 | 145.52 | 146.29 |
| PO-SH-47-H | South Flow Path | 308184 | 5195470 | 168.44 | Deltaic Aquifer | 156.82 | 144.04 | 142.54 | 143.29 |
| PO-SH-26-H-U | South Flow Path + Shannon Transect | 308372 | 5195500 | 168.57 | Deltaic Aquifer | 158.39 | 156.07 | 153.07 | 155.57 |
| PO-SH-26-H-L | South Flow Path + Shannon Transect | 308372 | 5195500 | 168.57 | Deltaic Aquifer | 158.39 | 156.07 | 153.07 | 153.57 |
| PO-SH-26-B-U | South Flow Path + Shannon Transect | 308374 | 5195498 | 168.57 | Deltaic Aquifer | 158.42 | 149.57 | 146.57 | 149.07 |
| PO-SH-26-B-L | South Flow Path + Shannon Transect | 308374 | 5195498 | 168.57 | Deltaic Aquifer | 158.42 | 149.57 | 146.57 | 147.07 |
| PO-117-H | South Flow Path | 308819 | 5195554 | 169.73 | Deltaic Aquifer | 161.47 | 160.41 | 155.91 | 158.09 |
| PO-116-H | South Flow Path | 308819 | 5195552 | 169.80 | Deltaic Aquifer | 161.56 | 154.31 | 149.81 | 152.03 |
| PO-117-B | South Flow Path | 308819 | 5195554 | 169.73 | Deltaic Aquifer | 161.48 | 149.20 | 144.70 | 146.86 |
| PO-116-B | South Flow Path | 308819 | 5195552 | 169.80 | Deltaic Aquifer | 161.57 | 144.10 | 139.60 | 141.89 |
| PO-126-H | South Flow Path | 309156 | 5195564 | 171.87 | Deltaic Aquifer | 162.42 | 161.51 | 156.93 | 159.19 |
| DP-PO-125 | South Flow Path | 309156 | 5195564 | 171.87 | Deltaic Aquifer | 162.74 | 162.64 | 150.44 | 156.34 |
| PO-126-B-U | South Flow Path | 309156 | 5195564 | 171.87 | Deltaic Aquifer | 162.44 | 151.45 | 146.87 | 150.21 |
| PO-126-B-L | South Flow Path | 309156 | 5195564 | 171.87 | Deltaic Aquifer | 162.44 | 151.45 | 146.87 | 148.01 |
| PO-125-H | South Flow Path | 309157 | 5195562 | 171.61 | Deltaic Aquifer | 162.39 | 137.30 | 135.78 | 136.68 |
| PO-143-H | South Flow Path | 310045 | 5195447 | 175.94 | Deltaic Aquifer | 166.50 | 165.94 | 162.94 | 164.34 |
| PO-142-H-U | South Flow Path | 310048 | 5195447 | 175.89 | Deltaic Aquifer | 166.51 | 161.44 | 156.94 | 160.28 |
| PO-142-H-L | South Flow Path | 310048 | 5195447 | 175.89 | Deltaic Aquifer | 166.51 | 161.44 | 156.94 | 158.03 |
| PO-143-B | South Flow Path | 310045 | 5195448 | 175.94 | Deltaic Aquifer | 166.47 | 156.44 | 151.94 | 154.13 |
| PO-142-B | South Flow Path | 310048 | 5195447 | 175.89 | Deltaic Aquifer | 166.51 | 151.77 | 147.27 | 149.48 |

| Sample | Objective | X | Y | Ground Elevation | Unit | Water Table Elevation | Elevation Top of Screen | Elevation Bottom of Screen | Sample Elevation |
|---|---|---|---|---|---|---|---|---|---|
| | | UTM m | UTM m | m | | m | m | m | m |
| *Shannon Transect* | | | | | | | | | |
| PO-SH-16-H | Shannon Transect | 308164 | 5195735 | 168.62 | Deltaic Aquifer | 158.25 | 149.40 | 147.90 | 148.67 |
| PO-SH-16-B | Shannon Transect | 308164 | 5195735 | 168.62 | Deltaic Aquifer | 158.25 | 133.80 | 143.30 | 144.07 |
| PO-SH-15-H | Shannon Transect | 308167 | 5195731 | 168.74 | Deltaic Aquifer | 157.23 | 143.20 | 141.70 | 143.24 |
| PO-SH-22-H-U | Shannon Transect | 308305 | 5195577 | 168.71 | Deltaic Aquifer | 157.76 | 157.81 | 154.81 | 157.41 |
| PO-SH-22-H-L | Shannon Transect | 308305 | 5195577 | 168.71 | Deltaic Aquifer | 157.76 | 157.81 | 154.81 | 155.91 |
| PO-SH-22-B-U | Shannon Transect | 308305 | 5195576 | 168.71 | Deltaic Aquifer | 157.76 | 151.71 | 148.71 | 151.28 |
| PO-SH-22-B-L | Shannon Transect | 308305 | 5195576 | 168.71 | Deltaic Aquifer | 157.76 | 151.71 | 148.71 | 149.78 |
| PO-SH-21-H | Shannon Transect | 308308 | 5195575 | 168.83 | Deltaic Aquifer | 157.76 | 146.33 | 144.83 | 145.91 |
| PO-SH-28-H | Shannon Transect | 308514 | 5195343 | 168.71 | Deltaic Aquifer | 159.29 | 156.10 | 151.60 | 153.84 |
| PO-SH-28-B | Shannon Transect | 308514 | 5195343 | 168.71 | Deltaic Aquifer | 160.11 | 148.40 | 143.90 | 147.66 |
| PO-SH-6-H-U | Shannon Transect | 308500 | 5195260 | 167.94 | Deltaic Aquifer | 159.16 | 155.64 | 151.14 | 154.47 |
| PO-SH-6-H-L | Shannon Transect | 308500 | 5195260 | 167.94 | Deltaic Aquifer | 159.16 | 155.64 | 151.14 | 152.27 |
| PO-SH-6-B-U | Shannon Transect | 308500 | 5195260 | 167.94 | Deltaic Aquifer | 159.14 | 147.64 | 143.14 | 146.44 |
| PO-SH-6-B-L | Shannon Transect | 308500 | 5195260 | 167.94 | Deltaic Aquifer | 159.14 | 147.64 | 143.14 | 144.24 |
| PO-SH-5-H | Shannon Transect | 308500 | 5195262 | 168.19 | Deltaic Aquifer | 159.17 | 139.29 | 134.79 | 137.03 |
| *Proglacial Aquifer Locations* | | | | | | | | | |
| PO-154-33 | Proglacial | 310147 | 5195372 | 175.56 | Proglacial Aquifer | 166.82 | 145.10 | 143.60 | 144.32 |
| PO-135-21 | Proglacial | 309473 | 5195582 | 176.29 | Proglacial Aquifer | 163.40 | 157.00 | 155.50 | 156.26 |
| PO-128-35 | Proglacial | 309258 | 5195274 | 172.24 | Proglacial Aquifer | 163.90 | 139.40 | 137.90 | 138.62 |
| PO-SH-25H | Proglacial | 308373 | 5195501 | 168.41 | Proglacial Aquifer | 159.39 | 143.41 | 138.41 | 140.91 |
| PO-SH-46-B | Proglacial | 308375 | 5195018 | 166.77 | Proglacial Aquifer | 162.02 | 148.90 | 147.40 | 148.12 |
| PO-SH-45-B | Proglacial | 308377 | 5195016 | 166.93 | Proglacial Aquifer | 162.11 | 143.00 | 141.50 | 142.28 |

**Table A2**. Projection of sample locations onto cross sections.

| Sample | Sample Depth Below W.T. | Elevation of Deltaic Aquifer Base | Real Saturated Thickness | Relative sampling position in saturated zone | Saturated Thickness on Tracking Flow Path | Elevation W.T. Projected on Tracks | Sample Elevation Projected on Tracks | Projected Depth Below W.T. | Horizontal Distance to Track Origin | Vertical Distance to Track Origin |
|---|---|---|---|---|---|---|---|---|---|---|
| | m | m | m | - | m | m | m | m | m | m |
| *North Flow Path* | | | | | | | | | | |
| PO-SH-8-H | 5.06 | 145.28 | 12.01 | 0.421 | 14.00 | 157.00 | 151.10 | 5.90 | 1755.50 | 13.60 |
| PO-SH-7-H | 8.86 | | | 0.738 | | | 146.67 | 10.33 | 3202.00 | 18.10 |
| DP-PO-122-1 | 3.35 | 132.74 | 30.25 | 0.111 | 27.50 | 161.25 | 158.20 | 3.05 | 669.50 | 5.50 |
| DP-PO-122-2 | 7.35 | | | 0.243 | | | 154.57 | 6.68 | 1527.00 | 12.60 |
| DP-PO-122-3 | 11.35 | | | 0.375 | | | 150.93 | 10.32 | 1854.00 | 17.40 |
| PO-122-H | 16.12 | | | 0.533 | | | 146.59 | 14.66 | 2078.50 | 22.30 |
| PO-122-B-U | 22.98 | | | 0.760 | | | 140.36 | 20.89 | 2239.50 | 29.20 |
| PO-122-B-L | 25.18 | | | 0.832 | | | 138.36 | 22.89 | | |
| PO-153-H-U | 6.77 | 136.19 | 30.27 | 0.224 | 24.75 | 165.00 | 159.46 | 5.54 | 193.00 | 7.30 |
| PO-153-H-L | 9.07 | | | 0.300 | | | 157.58 | 7.42 | 270.50 | 9.90 |
| PO-152-H | 14.07 | | | 0.465 | | | 153.50 | 11.50 | 425.00 | 14.90 |
| PO-153-B | 20.99 | | | 0.693 | | | 147.84 | 17.16 | 649.50 | 21.30 |
| PO-152-B | 28.1 | | | 0.928 | | | 142.03 | 22.97 | | |
| DP-C2-10-1 | 2.25 | 133.79 | 33.16 | 0.068 | 32.00 | 167.50 | 165.33 | 2.17 | 44.20 | 3.00 |
| DP-C2-10-2 | 5.25 | | | 0.158 | | | 162.43 | 5.07 | 77.00 | 6.00 |
| DP-C2-10-3 | 9.25 | | | 0.279 | | | 158.57 | 8.93 | 129.00 | 10.40 |
| C2-10-22m | 13.73 | | | 0.414 | | | 154.25 | 13.25 | 163.00 | 14.10 |
| C2-9-28m | 19.85 | | | 0.599 | | | 148.34 | 19.16 | 229.00 | 20.50 |
| C2-10-35m | 26.47 | | | 0.798 | | | 141.95 | 25.55 | | |
| *South Flow Path* | | | | | | | | | | |
| PO-SH-48-H-U | 2.89 | 138.73 | 18.05 | 0.160 | 20.50 | 157.00 | 153.72 | 3.28 | 345.00 | 5.90 |
| PO-SH-48-H-L | 4.29 | | | 0.238 | | | 152.13 | 4.87 | 604.00 | 8.30 |
| PO-SH-48-B-U | 9.09 | | | 0.504 | | | 146.68 | 10.32 | 2442.00 | 20.10 |
| PO-SH-48-B-L | 10.49 | | | 0.581 | | | 145.09 | 11.91 | 2596.00 | 22.70 |
| PO-SH-47-H | 13.53 | | | 0.750 | | | 141.63 | 15.37 | 2745.00 | 27.90 |
| PO-SH-26-H-U | 2.818 | 146.34 | 12.06 | 0.234 | 13.00 | 158.50 | 155.46 | 3.04 | 522.00 | 5.10 |
| PO-SH-26-H-L | 4.818 | | | 0.400 | | | 153.30 | 5.20 | 911.00 | 8.00 |
| PO-SH-26-B-U | 9.35 | | | 0.776 | | | 148.42 | 10.08 | 2404.00 | |

| Sample | Sample DepthBelow W.T. | Elevation of Deltaic Aquifer Base | Real Saturated Thickness | Relative sampling position in saturated zone | Saturated Thickness on Tracking Flow Path | Elevation W.T. Projected on Tracks | Sample Elevation Projected on Tracks | Projected Depth Below W.T. | Horizontal Distance to Track Origin | Vertical Distance to Track Origin |
|---|---|---|---|---|---|---|---|---|---|---|
| | m | m | m | - | m | m | m | m | m | m |
| *South Flow Path* | | | | | | | | | | |
| PO-SH-26-B-L | 9.63 | | | 0.799 | | | 148.12 | 10.38 | 2404.00 | 22.70 |
| PO-117-H | 3.38 | 135.62 | 26.24 | 0.129 | 25.50 | 160.50 | 157.17 | 3.33 | 334.00 | 4.10 |
| PO-116-H | 9.53 | | | 0.363 | | | 151.10 | 9.40 | 1621.00 | 15.10 |
| PO-117-B | 14.62 | | | 0.557 | | | 146.08 | 14.42 | | |
| PO-116-B | 19.68 | | | 0.750 | | | 141.09 | 19.41 | | |
| PO-126-H | 3.23 | 135.72 | 26.70 | 0.121 | 25.50 | 161.25 | 158.17 | 3.08 | 483.00 | 4.60 |
| DP-PO-125 | 6.4 | | | 0.240 | | | 155.14 | 6.11 | 1287.00 | 10.80 |
| PO-126-B-U | 12.23 | | | 0.458 | | | 149.57 | 11.68 | 1568.00 | 18.10 |
| PO-126-B-L | 14.43 | | | 0.540 | | | 147.47 | 13.78 | 1657.00 | 20.90 |
| PO-125-H | 25.71 | | | 0.963 | | | 136.69 | 24.56 | | |
| PO-143-H | 2.16 | 145.64 | 20.86 | 0.104 | 14.00 | 165.00 | 163.55 | 1.45 | 83.00 | 1.80 |
| PO-142-H-U | 6.23 | | | 0.299 | | | 160.82 | 4.18 | 403.00 | 5.60 |
| PO-142-H-L | 8.48 | | | 0.407 | | | 159.31 | 5.69 | 557.00 | 8.00 |
| PO-143-B | 12.34 | | | 0.592 | | | 156.72 | 8.28 | 738.00 | 12.60 |
| PO-142-B | 17.03 | | | 0.817 | | | 153.57 | 11.43 | | |
| *Shannon Transect* | | | | | | | | | | |
| PO-SH-22-H-U | 0.35 | 144.41 | 13.35 | 0.026 | 14.00 | 158.25 | 157.41 | 0.35 | | |
| PO-SH-22-H-L | 1.85 | | | 0.139 | | | 155.91 | 1.85 | | |
| PO-SH-22-B-U | 6.48 | | | 0.485 | | | 151.28 | 6.48 | | |
| PO-SH-22-B-L | 7.98 | | | 0.598 | | | 149.78 | 7.98 | | |
| PO-SH-21-H | 11.85 | | | 0.888 | | | 145.91 | 11.85 | | |
| PO-SH-6-H-U | | 134.89 | 24.27 | 0.193 | 10.50 | 159.50 | 154.47 | 4.69 | | |
| PO-SH-6-H-L | | | | 0.284 | | | 152.27 | 6.89 | | |
| PO-SH-6-B-U | | | | 0.523 | | | 146.46 | 12.70 | | |
| PO-SH-6-B-L | | | | 0.614 | | | 144.26 | 14.90 | | |
| PO-SH-5-H | | | | 0.912 | | | 137.02 | 22.14 | | |

**Table A3a.** $^{3}H$-$^{3}He$ Age Calculation

| Sample | Date water sample collection + gas sampler emplaced | Date gas sample collected | $^{3}H$ | Error (1σ) |
|---|---|---|---|---|
| | | | T.U. | T.U. |
| B69-2-6m | 08/11/07 | 27/11/07 | 12.3 | 0.9 |
| B69-2-23m | 08/11/07 | 27/11/07 | 11.3 | 0.9 |
| B70-1-10m | 08/11/07 | 27/11/07 | 12.3 | 0.9 |
| B70-1-21m | 08/11/07 | 27/11/07 | 10.5 | 1 |
| B98-1-13m | 08/11/07 | 27/11/07 | 10.6 | 1 |
| B98-1-22m | 08/11/07 | 27/11/07 | 8.8 | 0.8 |
| PO-SH-8-H | 02/11/07 | 21/11/07 | 12.3 | 1.1 |
| PO-SH-7-H | 02/11/07 | 21/11/07 | 11.3 | 1 |
| DP-PO-122-1 | 20/11/07 | 27/11/07 | 12.3 | 0.9 |
| DP-PO-122-2 | 20/11/07 | 27/11/07 | 13.8 | 1 |
| DP-PO-122-3 | 20/11/07 | 27/11/07 | 14.3 | 1.1 |
| PO-122-H | 03/11/07 | 23/11/07 | 12.9 | 1.2 |
| PO-122-B-U | 03/11/07 | 23/11/07 | 12.3 | 1.1 |
| PO-122-B-L | 03/11/07 | 23/11/07 | 11.9 | 1 |
| PO-153-H-U | 04/11/07 | 23/11/07 | 17.2 | 1.4 |
| PO-153-H-L | 04/11/07 | 23/11/07 | 20.6 | 1.5 |
| PO-152-H | 04/11/07 | 23/11/07 | 18.5 | 1.4 |
| PO-153-B | 04/11/07 | 23/11/07 | 12.9 | 1.1 |
| PO-152-B | 04/11/07 | 23/11/07 | 10.5 | 1 |
| DP-C2-10-1 | 27/11/07 | 27/11/07 | 14.3 | 1.1 |
| DP-C2-10-2 | 27/11/07 | 27/11/07 | 13.8 | 1 |
| DP-C2-10-3 | 27/11/07 | 27/11/07 | 12.3 | 0.9 |
| C2-10-22m | 09/11/07 | 27/11/07 | 13.1 | 1 |
| C2-9-28m | 09/11/07 | 27/11/07 | 13.7 | 1 |
| C2-10-35m | 09/11/07 | 27/11/07 | 15 | 1.1 |
| PO-SH-48-H-U | 08/11/07 | 23/11/07 | 12.9 | 1.2 |
| PO-SH-48-H-L | 08/11/07 | 23/11/07 | 14.5 | 1.2 |
| PO-SH-48-B-U | 08/11/07 | 23/11/07 | 11.3 | 1 |

| $^{3}He$ | Error (1σ) | $^{4}He$ | Error (1σ) | Ne | Error (1σ) |
|---|---|---|---|---|---|
| cc/cc | cc/cc | cc/cc | cc/cc | cc/cc | cc/cc |
| - | - | - | - | - | - |
| 2.12E-13 | 2.12E-14 | 9.69E-08 | 9.69E-09 | 3.14E-07 | 3.14E-08 |
| 1.22E-13 | 1.22E-14 | 8.26E-08 | 8.26E-09 | 2.5E-07 | 2.5E-08 |
| 3.34E-13 | 3.34E-14 | 1.57E-07 | 1.57E-08 | 6.33E-07 | 6.33E-08 |
| 1.28E-13 | 1.28E-14 | 8.63E-08 | 8.63E-09 | 2.48E-07 | 2.48E-08 |
| 1.57E-13 | 1.57E-14 | 8.56E-08 | 8.56E-09 | 2.46E-07 | 2.46E-08 |
| - | - | - | - | - | - |
| 1.53E-13 | 1.53E-14 | 1.98E-07 | 1.98E-08 | 3.2E-07 | 3.2E-08 |
| 1.52E-13 | 1.52E-14 | 8.63E-08 | 8.63E-09 | 4.12E-07 | 4.12E-08 |
| 1.51E-13 | 1.51E-14 | 6.74E-08 | 6.74E-09 | 3.06E-07 | 3.06E-08 |
| 1.77E-13 | 1.77E-14 | 8.94E-08 | 8.94E-09 | 4.14E-07 | 4.14E-08 |
| 1.62E-13 | 1.62E-14 | 8.61E-08 | 8.61E-09 | 3.58E-07 | 3.58E-08 |
| 2.61E-13 | 2.61E-14 | 9.91E-08 | 9.91E-09 | 4.06E-07 | 4.06E-08 |
| 2.86E-13 | 2.86E-14 | 1.28E-07 | 1.28E-08 | 3.7E-07 | 3.7E-08 |
| 1.23E-13 | 1.23E-14 | 1.03E-07 | 1.03E-08 | 2.96E-07 | 2.96E-08 |
| 1.44E-13 | 1.44E-14 | 1.04E-07 | 1.04E-08 | 3.72E-07 | 3.72E-08 |
| 1.16E-13 | 1.16E-14 | 8.59E-08 | 8.59E-09 | 2.99E-07 | 2.99E-08 |
| 1.21E-13 | 1.21E-14 | 8.95E-08 | 8.95E-09 | 3.12E-07 | 3.12E-08 |
| 2.9E-13 | 2.9E-14 | 2.81E-07 | 2.81E-08 | 4.14E-07 | 4.14E-08 |
| 1.3E-13 | 1.3E-14 | 7.14E-08 | 7.14E-09 | 3.44E-07 | 3.44E-08 |
| 1.32E-13 | 1.32E-14 | 9.9E-08 | 9.9E-09 | 3.03E-07 | 3.03E-08 |
| 1.94E-13 | 1.94E-14 | 1.54E-07 | 1.54E-08 | 4.44E-07 | 4.44E-08 |
| 1.23E-13 | 1.23E-14 | 8.55E-08 | 8.55E-09 | 2.41E-07 | 2.41E-08 |
| 1.32E-13 | 1.32E-14 | 9.13E-08 | 9.13E-09 | 2.59E-07 | 2.59E-08 |
| 3.8E-13 | 3.8E-14 | 1.75E-07 | 1.75E-08 | 2.85E-07 | 2.85E-08 |
| - | - | - | - | - | - |
| 2.51E-13 | 2.51E-14 | 1.49E-07 | 1.49E-08 | 3.05E-07 | 3.05E-08 |
| 2.53E-13 | 2.53E-14 | 3.16E-07 | 3.16E-08 | 3.29E-07 | 3.29E-08 |

| Sample | Date water sample collection + gas sampler emplaced | Date gas sample collected | $^{3}H$ | Error (1σ) | $^{3}He$ | Error (1σ) | $^{4}He$ | Error (1σ) | Ne | Error (1σ) |
|---|---|---|---|---|---|---|---|---|---|---|
| | - | - | T.U. | T.U. | cc/cc | cc/cc | cc/cc | cc/cc | cc/cc | cc/cc |
| PO-SH-48-B-L | 08/11/07 | 23/11/07 | 14.6 | 1.2 | 2.56E-13 | 2.56E-14 | 3.49E-07 | 3.49E-08 | 2.99E-07 | 2.99E-08 |
| PO-SH-47-H | 08/11/07 | 23/11/07 | 15 | 1.2 | 2.65E-13 | - | 2.6E-07 | - | 2.99E-07 | - |
| PO-SH-26-H-U | 09/11/07 | 21/11/07 | 16.5 | 1.4 | 1.71E-13 | 1.71E-14 | 7.08E-08 | 7.08E-09 | 3.8E-07 | 3.8E-08 |
| PO-SH-26-H-L | 09/11/07 | 21/11/07 | 15.2 | 1.3 | 2.08E-13 | 2.08E-14 | 1.34E-07 | 1.34E-08 | 4.17E-07 | 4.17E-08 |
| PO-SH-26-B-U | 09/11/07 | 21/11/07 | 12.5 | 1.1 | 1.93E-13 | 1.93E-14 | 8.27E-08 | 8.27E-09 | 3.95E-07 | 3.95E-08 |
| PO-SH-26-B-L | 09/11/07 | 21/11/07 | 14.6 | 1.1 | 2.17E-13 | 2.17E-14 | 1.4E-07 | 1.4E-08 | 4.93E-07 | 4.93E-08 |
| PO-117-H | 03/11/07 | 23/11/07 | 12.2 | 1 | 1.63E-13 | 1.63E-14 | 8.78E-08 | 8.78E-09 | 4.14E-07 | 4.14E-08 |
| PO-116-H | 03/11/07 | 23/11/07 | 14.4 | 1.2 | 2.04E-13 | 2.04E-14 | 1.11E-07 | 1.11E-08 | 4.79E-07 | 4.79E-08 |
| PO-117-B | 03/11/07 | 23/11/07 | 17.3 | 1.4 | 3.37E-13 | 3.37E-14 | 3.12E-07 | 3.12E-08 | 2.54E-07 | 2.54E-08 |
| PO-116-B | 03/11/07 | 23/11/07 | 13.5 | 1.1 | 2.03E-13 | 2.03E-14 | 1.49E-07 | 1.49E-08 | 2.68E-07 | 2.68E-08 |
| PO-126-H | 03/11/07 | 23/11/07 | 14.1 | 1.2 | 1.27E-13 | 1.27E-14 | 9.14E-08 | 9.14E-09 | 3.54E-07 | 3.54E-08 |
| DP-PO-125 | 20/11/07 | 27/11/07 | 13.5 | 1.1 | 1.31E-13 | 1.31E-14 | 9.52E-08 | 9.52E-09 | 3.44E-07 | 3.44E-08 |
| PO-126-B-U | 03/11/07 | 23/11/07 | 12.7 | 1.1 | 1.21E-13 | 1.21E-14 | 8.66E-08 | 8.66E-09 | 2.88E-07 | 2.88E-08 |
| PO-126-B-L | 03/11/07 | 23/11/07 | 14.5 | 1.2 | 1.27E-13 | 1.27E-14 | 8.91E-08 | 8.91E-09 | 3.65E-07 | 3.65E-08 |
| PO-125-H | 03/11/07 | 23/11/07 | 11.7 | 1.1 | 1.26E-13 | 1.26E-14 | 1.34E-07 | 1.34E-08 | 2.77E-07 | 2.77E-08 |
| PO-143-H | 03/11/07 | 23/11/07 | 13.8 | 1.1 | 5.28E-14 | 5.28E-15 | 4.08E-08 | 4.08E-09 | 1.94E-07 | 1.94E-08 |
| PO-142-H-U | 03/11/07 | 23/11/07 | 12.9 | 1.1 | 1.21E-13 | 1.21E-14 | 8.77E-08 | 8.77E-09 | 3.36E-07 | 3.36E-08 |
| PO-142-H-L | 03/11/07 | 23/11/07 | 12.5 | 1 | 1.35E-13 | 1.35E-14 | 9.87E-08 | 9.87E-09 | 3.66E-07 | 3.66E-08 |
| PO-143-B | 03/11/07 | 23/11/07 | 13.4 | 1.2 | 1.22E-13 | 1.22E-14 | 8.87E-08 | 8.87E-09 | 3.31E-07 | 3.31E-08 |
| PO-142-B | 03/11/07 | 23/11/07 | 12.1 | 1.1 | 6.75E-13 | 6.75E-14 | 3.96E-06 | 3.96E-07 | 3.21E-07 | 3.21E-08 |

| Sample | Date water sample collection + gas sampler emplaced | Date gas sample collected | $^{3}H$ | Error (1σ) | $^{3}He$ | Error (1σ) | $^{4}He$ | Error (1σ) | Ne | Error (1σ) |
|---|---|---|---|---|---|---|---|---|---|---|
| - | - | - | T.U. | T.U. | cc/cc | cc/cc | cc/cc | cc/cc | cc/cc | cc/cc |
| PO-SH-22-H-U | 02/11/07 | 21/11/07 | 13 | 1.1 | 2.18E-13 | 2.18E-14 | 1.28E-07 | 1.28E-08 | 5.17E-07 | 5.17E-08 |
| PO-SH-22-H-L | 02/11/07 | 21/11/07 | 12.3 | 1 | - | - | - | - | - | - |
| PO-SH-22-B-U | 02/11/07 | 21/11/07 | 11.8 | 0.9 | - | - | - | - | - | - |
| PO-SH-22-B-L | 02/11/07 | 21/11/07 | 10.8 | 1 | 2.02E-13 | 2.02E-14 | 9.29E-08 | 9.29E-09 | 4.49E-07 | 4.49E-08 |
| PO-SH-21-H | 02/11/07 | 21/11/07 | 10.4 | 0.8 | - | - | - | - | - | - |
| PO-SH-6-H-U | 04/11/07 | 21/11/07 | 16.1 | 1.2 | - | - | - | - | - | - |
| PO-SH-6-H-L | 04/11/07 | 21/11/07 | 13.2 | 1 | - | - | - | - | - | - |
| PO-SH-6-B-U | 04/11/07 | 21/11/07 | 15 | 1.1 | - | - | - | - | - | - |
| PO-SH-6-B-L | 04/11/07 | 21/11/07 | 14.9 | 1.1 | 2.17E-13 | 2.17E-14 | 1.4E-07 | 1.4E-08 | 4.93E-07 | 4.93E-08 |
| PO-SH-5-H | 09/11/07 | 21/11/07 | 9.9 | 0.8 | 2.56E-13 | 2.56E-14 | 2.27E-07 | 2.27E-08 | 5.35E-07 | 5.35E-08 |

**Table A3b.** $^{3}H$-$^{3}He$ Age Calculation.

| Sample | $^{4}He_{terrigenic}$ | $^{3}He_{tritiogenic}$ | $^{3}H + {}^{3}He_{tritiogenic}$ | Age | Error (1σ) |
|---|---|---|---|---|---|
| | cc/cc | T.U. | T.U. | years | years |
| B69-2-6m | - | - | - | - | - |
| B69-2-23m | 1.71E-08 | 40.93 | 52.23 | 27.2 | 3.1 |
| B70-1-10m | 2.09E-08 | 15.22 | 27.52 | 14.3 | 2.1 |
| B70-1-21m | 0 | 39.11 | 49.61 | 27.6 | 3.3 |
| B98-1-13m | 2.53E-08 | 17.69 | 28.29 | 17.4 | 2.6 |
| B98-1-22m | 2.53E-08 | 29.69 | 38.49 | 26.2 | 3.2 |
| PO-SH-8-H | - | - | - | - | - |
| PO-SH-7-H | 1.17E-07 | 15.58 | 26.88 | 15.4 | 1.9 |
| DP-PO-122-1 | 0 | 1.43 | 13.73 | 2 | 0.4 |
| DP-PO-122-2 | 0 | 18.24 | 32.04 | 15 | 2.1 |
| DP-PO-122-3 | 0 | 11.28 | 25.58 | 10.3 | 1.7 |
| PO-122-H | 0 | 13.92 | 26.82 | 13 | 2.2 |
| PO-122-B-U | 0 | 45.94 | 58.24 | 27.6 | 3.2 |
| PO-122-B-L | 3.19E-08 | 61.63 | 73.53 | 32.4 | 3.3 |
| PO-153-H-U | 2.8E-08 | 8.13 | 25.33 | 6.9 | 1.3 |
| PO-153-H-L | 7.35E-09 | 4.62 | 25.22 | 3.6 | 0.7 |
| PO-152-H | 1.01E-08 | 4.73 | 23.23 | 4 | 0.8 |
| PO-153-B | 1E-08 | 4.63 | 17.53 | 5.5 | 1.1 |
| PO-152-B | 1.72E-07 | 55.13 | 65.63 | 21.3 | 2.7 |
| DP-C2-10-1 | 0 | 3.64 | 17.94 | 4 | 0.8 |
| DP-C2-10-2 | 2.21E-08 | 10.57 | 24.37 | 10.1 | 1.6 |
| DP-C2-10-3 | 3.65E-08 | 12.65 | 24.95 | 12.6 | 1.9 |
| C2-10-22m | 2.64E-08 | 16.71 | 29.81 | 14.6 | 2.2 |
| C2-9-28m | 2.71E-08 | 17.48 | 31.18 | 14.6 | 2.1 |
| C2-10-35m | 1.03E-07 | 112.54 | 127.54 | 38 | 3.4 |
| PO-SH-48-H-U | - | - | - | - | - |
| PO-SH-48-H-L | 7.2E-08 | 57.78 | 72.28 | 28.6 | 3.2 |
| PO-SH-48-B-U | 2.32E-07 | 53.28 | 64.58 | 31 | 3.4 |
| PO-SH-48-B-L | 2.73E-07 | 59.18 | 73.78 | 28.8 | 3.2 |
| PO-SH-47-H | 1.84E-07 | 63.23 | 78.23 | 29.4 | 3.2 |
| PO-SH-26-H-U | 0 | 14.48 | 30.98 | 11.2 | 1.9 |
| PO-SH-26-H-L | 2.4E-08 | 22.66 | 37.86 | 16.2 | 2.4 |
| PO-SH-26-B-U | 0 | 20.65 | 33.15 | 17.3 | 2.5 |
| PO-SH-26-B-L | 8.37E-09 | 14.58 | 29.48 | 12.1 | 1.9 |
| PO-117-H | 0 | 5.72 | 17.92 | 6.8 | 1.3 |
| PO-116-H | 0 | 11.73 | 26.13 | 10.6 | 1.8 |
| PO-117-B | 2.49E-07 | 99.02 | 116.32 | 33.9 | 3.3 |
| PO-116-B | 8.21E-08 | 44.08 | 57.58 | 25.8 | 3 |

| Sample | $^4He_{terrigenic}$ | $^3He_{tritiogenic}$ | $^3H + {}^3He_{tritiogenic}$ | Age | Error (1σ) |
|---|---|---|---|---|---|
| | cc/cc | T.U. | T.U. | years | years |
| PO-126-H | 0 | 0.46 | 14.56 | 0.6 | 0.1 |
| DP-PO-125 | 6.56E-09 | 3.77 | 17.27 | 4.4 | 0.9 |
| PO-126-B-U | 1.41E-08 | 8.65 | 21.35 | 9.2 | 1.6 |
| PO-126-B-L | - | - | 13.22 | - | - |
| PO-125-H | 6.43E-08 | 11.92 | 23.62 | 12.5 | 2.1 |
| PO-143-H | - | - | 10.32 | - | - |
| PO-142-H-U | 1.3E-09 | 0.96 | 13.86 | 1.3 | 0.3 |
| PO-142-H-L | 3.73E-09 | 2.03 | 14.53 | 2.7 | 0.5 |
| PO-143-B | 3.9E-09 | 2.37 | 15.77 | 2.9 | 0.6 |
| PO-142-B | 3.88E-06 | 194.8 | 206.9 | 50.5 | 3.9 |
| PO-SH-22-H-U | 0 | 11.17 | 24.17 | 11 | 1.8 |
| PO-SH-22-H-L | - | - | - | - | - |
| PO-SH-22-B-U | - | - | - | - | - |
| PO-SH-22-B-L | 0 | 15.56 | 27.46 | 14.9 | 2.3 |
| PO-SH-21-H | - | - | - | - | - |
| PO-SH-6-H-U | - | - | - | - | - |
| PO-SH-6-H-L | - | - | - | - | - |
| PO-SH-6-B-U | - | - | - | - | - |
| PO-SH-6-B-L | 8.37E-09 | 14.58 | 29.48 | 12.1 | 1.9 |
| PO-SH-5-H | 8.33E-08 | 22.87 | 32.77 | 21.3 | 2.7 |

**Table A4.** $^{3}H$-$^{3}He$ Ages compared with models ages obtained from particle tracking at porosities (n) of 0.30, 0.35, 0.40 and 0.45.

| Sample | $^{3}H$-$^{3}He$ Dating Age | $^{3}H$-$^{3}He$ Dating Error (1σ) | Model Ages n=0.30 | n=0.35 | n=0.40 | n=0.45 |
|---|---|---|---|---|---|---|
| | years | years | years | years | years | years |
| *Prodeltaic Silt* | | | | | | |
| B69-2-6m | - | - | - | - | - | - |
| B69-2-23m | 27.2 | 3.1 | - | - | - | - |
| B70-1-10m | 14.3 | 2.1 | - | - | - | - |
| B70-1-21m | 27.6 | 3.3 | - | - | - | - |
| B98-1-13m | 17.4 | 2.6 | - | - | - | - |
| B98-1-22m | 26.2 | 3.2 | - | - | - | - |
| *North Flow Path* | | | | | | |
| PO-SH-8-H | - | - | 8.0 | 9.2 | 10.2 | 11.9 |
| PO-SH-7-H | 15.4 | 1.9 | 30.7 | 36.0 | 40.5 | 45.7 |
| DP-PO-122-1 | 2 | 0.4 | 3.6 | 4.2 | 4.8 | 5.4 |
| DP-PO-122-2 | 15 | 2.1 | 11.1 | 13.0 | 14.8 | 16.7 |
| DP-PO-122-3 | 10.3 | 1.7 | 18.8 | 22.0 | 25.2 | 28.3 |
| PO-122-H | 13 | 2.2 | 24.8 | 29.0 | 33.2 | 37.3 |
| PO-122-B-U | 27.6 | 3.2 | 31.0 | 36.2 | 41.5 | 46.6 |
| PO-122-B-L | 32.4 | 3.3 | n.d. | n.d. | n.d. | n.d. |
| PO-153-H-U | 6.9 | 1.3 | 6.6 | 7.7 | 8.8 | 9.9 |
| PO-153-H-L | 3.6 | 0.7 | 9.0 | 10.5 | 12.0 | 13.5 |
| PO-152-H | 4 | 0.8 | 15.2 | 17.7 | 20.2 | 22.7 |
| PO-153-B | 5.5 | 1.1 | 21.8 | 25.4 | 29.0 | 32.6 |
| PO-152-B | 21.3 | 2.7 | 25.2 | 29.3 | 33.5 | 37.6 |
| DP-C2-10-1 | 4 | 0.8 | 2.1 | 2.5 | 2.8 | 3.2 |
| DP-C2-10-2 | 10.1 | 1.6 | 4.7 | 5.5 | 6.2 | 7.0 |
| DP-C2-10-3 | 12.6 | 1.9 | 8.0 | 9.3 | 10.7 | 12.0 |
| C2-10-22m | 14.6 | 2.2 | 11.3 | 13.2 | 15.1 | 16.9 |
| C2-9-28m | 14.6 | 2.1 | 14.6 | 17.0 | 19.5 | 21.9 |
| C2-10-35m | 38 | 3.4 | n.d. | n.d. | n.d. | n.d. |
| *South Flow Path* | | | | | | |
| PO-SH-48-H-U | - | - | 2.2 | 2.5 | 2.9 | 3.3 |
| PO-SH-48-H-L | 28.6 | 3.2 | 3.5 | 4.1 | 4.6 | 5.2 |
| PO-SH-48-B-U | 31 | 3.4 | 12.0 | 14.0 | 16.0 | 18.2 |

| Sample | $^3H$-$^3He$ Dating | | Model Ages | | | |
|---|---|---|---|---|---|---|
| | Age | Error (1σ) | n=0.30 | n=0.35 | n=0.40 | n=0.45 |
| | years | years | years | years | years | years |
| PO-SH-48-B-L | 28.8 | 3.2 | 16.7 | 19.8 | 22.7 | 25.8 |
| PO-SH-47-H | 29.4 | 3.2 | 26.2 | 30.8 | 35.9 | 40.0 |
| PO-SH-26-H-U | 11.2 | 1.9 | 3.4 | 4.0 | 4.5 | 5.1 |
| PO-SH-26-H-L | 16.2 | 2.4 | 6.5 | 7.5 | 8.6 | 9.7 |
| PO-SH-26-B-U | 17.3 | 2.5 | 19.2 | 22.0 | 25.0 | 28.4 |
| PO-SH-26-B-L | 12.1 | 1.9 | 20.8 | 23.6 | 26.9 | 30.6 |
| PO-117-H | 6.8 | 1.3 | 1.7 | 2.0 | 2.3 | 2.6 |
| PO-116-H | 10.6 | 1.8 | 7.5 | 8.8 | 10.0 | 11.2 |
| PO-117-B | 33.9 | 3.3 | 13.4 | 15.7 | 17.9 | 20.2 |
| PO-116-B | 25.8 | 3 | n.d. | n.d. | n.d. | n.d. |
| PO-126-H | 0.6 | 0.1 | 2.8 | 3.2 | 3.7 | 4.2 |
| DP-PO-125 | 4.4 | 0.9 | 5.6 | 6.6 | 7.5 | 8.4 |
| PO-126-B-U | 9.2 | 1.6 | 10.7 | 12.6 | 14.3 | 16.1 |
| PO-126-B-L | - | - | 13.0 | 15.2 | 17.4 | 19.6 |
| PO-125-H | 12.5 | 2.1 | n.d. | n.d. | n.d. | n.d. |
| PO-143-H | - | - | 1.5 | 1.8 | 2.0 | 2.2 |
| PO-142-H-U | 1.3 | 0.3 | 4.3 | 5.0 | 5.7 | 6.4 |
| PO-142-H-L | 2.7 | 0.5 | 6.1 | 7.1 | 8.2 | 9.2 |
| PO-143-B | 2.9 | 0.6 | 10.8 | 12.2 | 14.0 | 15.6 |
| PO-142-B | 50.5 | 3.9 | n.d. | n.d. | n.d. | n.d. |
| *Shannon Transect* | | | | | | |
| PO-SH-22-H-U | 11 | 1.8 | - | - | - | - |
| PO-SH-22-H-L | - | - | - | - | - | - |
| PO-SH-22-B-U | - | - | - | - | - | - |
| PO-SH-22-B-L | 14.9 | 2.3 | - | - | - | - |
| PO-SH-21-H | - | - | - | - | - | - |
| PO-SH-6-H-U | - | - | - | - | - | - |
| PO-SH-6-H-L | - | - | - | - | - | - |
| PO-SH-6-B-U | - | - | - | - | - | - |
| PO-SH-6-B-L | 12.1 | 1.9 | - | - | - | - |
| PO-SH-5-H | 21.3 | 2.7 | - | - | - | - |

**Table A5**. Concentrations of major cations and anions in Valcartier groundwater.

| Sample | $Cl^-$ | $NO_3^-$ | $SO_4^{2-}$ | $HCO_3^-$ | $Ca^{2+}$ | $K^+$ | $Mg^{2+}$ | $Na^+$ | $Sr^{2+}$ | Si |
|---|---|---|---|---|---|---|---|---|---|---|
| | mg/L | mg/L | mg/L | mg/L | mg/L | mg/L | mg/L | mg/L | mg/L | mg/L |
| *Prodeltaic Silt* | | | | | | | | | | |
| B69-2-6m | 7.49 | 3.19 | 11.31 | 0.01 | 7.11 | 1.27 | 0.58 | 10.34 | 0.057 | 3.62 |
| B69-2-23m | 16.20 | bdl | 7.74 | 35.58 | 11.61 | 1.85 | 6.38 | 5.41 | 0.080 | 7.07 |
| B70-1-10m | 8.33 | bdl | 8.90 | 13.07 | 2.75 | 0.66 | 0.42 | 8.69 | 0.039 | 4.48 |
| B70-1-21m | 23.43 | bdl | 3.90 | 30.50 | 9.77 | 1.16 | 6.49 | 4.28 | 0.042 | 8.89 |
| B98-1-13m | 1.66 | bdl | 6.10 | 18.77 | 1.11 | 0.37 | 0.30 | 8.89 | 0.010 | 7.34 |
| B98-1-22m | 2.44 | bdl | 5.66 | 24.40 | 2.21 | 0.96 | 1.11 | 8.20 | 0.013 | 8.87 |
| *North Flow Path* | | | | | | | | | | |
| PO-SH-8-H | 60.29 | 8.79 | 19.73 | 17.08 | 11.53 | 1.33 | 2.66 | 50.32 | 0.090 | 9.39 |
| PO-SH-7-H | 95.96 | 6.75 | 21.91 | 31.72 | 26.77 | 1.66 | 7.22 | 52.67 | 0.190 | 9.27 |
| DP-PO-122-1 | 92.39 | 7.33 | 10.10 | 12.84 | 10.25 | 1.51 | 0.91 | 61.00 | 0.102 | 3.71 |
| DP-PO-122-2 | 83.57 | 7.64 | 13.66 | 20.33 | 11.69 | 2.01 | 2.14 | 55.51 | 0.123 | 5.18 |
| DP-PO-122-3 | 85.05 | 5.75 | 12.44 | 13.86 | 11.19 | 1.69 | 2.07 | 53.59 | 0.118 | 5.25 |
| PO-122-H | 7.93 | bdl | 4.86 | 34.16 | 2.00 | 0.55 | 0.58 | 13.76 | 0.016 | 8.16 |
| PO-122-B-U | 9.42 | 1.02 | 4.96 | 42.70 | 5.30 | 1.78 | 2.26 | 14.14 | 0.035 | 9.22 |
| PO-122-B-L | 9.82 | 0.00 | 4.91 | 35.88 | 5.39 | 1.77 | 2.30 | 14.09 | 0.034 | 8.70 |
| PO-153-H-U | 18.42 | 6.61 | 16.97 | 35.58 | 11.01 | 1.01 | 1.39 | 18.03 | 0.083 | 5.62 |
| PO-153-H-L | 21.64 | 7.75 | 16.55 | 50.83 | 11.09 | 1.08 | 1.43 | 20.21 | 0.087 | 6.00 |
| PO-152-H | 6.18 | 0.55 | 11.24 | 16.27 | 6.74 | 0.92 | 0.76 | 7.30 | 0.079 | 5.41 |
| PO-153-B | 11.56 | bdl | 7.75 | 22.47 | 2.41 | 0.87 | 0.85 | 16.34 | 0.021 | 6.39 |
| PO-152-B | 15.48 | bdl | 6.25 | 44.73 | 13.89 | 1.80 | 3.65 | 10.99 | 0.071 | 8.90 |
| DP-C2-10-1 | 43.15 | 9.306 | 24.76 | 89.47 | 24.64 | 5.42 | 1.72 | 45.06 | 0.167 | 3.01 |
| DP-C2-10-2 | 65.71 | 5.102 | 52.09 | 100.47 | 30.10 | 4.97 | 1.85 | 74.10 | 0.207 | 2.78 |
| DP-C2-10-3 | 65.71 | 4.829 | 50.18 | 115.90 | 31.06 | 5.07 | 1.89 | 73.25 | 0.215 | 2.78 |
| C2-10-22m | 55.04 | 6.59 | 24.94 | 33.55 | 11.06 | 1.38 | 0.89 | 52.99 | 0.102 | 3.84 |
| C2-9-28m | 71.40 | 4.60 | 18.03 | 30.50 | 21.94 | 2.33 | 6.05 | 38.21 | 0.155 | 6.52 |
| C2-10-35m | 4.37 | bdl | 8.51 | 156.86 | 32.34 | 2.47 | 3.85 | 13.37 | 0.141 | 6.28 |

| Sample | $Cl^-$ | $NO_3^-$ | $SO_4^{2-}$ | $HCO_3^-$ | $Ca^{2+}$ | $K^+$ | $Mg^{2+}$ | $Na^+$ | $Sr^{2+}$ | Si |
|---|---|---|---|---|---|---|---|---|---|---|
| | mg/L | mg/L | mg/L | mg/L | mg/L | mg/L | mg/L | mg/L | mg/L | mg/L |
| *South Flow Path* | | | | | | | | | | |
| PO-SH-48-H-U | 95.02 | 2.37 | 19.69 | 35.58 | 20.99 | 2.21 | 6.06 | 53.07 | 0.197 | 6.74 |
| PO-SH-48-H-L | 88.51 | 0.50 | 20.17 | 30.50 | 24.57 | 2.35 | 8.13 | 42.22 | 0.213 | 7.45 |
| PO-SH-48-B-U | 144.96 | 0.50 | 24.72 | 152.50 | 45.12 | 3.79 | 18.61 | 50.98 | 0.262 | 9.84 |
| PO-SH-48-B-L | 147.58 | bdl | 22.76 | 77.27 | 47.86 | 3.48 | 18.88 | 52.08 | 0.277 | 9.63 |
| PO-SH-47-H | 49.10 | bdl | 13.04 | 105.36 | 30.12 | 2.22 | 9.38 | 22.99 | 0.166 | 9.47 |
| PO-SH-26-H-U | 85.53 | 5.54 | 19.00 | 21.96 | 22.25 | 2.08 | 5.37 | 47.87 | 0.178 | 6.67 |
| PO-SH-26-H-L | 99.38 | 3.75 | 22.68 | 26.84 | 28.06 | 2.50 | 8.58 | 47.03 | 0.192 | 7.49 |
| PO-SH-26-B-U | 83.75 | 1.29 | 17.71 | 63.44 | 38.85 | 2.57 | 13.39 | 32.69 | 0.214 | 8.72 |
| PO-SH-26-B-L | 110.64 | 0.07 | 17.71 | 68.32 | 52.09 | 2.78 | 13.75 | 39.40 | 0.243 | 9.87 |
| PO-117-H | 54.22 | 1.62 | 11.99 | 36.60 | 8.10 | 1.71 | 1.62 | 45.43 | 0.096 | 5.08 |
| PO-116-H | 67.84 | 2.45 | 12.35 | 26.84 | 10.68 | 2.04 | 2.14 | 49.35 | 0.118 | 5.91 |
| PO-117-B | 86.16 | bdl | 14.32 | 73.20 | 33.14 | 3.16 | 12.26 | 27.00 | 0.198 | 10.20 |
| PO-116-B | 37.31 | bdl | 10.25 | 91.50 | 26.68 | 2.51 | 6.76 | 13.50 | 0.139 | 8.83 |
| PO-126-H | 42.17 | 3.30 | 12.59 | 28.71 | 9.46 | 1.40 | 1.27 | 31.29 | 0.097 | 3.21 |
| DP-PO-125 | 32.23 | 1.95 | 10.93 | 23.87 | 8.31 | 1.20 | 1.19 | 26.38 | 0.084 | 3.10 |
| PO-126-B-U | 27.87 | 3.02 | 12.15 | 46.36 | 9.12 | 1.48 | 1.18 | 22.68 | 0.090 | 3.50 |
| PO-126-B-L | 28.80 | 3.08 | 11.85 | 28.47 | 9.18 | 1.48 | 1.22 | 22.92 | 0.095 | 3.21 |
| PO-125-H | 28.15 | bdl | 8.93 | 37.54 | 11.53 | 1.50 | 3.41 | 19.36 | 0.066 | 5.09 |
| PO-143-H | 25.89 | bdl | 11.11 | 56.12 | 22.52 | 0.58 | 0.45 | 17.02 | 0.052 | 5.87 |
| PO-142-H- U | 1.35 | 0.98 | 7.14 | 4.88 | 2.57 | 0.66 | 0.36 | 1.87 | 0.021 | 3.04 |
| PO-142-H-L | 1.01 | bdl | 7.26 | 128.78 | 2.83 | 0.54 | 0.37 | 1.46 | 0.019 | 2.57 |
| PO-143-B | 0.48 | bdl | 5.66 | 33.55 | 2.52 | 0.33 | 0.36 | 1.04 | 0.015 | 3.29 |
| PO-142-B | 6.81 | 0.76 | 8.36 | 64.05 | 9.47 | 2.01 | 2.55 | 19.55 | 0.053 | 4.55 |

| Sample | $Cl^-$ | $NO_3^-$ | $SO_4^{2-}$ | $HCO_3^-$ | $Ca^{2+}$ | $K^+$ | $Mg^{2+}$ | $Na^+$ | $Sr^{2+}$ | Si |
|---|---|---|---|---|---|---|---|---|---|---|
| | mg/L | mg/L | mg/L | mg/L | mg/L | mg/L | mg/L | mg/L | mg/L | mg/L |
| *Shannon Transect* | | | | | | | | | | |
| PO-SH-16-H | 48.50 | 5.40 | 8.70 | 3.90 | 8.49 | 2.24 | 1.10 | 40.35 | 0.100 | 4.13 |
| PO-SH-16-B | 11.60 | 3.10 | 4.20 | 40.26 | 3.84 | 0.86 | 0.92 | 14.99 | 0.033 | 8.12 |
| PO-SH-15-H | 17.10 | 0.90 | 9.20 | 26.10 | 18.80 | 1.48 | 3.03 | 16.66 | 0.121 | 7.62 |
| PO-SH-22-H-U | 83.66 | 5.51 | 16.72 | 33.89 | 12.44 | 1.70 | 3.38 | 60.34 | 0.119 | 7.75 |
| PO-SH-22-H-L | 83.58 | 5.50 | 16.90 | 36.60 | 12.16 | 1.88 | 3.33 | 58.63 | 0.116 | 7.81 |
| PO-SH-22-B-U | 62.94 | 2.20 | 12.79 | 43.92 | 10.67 | 1.56 | 5.76 | 47.31 | 0.065 | 9.28 |
| PO-SH-22-B-L | 68.34 | 1.55 | 14.26 | 68.32 | 12.09 | 1.91 | 6.79 | 55.75 | 0.067 | 9.08 |
| PO-SH-21-H | 57.42 | bdl | 12.69 | 55.46 | 16.22 | 2.30 | 5.90 | 36.52 | 0.095 | 7.49 |
| PO-SH-28-H | 64.50 | 1.20 | 8.90 | 11.96 | 8.76 | 1.26 | 1.54 | 45.36 | 0.077 | 4.23 |
| PO-SH-28-B | 24.00 | 2.30 | 9.10 | 51.48 | 16.38 | 3.34 | 2.79 | 22.20 | 0.118 | 5.29 |
| PO-SH-6-H-U | 1.40 | 5.93 | 7.30 | 19.26 | 6.04 | 0.74 | 0.91 | 3.27 | 0.045 | 3.82 |
| PO-SH-6-H-L | 1.15 | 1.66 | 7.13 | 16.34 | 5.29 | 0.71 | 0.85 | 2.80 | 0.038 | 3.77 |
| PO-SH-6-B-U | 0.63 | bdl | 3.70 | 16.64 | 6.01 | 0.79 | 1.09 | 1.44 | 0.030 | 3.49 |
| PO-SH-6-B-L | 1.94 | bdl | 6.04 | 52.61 | 7.96 | 0.92 | 1.72 | 3.34 | 0.040 | 4.67 |
| PO-SH-5-H | 28.89 | bdl | 10.33 | 65.88 | 16.34 | 1.37 | 3.60 | 22.05 | 0.095 | 8.09 |
| *Proglacial* | | | | | | | | | | |
| PO-154-33 | 2.20 | 0.80 | 9.50 | 44.16 | 12.98 | 1.90 | 3.37 | 15.46 | 0.062 | 5.24 |
| PO-135-21 | 2.70 | 0.50 | 6.30 | 15.86 | 7.96 | 0.82 | 1.43 | 5.71 | 0.042 | 5.33 |
| PO-128-35 | 1.40 | 0.40 | 5.30 | 8.05 | 4.47 | 0.68 | 0.71 | 2.19 | 0.033 | 5.17 |
| PO-SH-25H | 1.80 | 0.50 | 8.70 | 42.70 | 16.71 | 1.91 | 3.40 | 3.83 | 0.046 | 5.46 |
| PO-SH-46-B | 35.20 | 8.10 | 16.00 | 54.66 | 43.16 | 2.17 | 4.74 | 10.99 | 0.153 | 4.00 |
| PO-SH-45-B | 23.20 | bdl | 16.30 | 47.34 | 32.00 | 2.97 | 3.69 | 7.94 | 0.153 | 4.77 |

**Table A6**. Stable isotope composition, terrigenic He, field parameters and contaminant concentrations

| Sample | $\delta^{18}O$ | $\delta^{2}H$ | $^{4}He_{terrigenic}$ | T | DO | Conductivity | pH | ORP | TCE | Perchlorate |
|---|---|---|---|---|---|---|---|---|---|---|
| | ‰ V-SMOW | ‰ V-SMOW | cc/cc x$10^{-8}$ | °C | % saturation | µS/cm | | mV | µg/L | µg/L |
| *Prodeltaic Silt* | | | | | | | | | | |
| B69-2-6m | -11.68 | -84.05 | | 10.31 | 33.8 | 295 | 6.37 | 41.9 | 4.1 | 73 |
| B69-2-23m | -12.61 | -88.39 | 9.7 | 7.93 | 10.75 | 210 | 5.87 | -95 | 430 | 0.07 |
| B70-1-10m | -12.3 | -86.48 | 8.3 | 7.99 | 19 | 290 | 5.64 | 92.7 | bdl | bdl |
| B70-1-21m | -12.51 | -89.67 | 0.0 | 7.32 | 9.6 | 320 | 5.69 | -113.5 | 81 | |
| B98-1-13m | -12.48 | -88.05 | 8.6 | 7.88 | 74 | 314 | 6.45 | 161 | | |
| B98-1-22m | -12.48 | -87.18 | 8.6 | 7.19 | 51.8 | 262 | 6.33 | 171 | | |
| *North Flow Path* | | | | | | | | | | |
| PO-SH-8-H | -12.11 | -86.2 | | 7.03 | 53.7 | 411 | 5.75 | 111.8 | <0.1 | 0.11 |
| PO-SH-7-H | -12.11 | -85 | 11.7 | 7.17 | 52.7 | 510 | 5.69 | 97.3 | <0.1 | 0.07 |
| DP-PO-122-1 | -12.4 | -88.28 | 0.0 | 8.66 | 74 | 375 | 5.67 | 149 | | |
| DP-PO-122-2 | -12.34 | -86.27 | 0.0 | 8.52 | 69.9 | 341 | 5.62 | 153.7 | | |
| DP-PO-122-3 | -12.43 | -87.45 | 0.0 | 8.41 | 69.2 | 321 | 5.61 | 153.9 | | |
| PO-122-H | -12.45 | -89.02 | 0.0 | 7.61 | 44.11 | 69 | 7.18 | 196 | 42 | 0.2 |
| PO-122-B-U | -12.2 | -85.4 | 0.0 | 7.3 | 35.48 | 98 | 7.38 | 184 | 120 | 0 |
| PO-122-B-L | -12.2 | -85.11 | 3.2 | 7.3 | 41.1 | 107 | 7.34 | 184 | 120 | 0 |
| PO-153-H-U | -12.16 | -87.85 | 2.8 | 8.22 | 64.91 | 127 | 5.94 | 247 | bdl | bdl |
| PO-153-H-L | -12.12 | -89.12 | 0.7 | 8.23 | 66.45 | 144 | 5.93 | 250 | | |
| PO-152-H | -12.24 | -87.2 | 1.0 | 7.87 | 71 | 83 | 6.07 | 274 | bdl | bdl |
| PO-153-B | -12.36 | -89.12 | 1.0 | 7.79 | 51.93 | 98 | 6.27 | 232 | 78 | 0.56 |
| PO-152-B | -12.09 | -87.62 | 17.2 | 7.29 | 30.4 | 149 | 6.93 | 243 | 9 | 0.16 |
| DP-C2-10-1 | -11.93 | -81.72 | 0.0 | 12.51 | 10.3 | 390 | 6.08 | 259 | | |
| DP-C2-10-2 | -12.02 | -87.11 | 2.2 | 12.02 | 15.8 | 632 | 6.28 | 264.2 | | |
| DP-C2-10-3 | -12.04 | -88.03 | 3.7 | 10.67 | 11.4 | 629 | 6.29 | 253.4 | | |
| C2-10-22m | -12.46 | -85.26 | 2.6 | 9.41 | 43.4 | 318 | 5.71 | 311.4 | 1.2 | 4.4 |
| C2-9-28m | -12.29 | -89.3 | 2.7 | 9.00 | 44.1 | 327 | 5.82 | 232.7 | 0.3 | 1.6 |
| C2-10-35m | -12.05 | -83.24 | 10.3 | 7.45 | 0 | - | 6.63 | -93 | | |

| Sample | $\delta^{18}O$ | $\delta^{2}H$ | $^{4}He_{terrigenic}$ | T | DO | Conductivity | pH | ORP | TCE | Perchlorate |
|---|---|---|---|---|---|---|---|---|---|---|
| | ‰ V-SMOW | ‰ V-SMOW | cc/cc x10-8 | °C | % saturation | µS/cm | | mV | µg/L | µg/L |
| *South Flow Path* | | | | | | | | | | |
| PO-SH-48-H-U | -11.99 | -82.78 | 6.0 | 7.88 | 50 | 426 | 5.9 | 204 | 60 | 0.49 |
| PO-SH-48-H-L | -11.96 | -81.95 | 7.2 | 7.87 | 38.53 | 411 | 5.94 | 209 | | |
| PO-SH-48-B-U | -11.98 | -85.07 | 23.2 | 7.61 | 31.13 | 658 | 6.31 | 204 | 40 | 0.08 |
| PO-SH-48-B-L | -11.94 | -85.02 | 27.3 | 7.58 | 23.98 | 676 | 6.47 | 198 | | |
| PO-SH-47-H | -11.92 | -83.51 | 18.4 | 7.62 | 16.39 | 322 | 6.53 | 142 | 100 | bdl |
| PO-SH-26-H-U | -11.99 | -86.2 | 5.3 | 8.11 | 57.2 | 508 | 6.71 | 91.3 | 90 | 0.11 |
| PO-SH-26-H-L | -12 | -85.6 | 9.5 | 7.94 | 34.9 | 519 | 5.71 | 94.8 | | |
| PO-SH-26-B-U | -11.98 | -82 | 87.4 | 7.89 | 18.6 | 671 | 6.37 | 47.3 | 88 | bdl |
| PO-SH-26-B-L | -12.06 | -82.8 | 33.7 | 7.77 | 13.4 | 632 | 6.46 | 40.5 | | |
| PO-117-H | -11.74 | -82.93 | 0.0 | 8.31 | 59.32 | 271 | 5.91 | 246 | 21 | 0.07 |
| PO-116-H | -11.8 | -82.66 | 0.0 | 8.02 | 38 | 318 | 5.79 | 183 | 55 | 0.08 |
| PO-117-B | -11.94 | -85.97 | 24.9 | 7.54 | 17.07 | 408 | 6.22 | 132 | 200 | bdl |
| PO-116-B | -11.81 | -83.78 | 8.2 | 7.18 | 29.2 | 235 | 6.62 | 138 | 87 | bdl |
| PO-126-H | -11.97 | -83.51 | 0.0 | 7.87 | 64.5 | 229 | 5.85 | 242 | 1.4 | bdl |
| DP-PO-125 | -12.11 | -83.26 | 0.7 | 7.76 | 59.4 | 256 | 5.54 | 150 | | |
| PO-126-B-U | -11.9 | -81.84 | 1.4 | 7.27 | 55.61 | 170 | 5.8 | 235 | 0.8 | 0.14 |
| PO-126-B-L | -11.95 | -82.47 | 0.0 | 7.55 | 52.37 | 172 | 5.79 | 239 | | 0.14 |
| PO-125-H | -11.99 | -82.48 | 6.4 | 6.55 | 63.34 | 48 | 6.13 | 236 | 12 | bdl |
| PO-143-H | -11.64 | -79.78 | 0.0 | 6.15 | 79.71 | 146 | 5.93 | 245 | bdl | bdl |
| PO-142-H- U | -11.55 | -80.3 | 0.1 | 6.28 | 68.04 | 29 | 5.25 | 296 | bdl | bdl |
| PO-142-H-L | -11.45 | -80.33 | 0.4 | 6.27 | 64.58 | 30 | 5.23 | 306 | | |
| PO-143-B | -11.88 | -83.8 | 0.4 | 6.26 | 72.37 | 25 | 5.59 | 267 | 6.2 | bdl |
| PO-142-B | -11.8 | -83.1 | 387.8 | 6.32 | 45.33 | 109 | 6.75 | 234 | 180 | bdl |

| Sample | $\delta^{18}O$ | $\delta^{2}H$ | $^{4}He_{terrigenic}$ | T | DO | Conductivity | pH | ORP | TCE | Perchlorate |
|---|---|---|---|---|---|---|---|---|---|---|
| | ‰ V-SMOW | ‰ V-SMOW | cc/cc x$10^{-8}$ | °C | % saturation | µS/cm | | mV | µg/L | µg/L |
| *Shannon Transect* | | | | | | | | | | |
| PO-SH-16-H | -12.49 | -91.5 | | 8.53 | 78.1 | 286 | 5.97 | 171.8 | bdl | 0.09 |
| PO-SH-16-B | -12.47 | -90.1 | | 8.27 | 71 | 145 | 6.82 | 138 | bdl | 0.06 |
| PO-SH-15-H | -12.42 | -85.5 | | 8.34 | 55 | 176 | 7.34 | 190 | bdl | 0.05 |
| PO-SH-22-H-U | -12.11 | -85.85 | 0.0 | 8.2 | 75 | 395 | 6.2 | 158 | 8.3 | 0.51 |
| PO-SH-22-H-L | -12.08 | -88.09 | | 8.2 | 74.2 | 392 | 6.2 | 165 | | |
| PO-SH-22-B-U | -12.32 | -87.48 | | 7.9 | 64.2 | 326 | 6.7 | 159 | 65 | 5.6 |
| PO-SH-22-B-L | -12.07 | -83.31 | 0.0 | 7.8 | 61.8 | 345 | 6.8 | 154 | | |
| PO-SH-21-H | -11.64 | -81.77 | | 7.6 | 48 | 334 | 6.8 | 122 | 4.4 | 0.46 |
| PO-SH-28-H | -11.99 | -84.3 | | 7 | 91.0 | 325 | 6.0 | 288 | | 0.06 |
| PO-SH-28-B | -11.9 | -81.7 | | 6.85 | 56.9 | 182 | 6.84 | 261.1 | | bdl |
| PO-SH-6-H-U | -11.72 | -82.79 | | 6.3 | 75.2 | 72 | 5.7 | 224 | bdl | bdl |
| PO-SH-6-H-L | -11.59 | -78.17 | | 6.3 | 75.7 | 75 | 5.7 | 230 | | |
| PO-SH-6-B-U | -12.72 | -90.18 | | 6.2 | 57.8 | 70 | 6.3 | 215 | 2.4 | bdl |
| PO-SH-6-B-L | -11.87 | -80.65 | 0.8 | 6.2 | 54.7 | 75 | 6.3 | 214 | | |
| PO-SH-5-H | -11.67 | -82.31 | 8.3 | 6.1 | 44.3 | 221 | 6.6 | 205 | 92 | bdl |
| *Proglacial Aquifer* | | | | | | | | | | |
| PO-154-33 | -11.98 | -85 | | 6.53 | 0.1 | 160 | 6.86 | 93 | 1600 | bdl |
| PO-135-21 | -11.97 | -83.3 | | 6.34 | 1.2 | 85 | 6.48 | 119 | 350 | bdl |
| PO-128-35 | -11.83 | -83.8 | | 6.18 | 65.6 | 44 | 5.71 | 52 | bdl | |
| PO-SH-25H | -11.92 | -82.3 | | 7.5 | 0.1 | 147 | 7.59 | 102 | bdl | bdl |
| PO-SH-46-B | -11.96 | -84 | | 7.19 | 53.2 | 362 | 7.32 | 124 | | 0.1 |
| PO-SH-45-B | -12 | -84.5 | | 7.96 | 0 | 247 | 7.32 | 113 | | bdl |

** Measurements highlighted in grey were not obtained by the author; values taken from 2007 sampling by Dessau-Soprin (B. Michaud, pers. comm., 2008)*

**Table A7**. Groundwater classification based on multivariate statistical analyses performed on geochemical data

| Sample | Cluster Analyses | | | Principal Component Loadings | | |
|---|---|---|---|---|---|---|
| | HCA Facies | AMBC Facies | AMBC Uncertainty | PC 1 | PC 2 | PC 3 |
| *Prodeltaic Silt* | | | | | | |
| B69-2-6m | A1 | 2 | 1.04% | 1.605 | 0.429 | 0.610 |
| B69-2-23m | A1 | 1 | 0.00% | 0.935 | 1.950 | -2.833 |
| B70-1-10m | A1 | 2 | 6.10% | 2.033 | 0.416 | -0.912 |
| B70-1-21m | A1 | 1 | 0.00% | 1.256 | 2.116 | -3.253 |
| B98-1-13m | A2 | 3 | 0.00% | 2.700 | 0.144 | -1.918 |
| B98-1-22m | A2 | 3 | 0.00% | 2.349 | 0.722 | -1.869 |
| *North Flow Path* | | | | | | |
| PO-SH-8-H | C1 | 6 | 0.00% | -0.991 | -1.800 | -1.403 |
| PO-SH-7-H | C1 | 6 | 0.00% | -2.748 | -1.262 | -0.926 |
| DP-PO-122-1 | C2 | 6 | 0.00% | -0.398 | -3.148 | -1.701 |
| DP-PO-122-2 | C2 | 6 | 0.00% | -0.771 | -2.761 | -1.204 |
| DP-PO-122-3 | C2 | 6 | 0.00% | -0.487 | -2.519 | -1.641 |
| PO-122-H | A2 | 3 | 0.00% | 2.076 | 1.187 | -2.183 |
| PO-122-B-U | A2 | 3 | 0.02% | 1.505 | 1.859 | -1.073 |
| PO-122-B-L | A2 | 3 | 0.02% | 1.687 | 1.753 | -0.946 |
| PO-153-H-U | C2 | 6 | 0.22% | 0.638 | -1.700 | -0.523 |
| PO-153-H-L | C2 | 6 | 0.01% | 0.347 | -1.846 | -0.686 |
| PO-152-H | A2 | 3 | 3.67% | 1.964 | -0.716 | -0.394 |
| PO-153-B | A2 | 3 | 0.00% | 2.163 | -0.139 | -1.481 |
| PO-152-B | A2 | 3 | 0.04% | 0.938 | 1.586 | -0.816 |
| DP-C2-10-1 | D1 | 4 | 0.00% | -2.369 | -1.200 | 1.843 |
| DP-C2-10-2 | D1 | 4 | 0.00% | -4.630 | -1.717 | 0.904 |
| DP-C2-10-3 | D1 | 4 | 0.00% | -4.773 | -1.402 | 0.737 |
| C2-10-22m | C2 | 6 | 0.00% | -0.797 | -2.801 | -0.317 |
| C2-9-28m | C2 | 6 | 0.00% | -1.292 | -1.431 | -1.317 |
| C2-10-35m | D2 | 5 | 0.05% | -1.373 | 4.129 | 0.356 |
| *South Flow Path* | | | | | | |
| PO-SH-48-H-U | C1 | 6 | 0.13% | -2.084 | -0.958 | 0.582 |
| PO-SH-48-H-L | C1 | 5 | 5.77% | -2.077 | -0.101 | 0.839 |
| PO-SH-48-B-U | D2 | 5 | 0.00% | -5.355 | 1.299 | 0.573 |
| PO-SH-48-B-L | D2 | 5 | 0.00% | -4.950 | 1.060 | 0.134 |
| PO-SH-47-H | D2 | 5 | 0.00% | -1.860 | 2.480 | 0.557 |
| PO-SH-26-H-U | C1 | 6 | 0.00% | -1.902 | -0.722 | -0.849 |
| PO-SH-26-H-L | C1 | 6 | 0.59% | -2.615 | -0.625 | -0.490 |
| PO-SH-26-B-U | D2 | 5 | 0.00% | -2.941 | 1.879 | 0.243 |
| PO-SH-26-B-L | D2 | 5 | 0.00% | -4.122 | 2.363 | -0.225 |
| PO-117-H | B | 7 | 0.04% | 0.205 | -1.056 | 1.436 |
| PO-116-H | B | 7 | 27.60% | -0.495 | -0.729 | 0.925 |
| PO-117-B | D2 | 5 | 0.00% | -2.495 | 1.826 | -0.313 |
| PO-116-B | D2 | 5 | 0.02% | -0.897 | 2.359 | 0.725 |

| Sample | Cluster Analyses | | | Principal Component Loadings | | |
|---|---|---|---|---|---|---|
| | HCA Facies | AMBC Facies | AMBC Uncertainty | PC 1 | PC 2 | PC 3 |
| PO-126-H | B | 7 | 0.19% | 0.686 | -1.560 | 1.050 |
| DP-PO-125 | B | 7 | 0.04% | 1.138 | -1.076 | 0.587 |
| PO-126-B-U | B | 7 | 0.00% | 0.841 | -0.910 | 1.668 |
| PO-126-B-L | B | 7 | 0.00% | 0.953 | -1.102 | 1.354 |
| PO-125-H | B | 7 | 0.00% | 1.291 | -0.114 | 1.081 |
| PO-143-H | B | 7 | 0.00% | 0.877 | 0.053 | 2.619 |
| PO-142-H- U | B | 7 | 0.00% | 3.040 | -1.204 | 2.989 |
| PO-142-H-L | B | 7 | 0.00% | 2.084 | -0.137 | 4.169 |
| PO-143-B | B | 7 | 0.00% | 2.996 | -0.743 | 1.540 |
| PO-142-B | B | 7 | 0.31% | 1.285 | 0.786 | 1.455 |
| *Shannon Section* | | | | | | |
| PO-SH-16-H | C2 | 6 | 0.01% | 0.766 | -2.443 | -2.448 |
| PO-SH-16-B | A2 | 3 | 0.00% | 1.861 | 0.212 | -2.583 |
| PO-SH-15-H | A2 | 3 | 0.01% | 0.570 | 1.155 | -1.282 |
| PO-SH-22-H-U | C1 | 6 | 0.00% | -1.188 | -1.714 | -0.897 |
| PO-SH-22-H-L | C1 | 6 | 0.00% | -1.175 | -1.765 | -1.250 |
| PO-SH-22-B-U | C1 | 6 | 11.19% | -0.223 | -0.140 | -1.826 |
| PO-SH-22-B-L | C1 | 6 | 0.45% | -0.764 | 0.343 | -0.268 |
| PO-SH-21-H | B | 7 | 2.23% | -0.467 | 1.228 | 1.180 |
| PO-SH-28-H | B | 7 | 0.56% | 0.961 | -2.089 | 0.674 |
| PO-SH-28-B | B | 7 | 0.01% | 0.421 | 0.318 | 1.397 |
| PO-SH-6-H-U | B | 7 | 0.00% | 2.283 | -1.461 | 1.601 |
| PO-SH-6-H-L | B | 7 | 0.00% | 2.634 | -0.592 | 2.990 |
| PO-SH-6-B-U | A2 | 3 | 0.00% | 2.871 | -0.295 | -2.127 |
| PO-SH-6-B-L | B | 7 | 0.01% | 2.089 | 0.767 | 1.814 |
| PO-SH-5-H | B | 7 | 0.20% | 0.118 | 1.370 | 1.414 |
| *Proglacial Aquifer Locations* | | | | | | |
| PO-154-33 | A1 | 2 | 0.00% | 0.839 | 2.082 | -0.059 |
| PO-135-21 | A1 | 2 | 0.00% | 1.754 | 1.747 | 0.268 |
| PO-128-35 | A1 | 7 | 0.23% | 2.640 | 0.301 | 0.463 |
| PO-SH-25H | A1 | 2 | 0.00% | 1.039 | 3.021 | 0.509 |
| PO-SH-46-B | D1 | 6 | 0.88% | -1.379 | 0.430 | 0.460 |
| PO-SH-45-B | A1 | 2 | 0.01% | -0.823 | 2.606 | 0.269 |

# Appendix B: Processing of $^{3}H$-$^{3}He$ Age Data

1) Equilibrium $^3He_{eq}$. The component of $^3He$ from equilibration with air ($^3He_{eq}$) can be easily determined using the Henry's constant $K_h$ appropriate from the recharge temperature. $K_h$ can be converted to the Bunsen coefficient $B$ to give the volumetric (cc) $^3He$ concentration in water (cc) per unit pressure (atmosphere) (cc $^3He$ / cc water / atm):

$$B = K_h RT \qquad \text{B.1}$$

The values for B used in this study were taken from Weiss (1971), assuming an average recharge temperature of 5°C: $B_{He}$ is 0.00915, and $B_{Ne}$ is 0.0117.

Where R is the gas constant (0.082057 L·mol/K·atm) and T is absolute temperature (K).

The volumetric mixing ratio of $^4He$ ($5.24 \times 10^{-6}$) and the $^3He/^4He$ ratio ($1.40 \times 10^{-6}$) in atmospheric air are known constants, and may be used with the fractionation factor of $^3He$ and $^4He$ (0.983) related to their dissolution in water to calculate $^3He_{eq}$ by the following two steps:

i) Find the equilibrium concentration of $^4He$ ($^4He_{eq}$) in water by multiplying the Bunsen coefficient, $B$, by the atmospheric $^4He$ mixing ratio ($5.24 \times 10^{-6}$):

$$^4He_{eq} = B \cdot 5.24 \times 10^{-6} \qquad \text{B.2}$$

ii) Converting $^4He_{eq}$ to $^3He_{eq}$ by multiplying by the $^3He/^4He$ ratio ($1.40 \times 10^{-6}$) and the fractionation factor (0.983):

$$^3He_{eq} = {}^4He_{eq} \cdot 1.40 \times 10^{-6} \cdot 0.983 \qquad \text{B.3}$$

2) Excess air $^3He_{ex}$. The excess air component of $^3He$ ($^3He_{ex}$) is calculated by first finding the total amount of excess air based on neon measurements, then by converting that value to $^3He$ using the following three steps:

i) Find the total amount of excess air by dividing the difference between the measured neon concentration ($Ne_{meas}$) and the concentration of atmospheric neon in equilibrium with water ($Ne_{eq}$ = $2.03 \times 10^{-7}$) by the atmospheric mixing ratio of neon ($1.82 \times 10^{-5}$):

$$\text{Total excess air} = \frac{Ne_{meas} - 2.03 \times 10^{-7}}{1.82 \times 10^{-5}} \qquad \text{B.4}$$

ii) Find the amount of excess $^4He$ ($^4He_{ex}$) by multiplying the total excess air by the atmospheric $^4He$ mixing ratio ($5.24 \times 10^{-6}$):

$$^4He_{ex} = \text{Total excess air} \cdot 5.24 \times 10^{-6} \qquad \text{B.5}$$

iii) Convert $^4He_{ex}$ to $^3He_{eq}$ by multiplying by the $^3He/^4He$ ratio ($1.40x10^{-6}$) and the fractionation factor (0.983):

$$^3He_{ex} = {}^4He_{ex} \cdot 1.40 \times 10^{-6} \cdot 0.983 \qquad \text{B.6}$$

3) Terrigenic $^3He_{ter}$. In shallow groundwaters, the terrigenic $^3He$ component ($^3He_{ter}$) is generally low, and can be detected by subtracting the excess air ($^4He_{ex}$) and equilibrium ($^4He_{eq}$) $^4He$ components from the total $^4He$ measured ($^4He_{meas}$), and multiplying by the mean crustal $^3He/^4He$ ratio of the Canadian Precambrian Shield ($2x10^{-8}$; Bottomley *et al*, 1984) in two steps:

i) Find the terrigenic $^4He$ component ($^4He_{ter}$):

$$^4He_{ter} = {}^4He_{meas} - {}^4He_{eq} - {}^4He_{ex} \qquad \text{B.7}$$

ii) Convert $^4He_{ter}$ to $^3He_{ter}$ by multiplying by the mean $^3He/^4He$ ratio for the Canadian Shield ($2x10^{-8}$; from Bottomley et al., 1984):

$$^3He_{ter} = {}^4He_{ter} \cdot 2 \times 10^{-8} \qquad \text{B.8}$$

4) Tritiogenic $^3He_{tri}$. To isolate the tritiogenic $^3He$ ($^3He_{tri}$), the additional components must be subtracted from the total measured $^3He$ ($^3He_{meas}$):

$$^3He_{tri} = {}^3He_{meas} - {}^3He_{eq} - {}^3He_{ex} - {}^3He_{ter} \qquad \text{B.9}$$

The tritiogenic $^3He$ concentration ($^3He_{tri}$) can then be used in the radioactive decay equation to determine the age of the groundwater, using the tritium $^3H$ measured concentration in groundwater and its half-life of 12.3 years (equivalent to equation 2.1):

$$Age = \frac{12.3}{\ln 2} \cdot \ln\left(1 + \frac{^3He_{tri}}{^3H}\right) \qquad \text{B.10}$$

# Appendix C: Quality Check of $^{3}H$-$^{3}He$ Age Data

There are several corrections that are applied to the measured $^3$He concentration in order to isolate $^3$He produced by tritium decay to calculate a groundwater age; at each correction stage, there is potential for error to be introduced. To verify the reliability of the $^3$He data, graphs of the isotopic ratios used to quantify the non-tritiogenic components can be constructed that compare the sample data with end-member isotopic compositions. This constrains the data to a valid isotopic composition range, and data that falls outside of this range may be regarded as poor quality and thus unreliable for use in age calculation. The component of $^3$He derived from solubility equilibration with air (referred to herein as "air-saturated water") is calculated using known solubility a constant (Henry's constant, $K_H$; see Appendix B) at a given temperature, and is used as an "endmember" in the data check graphs.

**Table B1**. Empirically measured values used to check $^3$H-$^3$He data.

| | Volume Mixing Ratio in **Air** | Volume Mixing Ratio in **Air Saturated Water** |
|---|---|---|
| He | $5.24 \times 10^{-6}$ | $4.802 \times 10^{-8}$ |
| Ne | $1.82 \times 10^{-5}$ | $2.144 \times 10^{-7}$ |
| Ne/He | 3.47 | 4.46 |
| $^3$He/$^4$He | $1.36 \times 10^{-6}$ | $1.38 \times 10^{-6}$ |

The graph that shows the Ne/He vs. $^3$He/$^4$He is a check on the computed terrigenic and tritiogenic $^3$He concentrations (Figure C1). Air-saturated water is plotted as an end-member, with pure terrigenic He and pure tritiogenic $^3$He representing the other two extreme compositions on this graph. Terrigenic He is a theoretical end-member that consists only of a dissolved gas component produced by radioactive decay of minerals in the earth and in the soil ($^3He_{meas}$ - $^3He_{ter}$ = 0). The Ne/He is zero because there is no terrigenic Ne production, so as the terrigenic component of He increases, the Ne/He decreases. The $^3$He/$^4$He of the terrigenic end-member is $2 \times 10^{-8}$, which is the average ratio produced in the Canadian Shield (Bottomley *et al.*, 1984). The line formed between air-saturated water and pure terrigenic He represents the addition of terrigenic He (moving towards the terrigenic end-member), and forms a boundary above which all valid sample data should fall. The other end-member composition is with a dissolved gas

composition of only tritiogenic $^3He$ (not plotted on the graph due o scale), where $^3He/^4He = \infty$ and Ne/He remains the same as air-saturated water. The lined formed moving from air-saturated water towards the tritiogenic end member represents the addition of $^3He$ produced from tritium decay, and forms a second line of which all sample data should fall to the left.

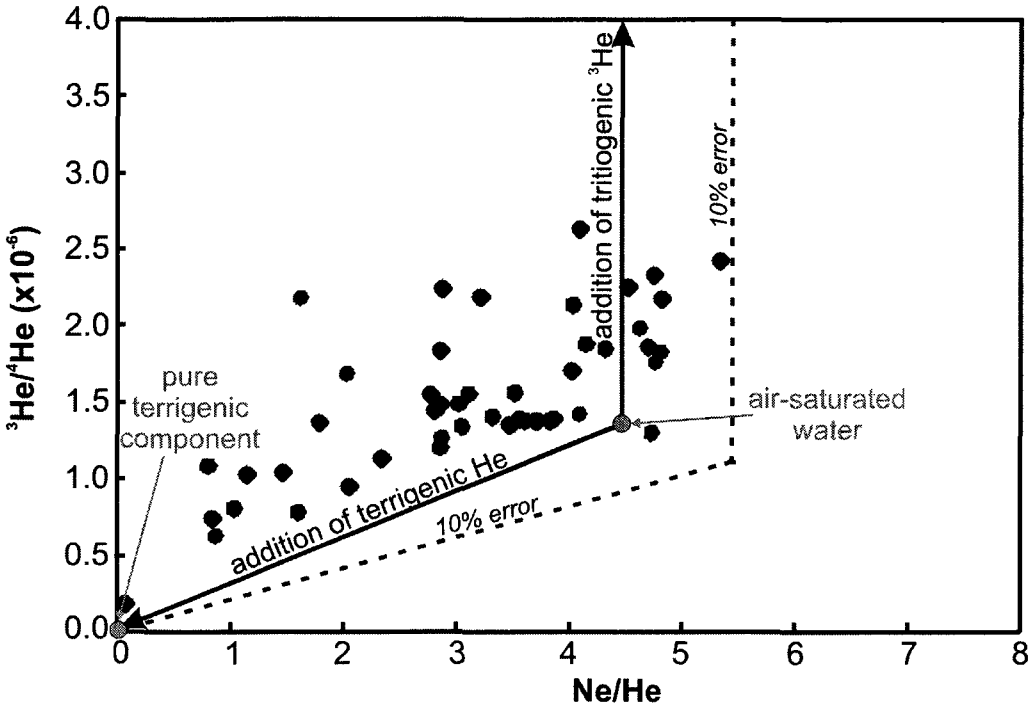


**Figure C1**. Ne/He versus $^3He/^4He$ for Valcartier groundwater samples.

Most of the Valcartier data plot within these two boundaries as they contain both tritiogenic and terrigenic He components. However, there are some data that plot to the right of air-saturated water; these data have a Ne/He ratio that is too large, as any additional component of $^3He$ added to the system should result in a Ne/He that is equal to (if only tritiogenic He is added) or less than (if terrigenic He and/or He from excess air are added) the Ne/He of air-saturated water. However, data plotting to the left of and above the line that defines 10% analytical error may be accepted as valid data points. Any data that plot outside of the range of error should be regarded as unacceptable and therefore inappropriate for use in the calculation of $^3H/^3He$ age.

The graph of total He concentration vs. total Ne concentration allows us to plot a line that defines the addition of excess air to a sample (Figure C2). Air -saturated water is the end-member used to compare with additions of unfractionated air; Ne and He concentrations will increase as excess

air is added to the system according to the relationship defined by the Ne and He ratio in unfractionated air (Ne = 3.47 * He). Data that plot along this line therefore have a component of excess air to account for. This graph also shows the presence of a terrigenic He component, as this contributes He but not Ne, so data with a terrigenic component of dissolved gas plot to the right of this line.

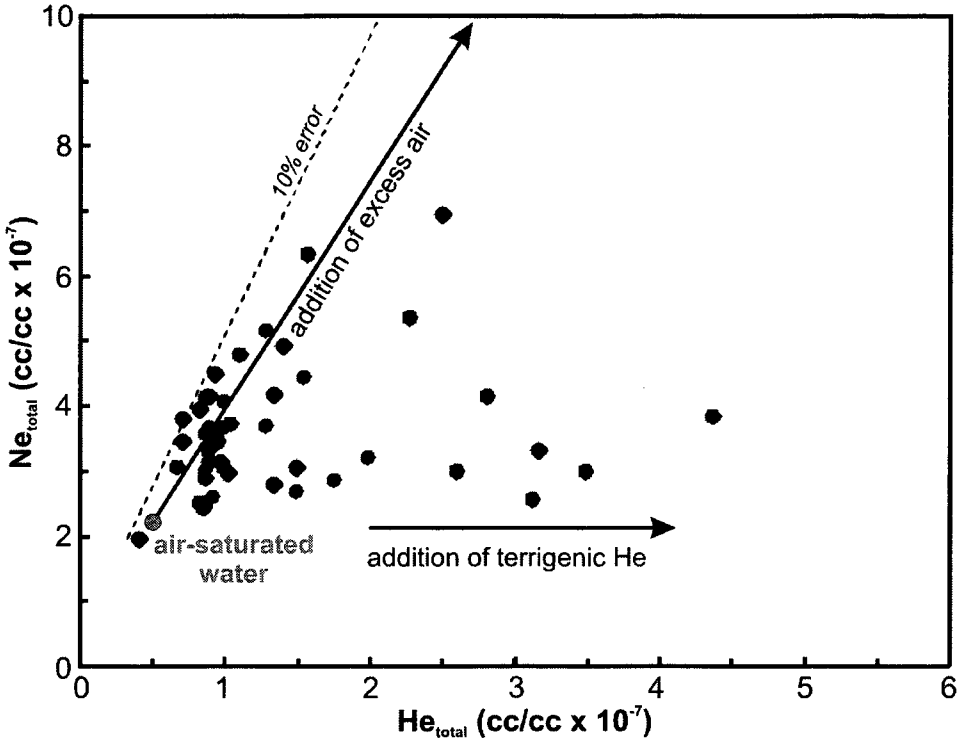


**Figure C2**. He concentration versus Ne concentration in Valcartier groundwater.

This graph illustrates how the corrections are made for excess air and terrigenic He. Excess air is directly quantified by the concentration of Ne in excess of that dissolved in air-saturated water; the Ne/He ratio of air (3.47) is used to determine the corresponding amount of He from excess air dissolved into the sample, so each data point is essentially "moved down" parallel to the line defined by excess air addition to the level of air saturated water. The amount of He remaining represents the terrigenic component, which is multiplied by the $^3He/^4He$ ratio of terrigenic gases from the Canadian Shield ($2x10^{-8}$) to estimate $^3He_{terrigenic}$. The terrigenic component can now be subtracted from the measured $^3He$, along with the amount from air-saturated water, to obtain the $^3He$ produced from tritium decay. Erroneous data can be identified if they plot to the left of the line for excess air addition, or below the value of He in air-saturated water ($4.802x10^{-8}$ cc/cc).